Overcoming Voltage Issues Associated with Integration of Photovoltaic Resources in the Electric Grid

Kaveh Rahimi

Dissertation submitted to the faculty of the Virginia Polytechnic Institute and State University in partial fulfillment of the requirements for the degree of

Doctor of Philosophy
In
Electrical Engineering

Robert P. Broadwater, Chair
Saifur Rahman, Co-Chair
Steve C. Southward
Virgilio A. Centeno
Amos L. Abbott

February 9, 2018
Blacksburg, VA

Keywords: Cloud Motion Simulator, Distribution Systems, Renewable Energy Resources, Smart Inverters, Solar Photovoltaic, Secondary Circuits, Voltage Flicker, Volt-var Control

Overcoming Voltage Issues Associated with Integration of Photovoltaic Resources in the Electric Grid

(Kaveh Rahimi)

Academic Abstract

The main challenge of dealing with solar energy, the fastest growing renewable energy, is its intermittent nature. Cloud shadows can cause drastic irradiance fluctuations and consequently impose voltage variations and flicker issues to power systems. However, in many cases those fluctuations are modeled and studied with simplified models, outdated standards and unrealistic approaches. Furthermore, distributed small-scale PV systems, a considerable portion of new PV installations, are usually connected to the secondary side of distribution systems. However, secondary circuits are either ignored or modeled with lumped models, causing a source of inaccuracy in the analysis. In addition, before the first amendment of IEEE 1547 standard in 2014, participation of distributed resources was not allowed in voltage regulation, blocking utilization of smart inverter features. High growth rate of PV resources, and fast and frequent fluctuations of irradiance, is becoming a challenge for power system planners and operators. The objective of this dissertation is to systematically tackle this challenge. To do so, three aspects of accurate analysis, accurate modeling, and effective control strategy are investigated.

To address accurate analysis, a comparison between Quasi Steady-State (QSS) and steady-state analysis approaches is performed. Moreover, IEEE 1453-2015, the latest voltage flicker standard, in conjunction with the QSS approach is used. Regarding accurate modeling, realistic models of cloud shadows, mimicking the gradual change in irradiance, are implemented. A cloud motion simulator has been developed to model cloud shadow motion in a more efficient and realistic manner. In addition, detailed secondary circuit models as well as distributed models of large PV systems, instead of point models, are employed. To address effective control strategy, the effectiveness of disturbed VVC schemes is assessed. Furthermore, a comprehensive comparison between various control strategies of smart inverters has been performed in terms of voltage regulation performance.

This dissertation presents new and effective analysis approaches and models to improve the accuracy of solar PV studies. Simulations show that using QSS analysis, new flicker standards, and distributed PV models leads to a significant increase in PV penetration levels. It is also demonstrated that detailed secondary models are essential for precisely detecting locations with voltage issues.

Overcoming Voltage Issues Associated with Integration of Photovoltaic Resources in the Electric Grid

(Kaveh Rahimi)

General Audience Abstract

Power generation from solar energy has significantly increased, and the growth is projected to continue in the foreseeable future. The main challenge of dealing with solar energy is its intermittent nature. The received irradiation energy of the sun on the earth's surface can fluctuate in a matter of seconds and cause voltage issues to power systems. Considering the high growth rate of solar photovoltaic (PV) resources, it is essential to be prepared to encounter and manage their high penetration levels.

Currently, simplified approaches are used to model the impacts of cloud shadows on power systems. Using outdated standards also limits the penetration levels more than required. Approximately 40% of the new PV installations are residential, or installed at a low voltage level. Currently, all components between utility distribution transformers and customers/loads are either ignored or modeled with oversimplification. Furthermore, large PV systems require a considerable amount of land. However, point sensor models are currently used to simulate those systems. With a point model, the irradiance values measured at a point sensor are used to represent the output of a large PV system. However, in reality, clouds cover photovoltaic resources gradually and if the solar arrays are widespread over a large geospatial area, it takes some time for clouds to pass over the solar arrays. Finally, before 2014, participation of small-scale renewable resources was not allowed in controlling voltage. However, they can contribute significantly in voltage regulation. The main objective of this dissertation is to address the abovementioned issues in order to increase the penetration levels as well as precisely identify and locate voltage problems.

A time-series analysis approach is used in modeling cloud motion. Using the time-series approach, changes of the received irradiation energy of the sun due to cloud shadows are simulated realistically with a Cloud Motion Simulator. Moreover, the use of the time-series approach allows implementation of new grid codes and standards, which is not possible using the old step change methods of simulating cloud impacts. Furthermore, all electrical components between utility transformers and customers are modeled to eliminate the inaccuracy due to using oversimplified models. Distributed PV models are also developed and used to represent large photovoltaic systems. In addition, the effectiveness of more distributed voltage control schemes compared to the traditional voltage control configurations is investigated. Inverters connect renewable energy resources to the power grid and they may use different control strategies to control voltage. Different control strategies are also compared with the current practice to investigate voltage control performance under irradiation variations.

This dissertation presents a comprehensive approach to study impacts of solar PV resources. Moreover, simulation results show that by using time-series analysis and new grid codes, as well as employing distributed PV models, penetration of solar PV resources can increase significantly with no unacceptable voltage effects. It is also demonstrated that detailed secondary models are required to accurately identify locations with voltage problems.

To my wonderful parents, my very first teachers,

my beloved sisters,

and the love of my life, my wife.

Acknowledgements

Words cannot express my sincere gratitude to my advisor, Dr. Robert Broadwater for the continuous encouragement and support that I have received from him throughout my PhD program. His character, especially his patience, is exceptional and I will always look up to him as a role model. Moreover, I would like to thank Dr. Broadwater for the engineering principles that he taught me which are very practical to industry.

Besides my advisor, I would like to thank the rest of my committee: Dr. Saifur Rahman, Dr. Steve Southward, Dr. Virgilio Centeno, and Dr. Amos Abbott for serving on my committee, and the invaluable materials that I learned from their classes, and providing me with consistent guidance and support.

I take this opportunity to thank my labmates during these years for the great discussions and the exchange of ideas on almost every topic. I learnt a lot from them, and having them around made the PhD experience more fun.

This long journey would have been impossible without the support of my family. I would like to thank my parents for their endless support and encouragement, not only during my graduate studies, but also during my entire life. Further, I want to thank my beloved sisters who always had my back; and I know that I can always count on them. Last but not the least, I want to thank my lovely wife for helping me in overcoming the hardships of graduate life. She encouraged me when I was doubtful and she was always there for me when I needed her.

Table of Contents

List of Figures

List of Tables

Chapter 1: Introduction and Literature Review

1.1 Renewable energy resources, benefits and challenges

High penetration of Renewable Energy Resources (RERs) is inevitable and is rapidly becoming a reality in many places. Renewable Portfolio Standards (RPSs) in the United States, National Action Plans (NAPs) in Europe, and aggressive plans for very high penetration of RERs all over the world are explicit instances of the drastic shift toward renewable energies.

RERs integration has many benefits such as energy independence and the security factor associated with lower dependency on fossil fuels [1], environmental impacts by decreasing carbon emission [2], [3], increasing resilience of power systems [4], [5], and overall economic benefits [6], [7]. On the other hand, the high growth rates of RERs also introduce new challenges to system planners and operators mainly due to the volatile and intermittent nature of renewable energies such as wind and solar.

Among RERs, solar Photovoltaic (PV) resources had the greatest global growth rate during 2010-2016 [8], [9]. They also had the greatest growth rate in 2016, and the growth of PV resources has been projected to continue into the future. As an example, China has already surpassed its 2020 solar goal of 105 GW installed capacity in 2017. The main challenge of dealing with solar energy is its intermittent nature. Figure 1.1 presents how Global Horizontal Irradiance (GHI) can fluctuate during a day. As shown in Figure 1.1, fast and frequent irradiance fluctuations can occur in a matter of seconds/minutes, which means fluctuations with the same pattern in the generated power and voltage of the point of interconnection. The mentioned fluctuations can cause power quality issues, voltage flicker, over/under-voltages, and reverse power flows [10]-[13]. Another critical

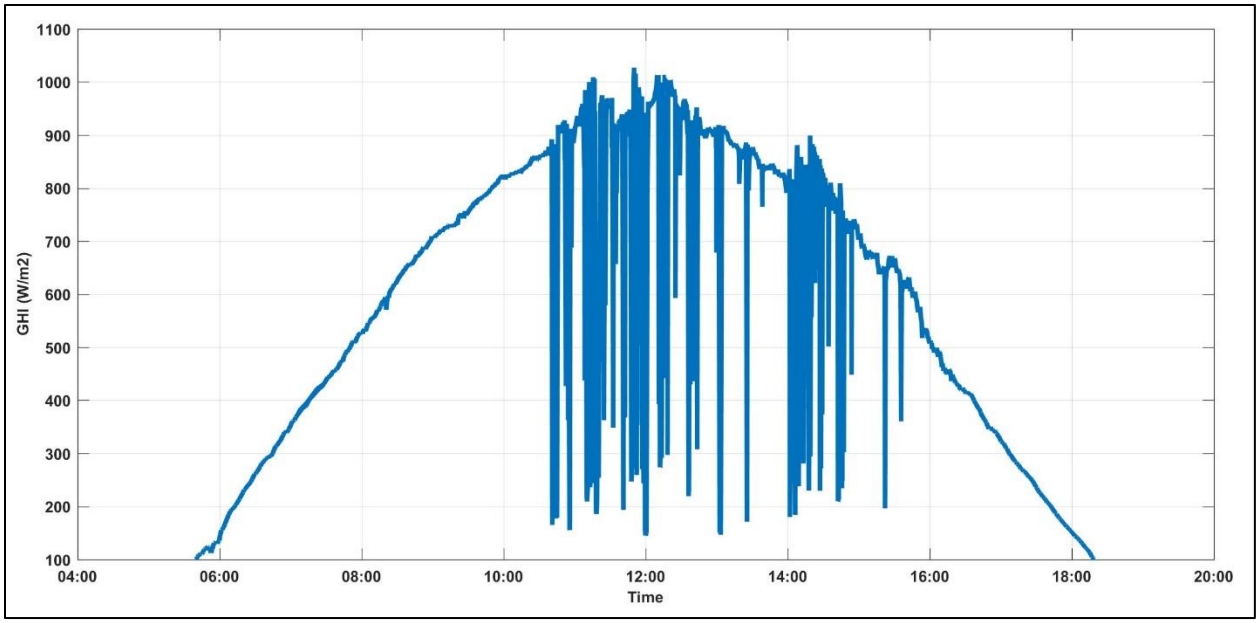

Figure 1.1. An example of how irradiance can fluctuate significantly and frequently during a day

operational challenge is determining how the rapid loss of power can be supplied with conventional power plants, which have low generation ramp rates. However, the scope of this work is mainly on the voltage variations associated with irradiance fluctuations of PV resources.

Output variations of solar PV arrays can be as significant as 80% of their rated capacity [14], and 20% per second in terms of rate of change [15]. On the other hand, delay of conventional Volt-var Control (VVC) devices is usually in the range of 30 to 90 seconds. Therefore, irradiance fluctuations can cause under/over voltages that exist for a considerable amount of time due to the slow-acting controllers. Therefore, accurately identifying locations with voltage issues and finding appropriate mitigation techniques are essential for the systems with high penetration of PV resources.

To mitigate voltage issues induced by PV resources, different solutions have been introduced, such as employing battery storage systems [14]-[18], taking advantage of reactive power control [13], [19]-[22], using combination of active and reactive powers control [23], [24], employing network reconfiguration techniques [25], [26], and using smart inverter functions [27]-[30].

However, there are still many issues and challenges that needed to be addressed. In the following section, some of those issues/challenges are introduced and discussed.

1.2 Flaws and inaccuracies in current analysis approaches

1.2.1 Steady state approach and its flaws

Currently many power analyses are performed using Steady State (SS) models and through power-flow, or load-flow analysis in transmission or distribution domains, respectively. The SS method is being used extensively in power analysis from power market studies to integration of RERs [31]-[39]. However, the SS approach cannot be used efficiently to assess a system whose inputs, load and generation, change frequently over time. A good example is the variations in output of RERs such as PV systems.

To precisely investigate the response of a power system to a sequence of rapid disturbances, a detailed analysis approach is required which can monitor the disturbances and track the following controller reactions with an appropriate time-step. The SS approach simply cannot perform the analysis accurately because it does not have a clear answer for this question: “Which controller will act first in response to a disturbance if the controllers have equal time delays?”

1.2.2 Using flicker curves for flicker studies

Currently to perform voltage flicker studies and identifying flicker issues, flicker curves presented in the IEEE 141-1993 [40] and IEEE 519-1992 [41] standards, also known as GE flicker curves in industry, are used. To perform voltage flicker studies, induced by PV resources, a utility typically uses computer-based circuit models. The PV system in question is placed at the appropriate location in the circuit model and its power output is adjusted to represent how the system will behave when clouds pass over the PV arrays. The resulting changes in voltage are then measured to determine if that location will experience irritating levels of voltage flicker.

The flicker curves were designed for rectangular fluctuations occurring at a constant frequency typically caused by motors, pumps, and furnaces. Therefore, applying those curves to solar energy, which is more random and slower-ramping in nature, can produce overly conservative limitations on PV penetration. Although the flickermeter method employed in the IEEE 1453-2015 standard [42] is the most updated and applicable method of computing flicker severity, its complex implementation and intensive computations have resulted in extensive use of flicker curves in flicker studies as the current practice.

1.2.3 Complexity of current cloud motion simulations

The abovementioned issues in investigating solar PV integration illustrates the necessity of a practical tool, capable of simulating the impacts of cloud shadows on power systems. Many studies have probed cloud cover/shape simulations and their distributions. In [43], computer models which simulate cloud cover, from the simulation of the steady state probability distribution up to the generation of cloud cover, have been developed as a function of time. The authors in [44] have used satellite images to determine cumulus cloud distribution and their characteristics for western Kansas during four months. Research conducted in [45] has concluded synthetic irradiance fields coupled with wind vector information could produce realistic simulations of photovoltaic power generation. In [46], a cloud shadow model that could be used to recreate the power generation of PV systems during days with cumulus clouds has been proposed using fractals. [47] has suggested that forecasting the irradiance and the cell temperature were the best approaches to precisely forecast rapid PV power fluctuations due to the cloud cover. The mentioned studies have focused mainly on simulating the cloud shapes, patterns or distributions rather than the impacts on power systems. Furthermore, some cloud simulation approaches are very sophisticated due to use of complex techniques, making them almost impossible to implement in commercial power

simulators, or require very special input data, such as satellite images. However, in reality what is of utmost importance for power engineers is the impact of cloud shadows, rather than the shape of the clouds. Therefore, there is a need of a practical Cloud Motion Simulator (CMS), meeting the following criteria:

- Can provide a trade-off between accuracy and feasibility of simulation
- Its parameters can be obtained/estimated from publicly available meteorological data

1.2.4 Inaccurate secondary circuit and connection models

While actual distribution feeders have both primary and secondary circuits, the utilities corresponding circuit models typically only contain the primary assets. The models usually exclude the secondary circuits and connections downstream of distribution service transformers, which connect primary circuits to customers at lower voltage levels. In case of modeling a secondary circuit, it is usually simplified into a lumped single equivalent load and generator with the secondary conductors not included. In some cases, even service transformers are also ignored and load and generation are connected directly to the primary system [12], [48]-[52].

By considering large number of components in distribution feeders, adding service transformers, secondary conductors, and service drop conductors can increase the number of components exponentially, which eventually could cause divergence or memory issues in the past due to the large size of the problem [48]. However, with recent technological advancements and the increasing computational power of computers, the mentioned issue can be prevented. Moreover, with the high growth rate of small-scale distributed PV resources, which are often connected to the secondary side of distribution systems, modeling of the secondary circuits has become a necessity to accurately analyze voltage variations of PV resources. It is obvious that

without modeling the circuits to which PV resources are connected, precise analysis of voltage issues is not feasible.

1.2.5 Employing point models while dealing with large PV systems

Currently PV generation is estimated with irradiance point sensor data, regardless of PV system size. However, the irradiance measured at a single point cannot be an accurate representation of the output of a large PV generator, because with large PV systems, covering a considerable geospatial area, the received irradiance is not equal in different panel locations [53]-[55]. A clear example is a large PV system, which is partially covered by a cloud shadow. Some studies have proposed averaging methods and wavelet variability models [56]-[58] to mitigate the inaccuracy introduced by point models, which can over-represent the variability in generation output of PV resources. However, those studies are suffering from inaccuracies mainly from the fact that they cannot simulate cloud shadow motion realistically.

1.2.6 Preventing smart inverters from participating in voltage regulation

Participation of Distribute Resources (DR) in voltage or frequency regulation was not allowed by grid codes or standards in the past. The first version of the IEEE 1547, the IEEE Standard for Interconnecting Distributed Resources with Electric Power Systems [59] issued in 2003, did not authorize the involvement of DRs in voltage regulation. However, due to steady growth of RERs and distributed RERs, and emergence of under/over voltage issues, bi-directional power flows, high-frequency harmonics and grid instability [10]-[13], [60]-[62], participation of DRs was revisited carefully. France and Germany were the first countries to update their grid codes to facilitate integration of RERs [63]. In the US, the state of California also updated its interconnection requirements in terms of allowing reactive power control by Distributed RERs [64]. Finally, in 2014, the first amendment of the IEEE 1547 standard [65] allowed the engagement

of DRs in voltage regulation by controlling real and reactive power. However, there is still a need to examine different control strategies of smart inverters to select the best performing control while dealing with different voltage levels as well as random voltage variants induced by PV resources.

1.3 Addressing the flaws and inaccuracies

In this section, the proposed approach to address the aforementioned flaws and challenges is discussed briefly.

In order to address the issue of the steady state analysis approach to assessing intermittent renewable generation, Quasi Steady State (QSS), or quasi static or time series analysis, is employed [27], [66]-[68]. The significant advantage of the QSS approach over the SS approach is the capability of varying load or generation for specific elements of a power system during a QSS simulation. Therefore, PV systems irradiance fluctuations and consequent voltage variations can be accurately modeled. Moreover, with the QSS approach, the concept of time or sequence can be implemented. Hence, the order in which solar arrays are covered by cloud shadow(s) can be precisely simulated. Finally, the interactions of controllers, and the sequence of their reactions to disturbances, can be modeled more realistically.

To address the issue of the flicker curves, which can lead to overly conservative limitations on PV penetration, the flickermeter method employed in the IEEE 1453-2015 standard is applied to compute flicker severity. Using the QSS approach allows computation of short-term flicker severity (P_{st}), which requires 10 minutes of voltage values/measurements. The QSS analysis approach can perfectly handle the computation of P_{st} values, as it can follow load and generation variations in the mentioned 10-minute window.

As mentioned, a practical cloud motion simulator, which can be used by power engineers without difficulty, would be an extremely useful asset in this industry. In this dissertation, a novel

CMS is developed and introduced. The proposed CMS provides a trade-off between accuracy and practicality with a focus in simulating impacts of cloud shadows on power systems rather than cloud shapes. The CMS incorporates the QSS approach and the IEEE 1453 standard to simulate cloud motion considering six parameters, and also computes the flicker severity. A practical method to estimate the CMS parameters from publicly available meteorological data is also introduced.

To address the inaccuracy caused by ignoring or oversimplification of secondary circuits, detailed secondary circuits of distribution systems, modeling all of the components downstream of service transformers, are developed and added to the corresponding primary circuit models.

Moreover, a new approach of modeling large PV systems is proposed to accurately model voltage variations of such systems. Being equipped with the CMS and distributed models of large PV systems, precise analysis of voltage changes of PV systems and flicker severity can be achieved.

With steady growth of distributed RERs, it seems distributed VVC schemes are more effective in voltage regulation by addressing the issues at their locations. In this dissertation, performance of distributed VVC schemes is investigated. Furthermore, voltage regulation performance of unity power factor control, which is the current practice, is compared with the performance of Volt-var and Volt-Watt control strategies.

1.4 Dissertation objectives

The objective of this dissertation is to introduce more accurate analysis approaches, models, and tools to precisely study impacts of RERs, particularly solar PV resources, on power systems. The ultimate goal is to increase penetration levels of PV resources considerably, while being able to accurately identify locations with problems through:

- Investigating state-of-the-art analysis approaches and proposing more efficient approaches
- Employing more accurate models to eliminate flaws and inaccuracies with current models
- Proposing effective control strategies to deal with the interment nature of solar energy and integration of distributed RERs

1.5 Dissertation organization

Chapter 2: This chapter is devoted to presenting new approaches to increase the accuracy of RERs integration analysis. In this chapter, the SS and QSS analysis approaches are compared to investigate the differences in their results and the causes of those differences. Identifying penetration limits based on flicker curves and flickermeter methods is probed and discussed with multiple case studies. Finally, the proposed CMS is introduced, and how its parameter can be estimated from statistical analysis of meteorological data is discussed.

Chapter 3: This chapter discusses flaws in currently used models, such as ignoring secondary circuits as well as using point sensor models with large PV systems. This chapter also investigates how much using detailed secondary models and appropriate models of large PV systems can change the penetration levels.

Chapter 4: This Chapter studies the effectiveness of distributed VVC schemes in order to perform voltage regulation to achieve energy-saving initiatives, such as Conservation Voltage Reduction (CVR). Chapter 4 also examines and compares different smart inverter functions with the current practice in terms of voltage regulation with two case studies.

Chapter 5: In this chapter, irradiance variations of a PV system due to a cloud shadow are simulated, and their effects on power quality indices, such as Total Harmonic Distortion (THD) and Individual Harmonic Distortion (IHD), are investigated.

Chapter 6: This chapter summarizes the research contributions and provides recommendations for further investigation.

Chapter 2: Accurate Analysis of Photovoltaic Resources

2.1 Introduction and chapter objective

In this section, Steady State (SS) analysis approach, which is extensively used in transmission and distribution domains, is compared with Quasi Steady State (QSS) or quasi static or time series analysis approach using case studies with Volt-var Control (VVC) devices. First, a simple case study is used to demonstrate the differences of employing the SS and QSS approaches and their causes. Then a Cloud Motion Simulator (CMS), along with its parameters, is introduced, which performs the QSS simulations in the rest of this dissertation. A new analysis of estimating the CMS parameters based on the statistical analysis of meteorological data is then presented. The second case study of this chapter, which is a realistic distribution feeder, illustrates the differences of the QSS and SS simulation results and also examines the impact of controller settings such as dead-band or delay on final state of a system.

In the second part of this chapter, the advantages and disadvantages of current flicker standards, such as flicker curves presented in IEEE 141-1993 [40] and IEEE 519-1992 [41], and the flicker method employed in the IEEE 1453-2015 [42], are probed. Furthermore, how the CMS incorporates the QSS approach and computes flicker severity values is discussed. The impacts of the CMS parameters on short-term flicker is then investigated. Finally, a detailed comparison is performed between the flicker curve and flickermeter methods in term of identifying the maximum allowable solar PV penetration.

The main objective of this chapter is to improve the accuracy of current PV integration analysis through applying the CMS, which takes advantage of QSS simulations, and the flickermeter method.

2.2 QSS approach versus SS approach

In this section, how the SS step-change approach is applied to simulate cloud covering of solar arrays is discussed. Currently, to study impacts of cloud shadows and a decrease/increase in the outputs of the solar arrays of a PV system, only two states are considered. The initial state, in which it is assumed that there is no cloud shadow on solar arrays, and the final state in which cloud shadow covers all of the solar arrays. If uncovering of solar arrays needs to be simulated, the same approach will be used, but the initial and final states will be replaced. In addition, in practice the received irradiance will change continuously and gradually if a cloud shadow covers a PV system, but with the SS approach, irradiance or output of PV systems discretely jumps from the initial state level to the final state level. Another unrealistic assumption with the SS step-change approach is that a cloud shadow hits all of the solar arrays distributed over a geographical area all at once. Obviously this is not the case with large PV systems, spanning over multiple acres of land. As a result, there is no difference in the direction of cloud motion, and the sequence that the cloud shadow hits the solar arrays in the SS approach. Volt-var controllers in the field have time delays. Using the SS approach, cloud speed also cannot be considered in the analysis, but in reality, duration of a disturbance and delays of controllers can make a notable difference. For example, if a small cloud covers a PV system and causes a short-term voltage decrease, and if delays of VVC devices are long-enough so that the cloud passes over the system before the controller delays end, there will be either no control actions or control actions, which may cause over-voltages based on the controller logic. However, the SS approach is not capable of analyzing those situations.

Quasi steady state analysis approach with a proper time-step can address the aforementioned flaws of the SS approach. In a QSS simulation, inputs, load and generation in case of a power system, can vary over time steps for desired components. Therefore, outputs of solar arrays can be

adjusted during a QSS simulation based on realistic curves, mimicking the fluctuations of PV systems in reality. Being able to implement the concept of time/sequence in a QSS simulation allows simulation of cloud shadow motion, by defining the cloud shadow speed and motion direction. As a result, the order a cloud shadow, or a set of cloud shadows, covers PV arrays spread over a geographical area can be determined and simulated. Obviously, all solar arrays are not affected at the same time and controllers act in the right order, leading to more realistic results. In the next section, a case study is used to illustrate the impacts of a disturbances sequence and non-linear controllers on the final state of a system, emphasizing the importance of the QSS analysis to achieve accurate results.

2.2.1 Importance of disturbances sequence in a system with non-linear controllers

A simple case study, shown in Figure 2.1, is used to illustrate how the sequence of disturbances can lead to different final states, even when the initial and final load and generation are equal. Two cloud motion directions of East-to-West and North-to-South are considered in scenarios 1 and

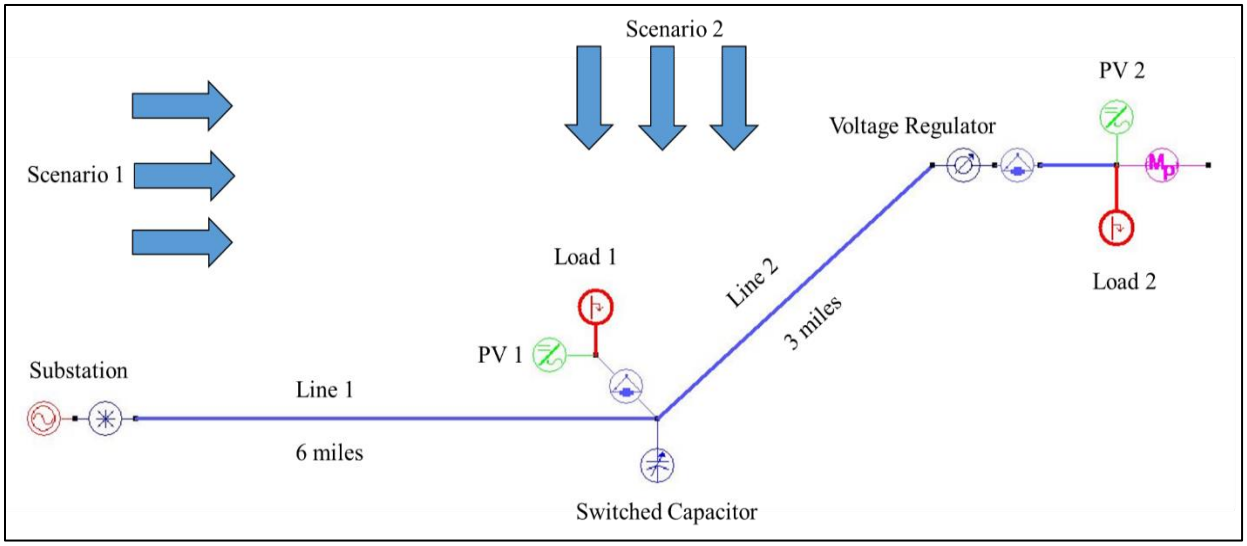

Figure 2.1. Case study to illustrate the importance of the QSS analysis to achieve accurate results.

2, respectively. It is assumed that the cloud shadow is large enough to cover both PV systems ultimately in both scenarios. Moreover, covering the PV systems decreases their outputs from 75 kW to 15 kW, simulating an 80% decrease in their delivered real power. The inverters are working under unity power factor. The set-point of the controllers is 120V and their dead-band is 2 V. Therefore, as long as the voltage is between 119 and 121 V, they are not expected to respond to voltage variations. In the following, every state between initial and final states is briefly discussed for both scenarios.

Scenario 1: A cloud shadow, with East-to-West direction, covers both PV systems eventually.

State 1 (initial state): No cloud cover. Both PV units generate 75 kW.

State 2: PV 1 is covered by the cloud, and its generation goes down from 75 kW to 15 kW. PV 2 is still generating 75 kW. The voltage of load 1 goes below 119 V, therefore, the switched capacitor should respond to the voltage decrease. The voltage of load 2 is still in the dead-band. Therefore, the voltage regulator is not supposed to function.

State 3: The switched capacitor operates, and returns the voltage of load 1 to the range of 119-121 V. However, now the voltage of load 2 is more than 121 V. Therefore, the voltage regulator is expected to react to the out of band voltage.

State 4: The voltage regulator operates, and returns the voltage of load 2 into the range of 119-121 V.

State 5: The cloud covers PV 2, and its generation goes down from 75 kW to 15 kW. The voltage of load 2 decreases but it is still in the range of 119-121 V.

State 6 (final state): Both PV systems generate 15 kW and both controllers are not supposed to operate because the voltages of load 1 and 2 are not out of band.

Scenario 2: A cloud shadow, with North-to-South direction, covers both PV systems eventually.

State 1 (initial state): No cloud cover. Both PV units generate 75 kW.

State 2: Due to the motion direction, this time PV 2 is first covered by the cloud, and its generation goes down from 75 kW to 15 kW. PV 1 is still generating 75 kW. The voltage of load 2 goes below 119 V. Hence, the voltage regulator should respond to the voltage decrease. The voltage of load 1 is still in the dead-band. Therefore, the switched cap is not supposed to function.

State 3: The voltage regulator operates, and returns the voltage of load 2 to the range of 119-121 V. The voltage of load 1 is still in the band.

Step 4: The cloud also covers PV 1. Therefore, its generation goes down from 75 kW to 15 kW. The voltage of load 1 goes below 119. Thereafter, the switched capacitor is supposed to function.

Step 5: The switched capacitor operates and returns the voltage of load 1 to the range of 119-121 V. However, by turning on the switched capacitor, the voltage of load 2 goes above 121V. Hence, the voltage regulator is expected to function to decrease the voltage of load 2.

Step 6: The Voltage regulator operates and returns the voltage of load 2 to the band.

State 7: (final state): both PV systems generate 15 kW and both controllers are not supposed to operate because the voltages of load 1 and 2 are not out of band.

Table 2.1 summarizes the discussed states of scenarios 1 and 2. It also shows the switch capacitor's on-or-off state as well as the tap number of the voltage regulator.

Table 2.1. Summary of all states occurring in scenarios 1 and 2, controller actions and their status/setting.

Scenario	State	Cloud Coverage	Controllers Actions	PV1 (kW)	PV2 (kW)	Laod1 Voltage (V)	Laod2 Voltage (V)	Switched Cap On or Off	Voltage Regulator Tap
1	1 (Initial state)	No Cloud Cover	Controllers Standby, no Action Needed	75	75	119.36	119.63	0	1
1	2	Cloud Covers PV1	Both Controllers Frozen	15	75	118.46	119.32	0	1
1	3	Cloud Covers PV1	Switched Cap Operates	15	75	120.51	121.37	1	0
1	4	Cloud Covers PV1	Voltage Regulator Operates	15	75	120.52	120.62	1	0
1	5	Cloud also Covers PV2	Both Controllers Frozen	15	15	120.19	119.61	1	0
1	6 (Final State)	Cloud also Covers PV2	Controllers Standby, no Action Needed	15	15	120.19	119.61	1	0
2	1 (Initial state)	No Cloud Cover	Controllers Standby, no Action Needed	75	75	119.36	119.63	0	1
2	2	Cloud Covers PV2	Both Controllers Frozen	75	15	119.04	118.6206293	0	1
2	3	Cloud Covers PV2	Voltage Regulator Operates	75	15	119.0374388	119.3587668	0	2
2	4	Cloud also Covers PV1	Both Controllers Frozen	15	15	118.1384987	119.0395273	0	2
2	5	Cloud also Covers PV1	Switched Cap Operates	15	15	120.1858659	121.1121733	1	2
2	6	Cloud also Covers PV1	Voltage Regulator Operates	15	15	120.19	120.36	1	1
2	7 (Final State)	Cloud also Covers PV2	Controllers Standby, no Action Needed	15	15	120.19	120.36	1	1

Table 2.1 shows that the final states in scenarios 1 and 2 are different, and the difference is due to the sequence of the controller actions as a response to the sequence of system disturbances. That is why utilization of the QSS analysis approach is of importance. It can respond to a sequence of disturbances as they occur, which provides realistic results. Note that the final voltages of loads 1 and 2 are different, but in the dead-band of the controllers. Realizing the importance of the QSS simulations to achieve accurate results, in the next section a cloud motion simulator is introduced and discussed, which is designed to perform QSS simulations to probe the impacts of cloud shadows on power systems.

2.3 Could motion simulator

In this section, the cloud motion simulator, which applies the QSS approach and simulates cloud motion, is introduced. Furthermore, the CMS parameters, and their estimation based on meteorological data, are discussed. In addition, the CMS is used to carry out a comparison between the QSS and SS analysis approaches with a realistic distribution feeder as the case study. Impacts of controller settings are also examined through various scenarios.

A portion of [69] is re-formatted and reused in this section. The first author of [69] is the author of this dissertation and the reuse is in compliance with IEEE policy at the time of writing this dissertation. The policy can be found in the appendix. Note that IEEE holds the copyright of [69], whose citation is provided in the bibliography.

2.3.1 Cloud motion simulator and its parameters

Clouds may have different and varying shapes. Some studies have considered clouds to have rigid shapes/patterns, such as circular or rectangular shapes [44], [67], [70], [71]. Some studies have proposed cloud shape simulation using more sophisticated shapes, such as fractals [44], [46], [72]. In this work, rectangular shapes are used for cloud motion simulations due to the ease of implementation. Rectangular shapes also help to estimate the widths of the clouds, which will be explored later in this section. As discussed before, the focus of previous studies has mainly been on simulating the cloud patterns, shapes or distributions rather than the impacts on power systems. Furthermore, some cloud simulation techniques are very complex and require a meteorology background, making them almost impossible to implement in commercial power simulators, or require very special input data, such as satellite images. The CMS in this dissertation can be used by engineers without being puzzled by the complex methodologies involved with obtaining precise meteorological data for clouds.

To achieve a trade-off between being comprehensive and the feasibility of the simulation, the parameters shown in Table 2.1 are selected for the CMS. Regarding parameter 6 in Table 2.1, when a cloud shadow covers or uncovers a PV generator, the generation does not instantaneously step down or up, but changes according to the piecewise linear curve, referred to later as a decay curve, specified in parameter 6 [73] as shown in Figure 2.2. Figure 2.2 also demonstrates the difference of the QSS approach, employed by the CMS, with the step-change SS approach in

Table 2.2. Cloud motion simulator parameters [69].

Parameter	Parameter Description
P_1	Number of cloud(s)
P_2	Direction of cloud motion
P_3	Speed of cloud(s)
P_4	Time interval between two successive clouds
P_5	Width of cloud(s)
P_6	Points for a curve specifying percent rate of change of PV generation as a cloud shadow either covers or uncovers a PV generator [73]

modeling the impacts of cloud shadows. In addition, decay and recovery curves and coverage time are illustrated in Figure 2.2.

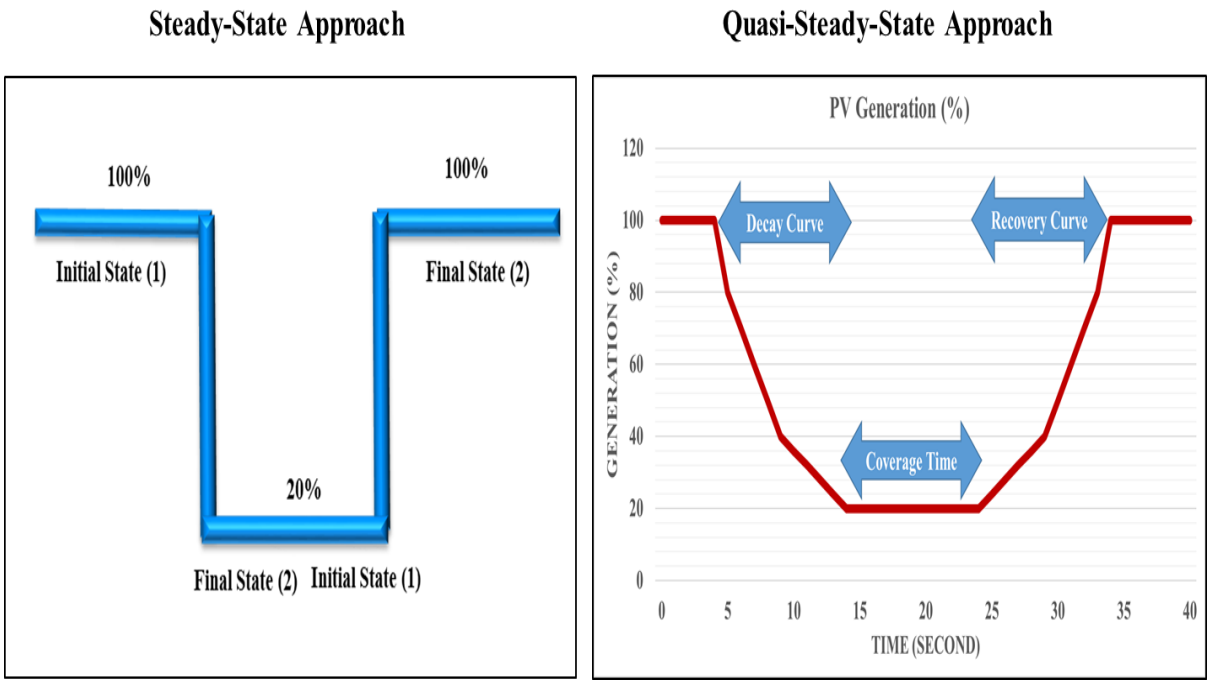

Figure 2.2. The difference between generation level changes in the QSS and step-change SS approaches.

Figure 2.3 presents the mentioned CMS parameters, when three clouds pass over a distribution network. How generation is adjusted based on the decay curve is also illustrated in Figure 2.3, using different shadings, where no shading represents 100% generation, and the darkest shading represents 20% generation. How the output of the PV generator goes back to the initial level is

based on the reverse of the decay, here called the recovery curve, shown in Figure 2.3. Note that decay and recovery curves are user specified and can be used to take into account parameters not considered in the CMS, such as cloud altitude, thickness/density, and type of clouds.

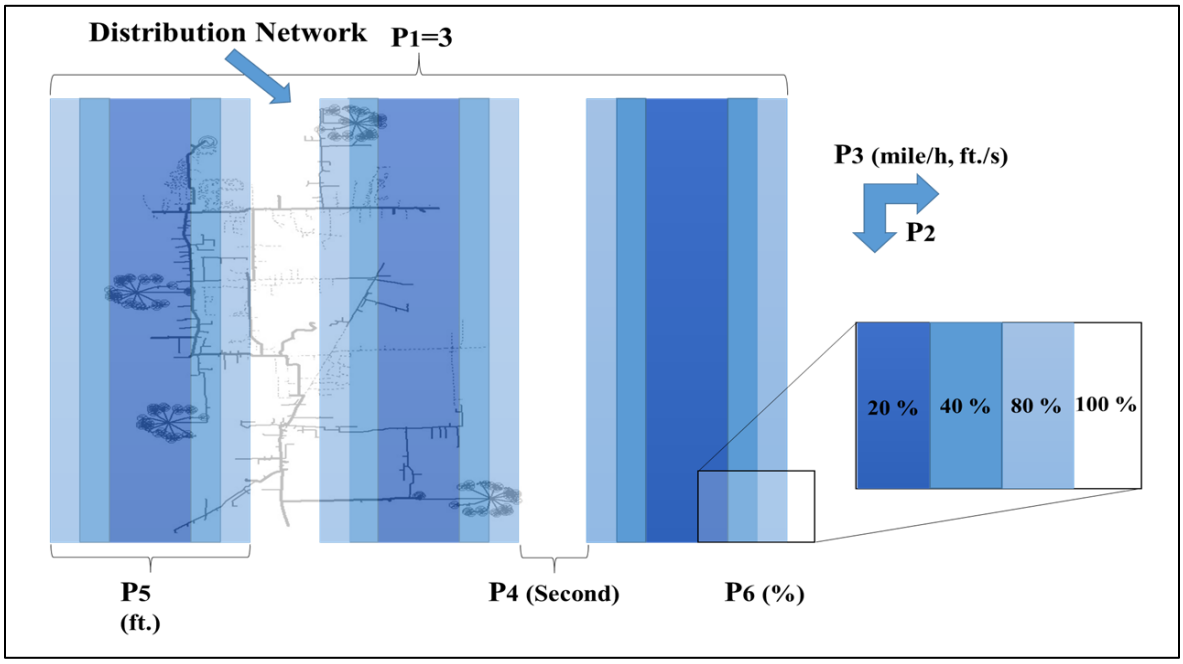

Figure 2.3. Illustration of Cloud Motion Simulator parameters P1-P6 [69]. © 2018 IEEE

The CMS uses the QSS approach, where the simulation step size is selected to be one second. That is, a power-flow calculation is performed every second, computing the varying voltages and currents as a result of the altering PV generation. Smart inverters can reach steady state in matter of cycles. Therefore, the step size of one second allows all transients to decay prior to the next QSS analysis time point.

At each second of the simulation, the PV inverters, which cloud shadows cover, are detected, and their outputs are updated based on decay and recovery curves. The analysis is performed by considering the (X,Y) coordinates of the PV generators as well as the (X,Y) coordinates of the simulated cloud shadows, which vary over the simulation time. Thus, at each second of the simulation, the CMS identifies the affected PV inverters and adjusts their output power

accordingly. Figure 2.4 presents how coordinates of each edge of a cloud change over simulation time.

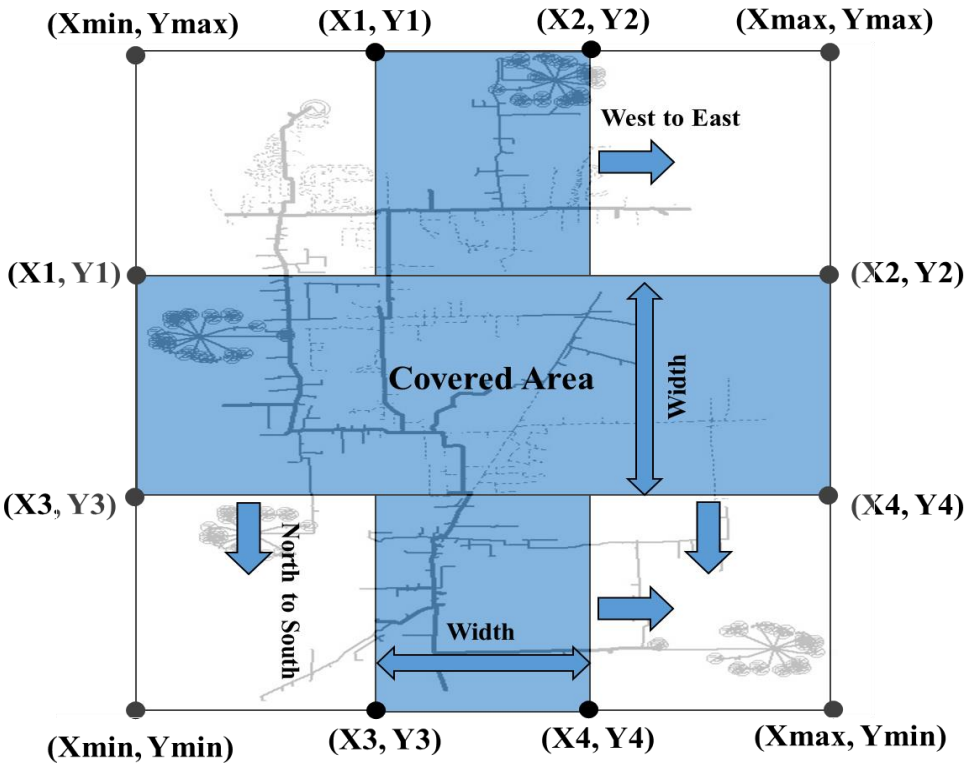

Figure 2.4. Coordinates of edges of clouds while considering two motion directions, West-to-East and North-to-South [69]. © 2018 IEEE

Coordinates of the four edges will be computed by equations (2.1)-(2.8), when the motion direction is West-to-East. Note that for simplicity it is assumed that the coordinates are presented in length units.

$$X_1 = X_{min} + V * T - W \quad (2.1)$$

$$Y_1 = Y_{max} \quad (2.2)$$

$$X_2 = X_{min} + V * T \quad (2.3)$$

$$Y_2 = Y_{max} \quad (2.4)$$

$$X_3 = X_{min} + V * T - W \quad (2.5)$$

$$Y_3 = Y_{min} \quad (2.6)$$

$$X_4 = X_{min} + V * T \quad (2.7)$$

$$Y_4 = Y_{min} \quad (2.8)$$

Similarly, the coordinates can be calculated by (2.9)-(2.16) when the motion direction is North-to-South.

$$X_1 = X_{min} \quad (2.9)$$

$$Y_1 = Y_{max} - V * T - W \quad (2.10)$$

$$X_2 = X_{max} \quad (2.11)$$

$$Y_2 = Y_{max} - V * T - W \quad (2.12)$$

$$X_3 = X_{min} \quad (2.13)$$

$$Y_3 = Y_{max} - V * T \quad (2.14)$$

$$X_4 = X_{max} \quad (2.15)$$

$$Y_4 = Y_{max} - V * T \quad (2.16)$$

where

T: Simulation time

V: Cloud speed

W: Cloud Width

X_{max}: Maximum X coordinate of all components

X_{min}: Minimum X coordinate of all components

Y_{max}: Maximum Y coordinate of all components

Y_{min}: Minimum Y coordinate of all components

(X,Y) coordinates of PV generators are known. Moreover, in each time-step the area covered by clouds, through computing edges coordinates, is calculated. Therefore, if the coordinates of PV generators fall into the calculated area, their outputs are adjusted based on the decay/recovery curve. Figure 2.5 demonstrates the flowchart of the algorithm, which takes into account X1-X4 and Y1-Y4 values as well as (X,Y) coordinates of PV generators and updates their outputs in each time-step according to decay/recovery curve.

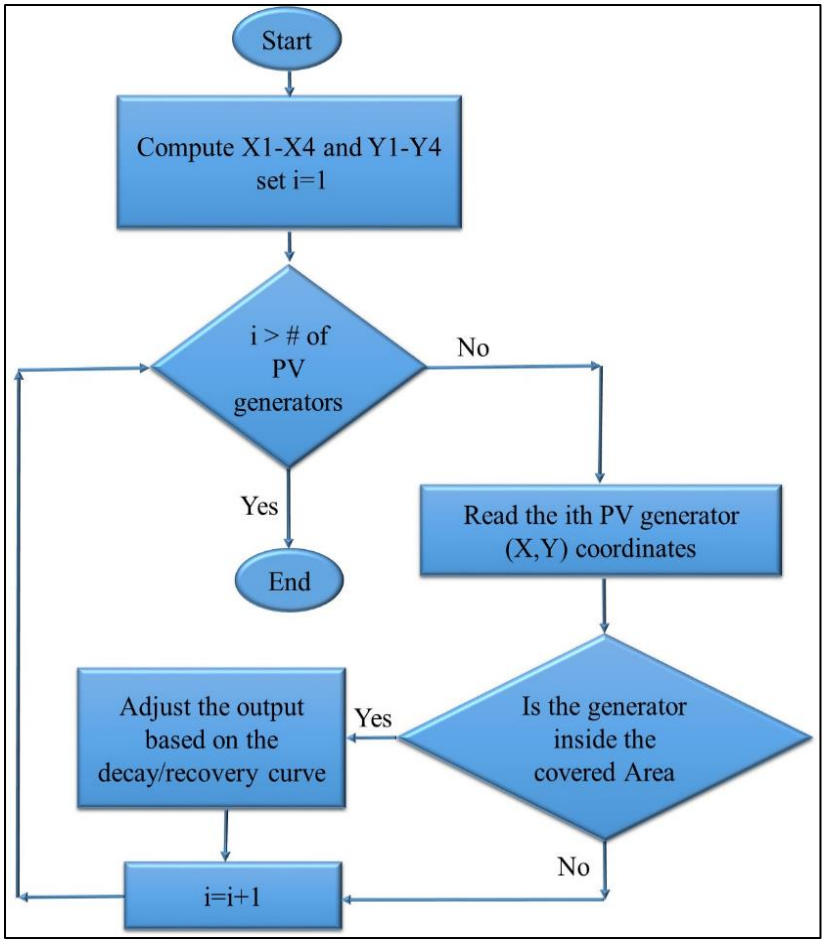

Figure 2.5. Flowchart of the algorithm used to detect impacted PV generators and to adjust their outputs [69]. © 2018 IEEE

2.3.2 Parameters determination

This section provides insight into how the CMS parameters can be estimated from statistical analysis of publicly available meteorological data. This is an advantage of the proposed CMS over other simulation methods that require special input data, such as satellite images. If only evaluating worst-case scenarios, such as a drastic irradiance changes or full coverage by a large cloud shadow is the objective, some of the CMS parameters can be selected according to the objectives. Although engineering studies of large PV installations would tend to use statistical parameters that would have the largest effect on voltages, the proposed method can also provide insight into the use of statistical parameters that mimic the most probable scenarios. Note that results of the analysis are

time-and-location dependent, but the procedure is the same for different locations. For many locations, average wind speed, wind gust speed, and wind direction can be obtained through public sources, such as the US National Weather Service (NWS).

One-second measurements of the Global Horizontal Irradiance (GHI), obtained from a pyranometer, and wind speed values are utilized to calculate cloud statistics. The employed data was recorded in 2013 at a location in the state of New York. The months that showed the greatest and most frequent variations in GHI values at this location were January, April, July, and October, and the GHI data from those months was selected for analysis. Irradiance percentage change and its rate of change, number of clouds, and time interval between two successive clouds, can be extracted from GHI measurements, as presented in Figure 2.6.

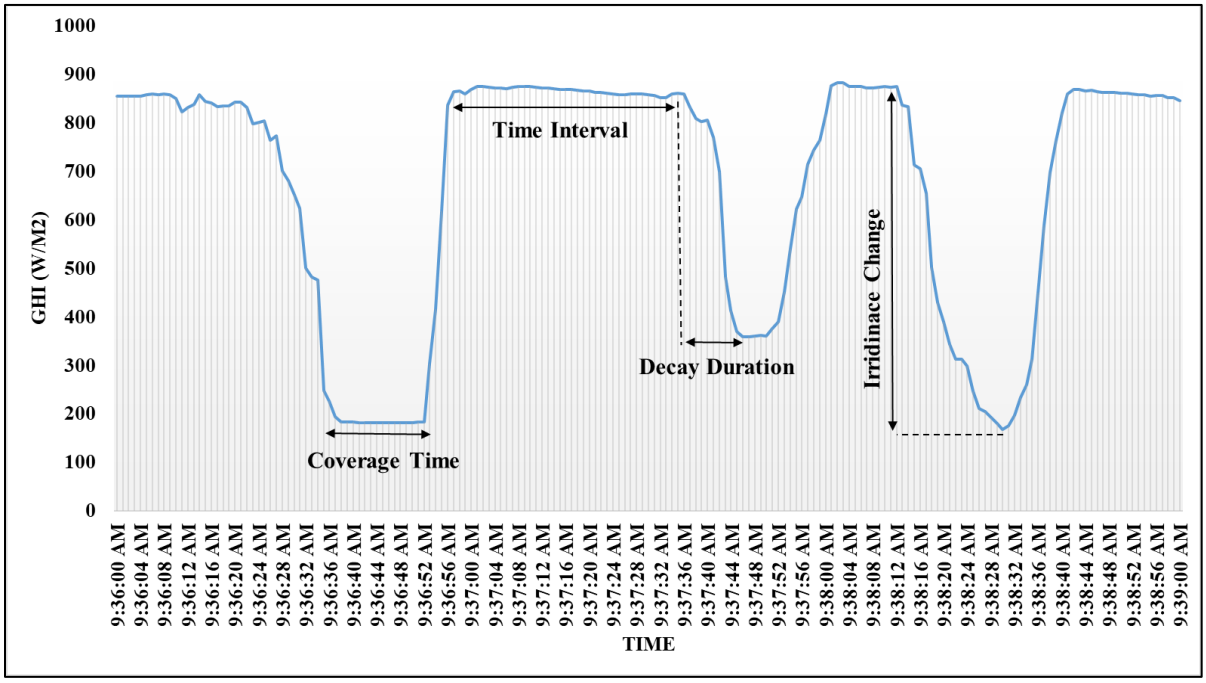

Figure 2.6. Illustrating use of irradiance values, changes in GHI values and their rate change values to calculate the CMS parameters [69]. © 2018 IEEE

From Figure 2.6, it can be interpreted that three clouds have passed over the pyranometer, and that the received irradiance dropped from 880 W/m^2 to the neighborhood of 200 W/m^2 in two cases

and dropped approximately to 350 W/m^2 in another case. Coverage time values are approximately 0, 8, and 20 seconds, and the time interval between clouds varies from about 8 to 20 seconds.

To calculate the statistical values, different bins are defined for each parameter based on the required accuracy or resolution of the data. By counting the number of values in each bin, and then dividing by the total number of values over all bins, the Probability Density Functions (PDF) of the parameters can be formed. The Cumulative Density Functions (CDF) for each parameter may then be computed, as illustrated in Figure 2.7. From the CDF, valuable information can be obtained. For example, Figure 2.7 shows that for 96 % of the time, the percentage irradiance variation is less than 80 %.

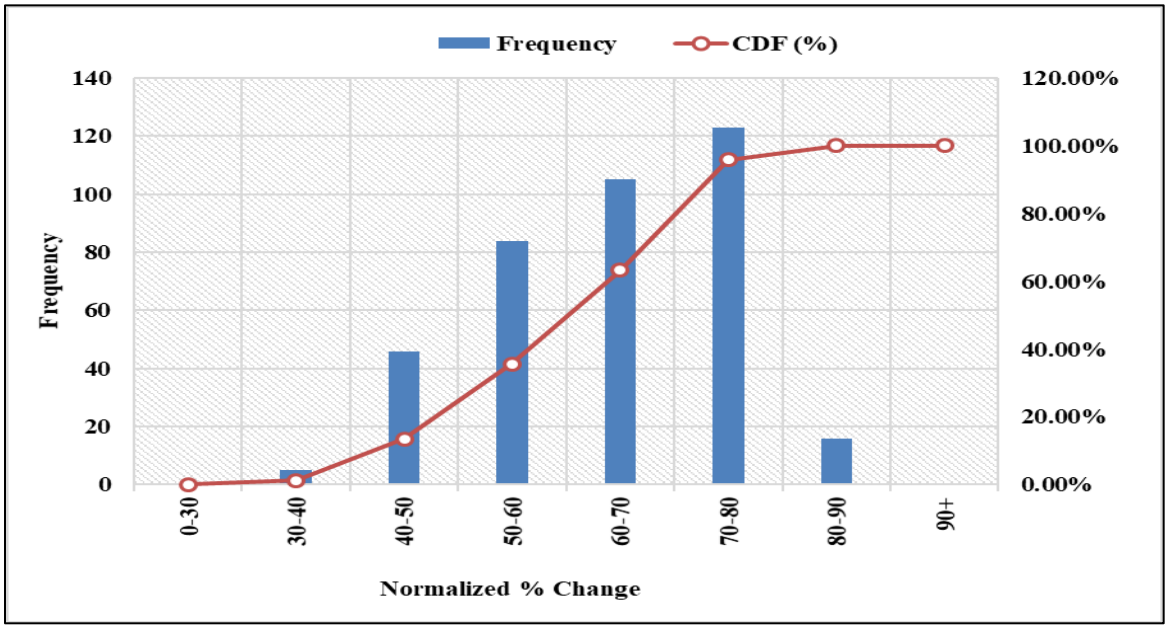

Figure 2.7. Results of statistical analysis of irradiance percentage changes [69]. © 2018 IEEE

To estimate cloud width, average wind speed plus cloud coverage times can be used. Width of the clouds can be estimated by multiplying the average wind speed by the coverage time. Average wind speeds can also be used for the cloud speed estimation. Similar PDFs and CDFs can be

formed for other parameters in the same manner, and engineers can use desired parameters based on the application, such as the most probable case or the worst-case scenario.

2.3.3 Effect of controller setting on voltage analysis

A common perception between power engineers is that the QSS and SS analysis approaches provide the same results if initial and final inputs of a system are the same, even in the existence of Volt-var controllers. The case study of section 2.2.1 showed the falsehood of this assumption with a simple example, and this section takes advantage of the CMS and uses a more realistic case study. Moreover, effects of dead-band and time-delay of controllers, as well as cloud motion speed and direction, on voltage changes computed by the SS and QSS approaches are investigated through various scenarios.

Methodology

The greatest voltage changes and their corresponding locations are of interest to detect voltage issues, as well as to select appropriate mitigation approaches. To compute and compare voltage changes coming from the SS and QSS simulations, the following procedure is used. With the SS analysis, two steady state simulations are performed. First, all PV generators are assumed to be at rated output, simulating the case with no cloud cover, and power flow analysis is performed. Then all PV generator outputs are set to a lower level, corresponding to the final generation level reached in the QSS simulations described below, simulating the condition with cloud cover over the whole feeder, and power flow analysis is again performed. In this study, a 65% reduction in PV generation is used for the final states of the SS and QSS simulations. The 65% reduction in PV generation is sufficient to cause controller actions. At all load buses, the voltage differences between the two SS simulations are then calculated. Next, the locations with the greatest voltage changes are identified. Figure 2.8 illustrates the SS analysis process.

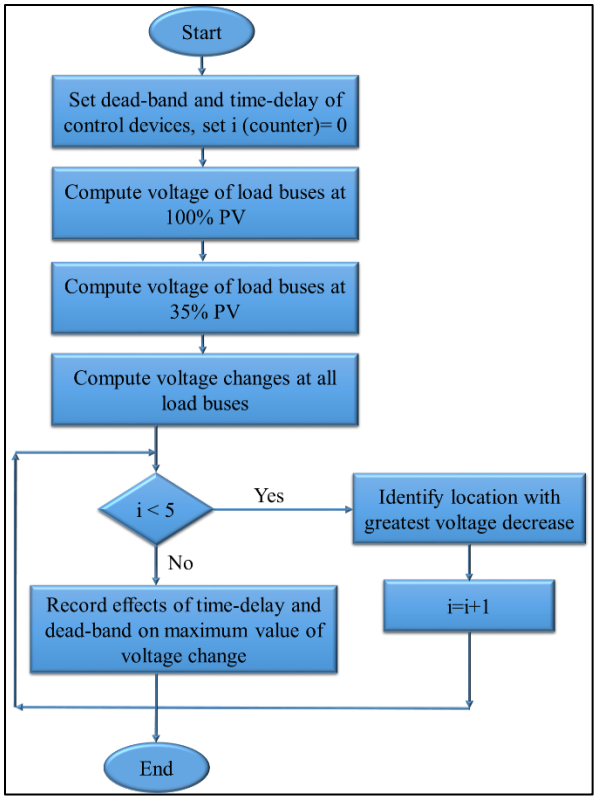

Figure 2.8. Steady state (SS) analysis process.

With the QSS approach, power flows are performed on a second-by-second basis. Thus, with the QSS simulations, one-second voltage changes for all load buses are calculated. Also, similar to the SS simulations, the locations with the greatest one-second voltage change, either increase or decrease, are identified. In the remainder of the paper, the phrase "***QSS voltage change***" refers to one-second voltage change, and the phrase "***final QSS voltage change***" refers to the final state of the voltage minus its initial state computed by the QSS simulations. High QSS voltage changes can be a good indicator of flicker issues. A comparison of the results between the SS and QSS approaches is performed, where the comparison evaluates the highest voltage changes and the corresponding locations. With the QSS simulations the effects of controller settings, such as time-delays and dead-bands, as well as cloud motion direction and cloud speed, are studied through 16 scenarios. Due to the gradual change in output of PV generators with the QSS approach, and the

fact that not all of the PV generators are affected at the same time, it is expected that the SS approach provides more conservative results than the QSS approach. Figure 2.9 illustrates the QSS analysis process.

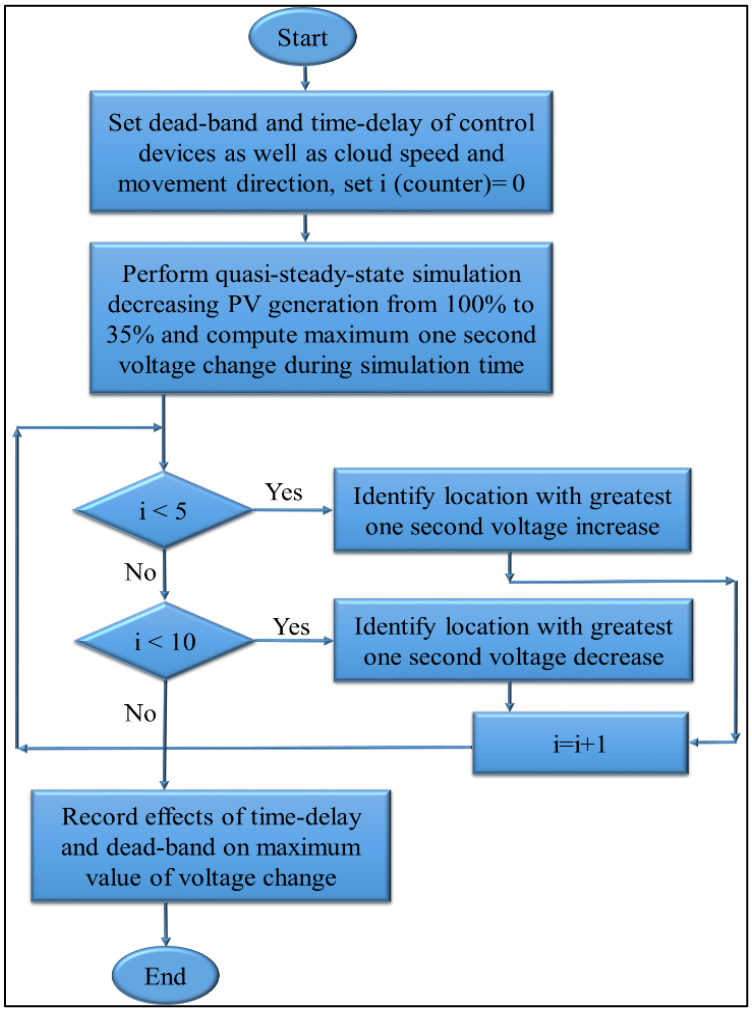

Figure 2.9. Quasi Steady state (QSS) analysis process.

Case study and scenarios

A distribution feeder with two voltage levels, 13.2 and 4.8 kV, is used in the case study. The feeder circuit model is shown in Figure 2.9. The black colored lines are the 4.8 kV sections, while the 13.2 kV sections are displaced in red. The feeder contains 1100 loads, 116 PV generators (all connected to the 4.8 kV sections), 7 tap-changers, and 3 switched shunt capacitors. The umbrella-

like shapes in Figure 2.10 are where PV generators are located. The simulations are performed at noon when the solar irradiance is maximum. The rated kVA range of the PV generators varies from 5 to 16 kVA. The total real power measured at the substation is 7354 kW (with no PV injection). The total output of the PV generators is 1004 kW at 100% generation, and PV generators operate at unity power factor.

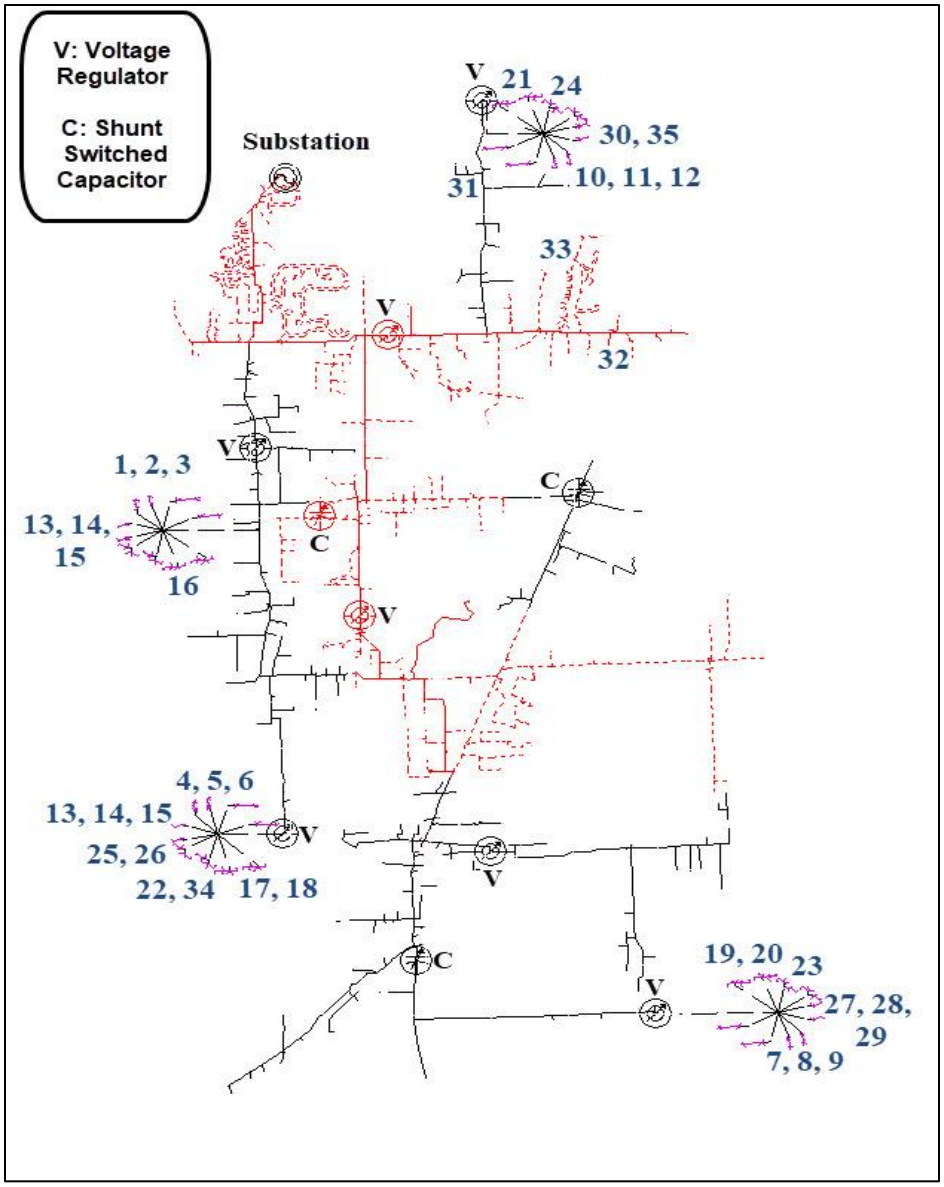

Figure 2.10. Realistic distribution feeder and locations of its Volt-var control devices.

Discrete models are used to model tap-changer voltage regulators and switched capacitors [74], [75]. The tap movements of tap-changers are modeled by:

$$n(k) = n(k-1) - mf(\Delta V) \quad (1)$$

$$\Delta V = V - V_{Ref} \quad (2)$$

Where

n(k): tap ratio in the kth time step
ΔV: Voltage Error
V_{Ref}: Reference Voltage
m: Tap Step Size
Denoting the dead-band as ± ε, $f(\Delta V)$ is given by:

$$f(\Delta V) = \begin{cases} 1 & if \Delta V > \varepsilon \; for \; t_d \\ -1 & if \Delta V < -\varepsilon \; for \; t_d \\ 0 & otherwise \end{cases} \quad (3)$$

where

t_d : Time delay of controller

Three situations are possible for switched capacitors, turning on, turning off, or keeping the previous state.

Sixteen scenarios are used to investigate the effect of controller settings, cloud shadow speed and motion direction. In each scenario only one parameter is changed to monitor its effect. Table 2.3 presents the scenarios. In each scenario results of the QSS simulations computed by the CMS are compared with the SS results, and the effect of controller dead-band and time-delay on the simulation results is probed.

Table 2.3. Cloud speed and motion direction and controller settings of the scenarios.

Scenario	Cloud Shadow Speed (m/s)	Controller Dead-Band (V)	Controller Delay (s)	Cloud Shadow Movement Direction
1	16	2	30	West to East
2	8	2	30	West to East
3	16	3	30	West to East
4	8	3	30	West to East
5	16	2	45	West to East
6	8	2	45	West to East
7	16	Frozen	Frozen	West to East
8	8	Frozen	Frozen	West to East
9	16	2	30	North to South
10	8	2	30	North to South
11	16	3	30	North to South
12	8	3	30	North to South
13	16	2	45	North to South
14	8	2	45	North to South
15	16	Frozen	Frozen	North to South
16	8	Frozen	Frozen	North to South

Two cloud shadow speeds, 8 and 16 m/s (corresponding to 18 and 36 miles per hour, respectively) are used to evaluate the effects of cloud speed on the QSS voltage changes. 16 m/s, which is a fast cloud shadow speed [76], is selected to provide a high rate of change of PV generator output. Two directions of motion, West-to-East and North-to-South, are also considered to study impacts of cloud motion direction on the QSS voltage changes, as well as control responses. In the QSS simulations the cloud takes approximately 7 minutes to entirely cover the feeder when it moves from the West to the East and the cloud speed is 16 m/s, and twice the time, 14 minutes, when the cloud speed is 8 m/s. While moving in the North-South direction the cloud takes about 10 minutes to entirely cover the feeder when moving at 16 m/s, and approximately 20 minutes when moving at the speed of 8 m/s.

Time delays of 30 and 45 seconds and dead-bands of 2V and 3V are considered to assess the impact of controller settings on the QSS and total voltage changes. In four scenarios controllers are intentionally frozen to study the effects of control devices by comparing computed voltage

changes with the scenarios where controllers are allowed to act, as well as to validate the results of the QSS approach with the SS approach. That is, when controllers are frozen, the QSS and SS approaches should provide the same results.

Based on the direction of cloud motion, two sets of scenarios are performed, where each set includes eight scenarios. For each scenario the five locations with the greatest voltage change computed by the SS simulations are identified. With the QSS simulations the five locations with the greatest voltage increase and the five locations with the greatest voltage decrease are identified, totaling ten locations for each QSS scenario. All locations identified by both SS and QSS simulations are illustrated in Figure 2.10. The detailed results of the SS and QSS simulations are presented in Tables 2.4-2.7. Note that in this analysis the cloud length is selected long enough so that it can cover the entire feeder, mimicking the final state of the SS approach.

When the QSS voltage change is negative for a location, it means that the interaction of the PV generation loss and the controller actions resulted in a voltage decrease. If the QSS voltage change is positive, it means the result of the interaction caused a voltage increase. Note that for the five locations identified by the SS simulations all voltage changes (Voltage at 100% PV-Voltage at 35% PV) are negative, which means a voltage decrease resulted from the loss of generation. Figure 2.11 provides a description for the quantities presented in Tables 2.4-2.7. Observations from all of the scenarios are summarized in the tables, but only results from the first scenario are discussed in detail. Note that in each scenario results from QSS simulations, greatest voltage changes and their locations, computed by the CMS, are compared with results from the SS simulations.

Table 2.4. Results for scenarios 1-8 for West-to-East cloud motion. Five customer load locations with the greatest SS voltage change, their corresponding maximum QSS voltage change, and final QSS voltage change.

Scenario	Location	Phase	SS Voltage Change (V)	SS Voltage Change (%)	Maximum QSS Voltage Change (V)	Time of Maximum QSS Voltage Change	Difference of SS Voltage Change and Max QSS Voltage Change (V)	Final QSS Voltage Change (V)	Final QSS Voltage Change (%)	Difference of SS Voltage Change and Final QSS Voltage Change (V)
1	1	AC	-6.2373	-4.90%	-1.1104	12:00:14 PM	5.1269	-5.4633	-4.29%	0.7740
	3	AC	-5.9365	-4.67%	-0.9791	12:00:14 PM	4.9574	-5.1633	-4.06%	0.7732
	2	AC	-5.9006	-4.65%	-0.9725	12:00:14 PM	4.9281	-5.1265	-4.04%	0.7741
	10	AB	-5.6431	-4.48%	-1.1181	12:04:16 PM	4.5250	-6.3832	-5.07%	0.7401
	12	AB	-5.4444	-4.35%	-1.1267	12:04:16 PM	4.3177	-6.1834	-4.94%	0.7389
2	1	AC	-6.2373	-4.90%	-0.7198	12:00:27 PM	5.5174	-5.4633	-4.29%	0.7740
	3	AC	-5.9365	-4.67%	-0.7001	12:00:24 PM	5.2364	-5.1633	-4.06%	0.7732
	2	AC	-5.9006	-4.65%	-0.7598	12:00:24 PM	5.1408	-5.1265	-4.04%	0.7741
	10	AB	-5.6431	-4.48%	0.7752	12:08:32 PM	4.8679	-6.3832	-5.07%	0.7401
	12	AB	-5.4444	-4.33%	-0.8389	12:08:32 PM	4.6055	-6.1834	-4.91%	0.7389
3	7	BC	-6.4708	-5.16%	-1.0823	12:06:27 PM	5.3885	-5.8811	-4.69%	0.5896
	9	BC	-6.1658	-4.93%	-1.1132	12:06:27 PM	5.0526	-5.5760	-4.45%	0.5898
	8	BC	-6.1296	-4.90%	-1.0561	12:06:27 PM	5.0735	-5.5392	-4.43%	0.5904
	10	AB	-5.7447	-4.54%	-1.1070	12:04:16 PM	4.6377	-6.3720	-5.03%	0.6273
	12	AB	-5.5473	-4.38%	-1.1157	12:04:16 PM	4.4316	-6.1734	-4.88%	0.6261
4	7	BC	-6.4708	-5.16%	0.7335	12:13:29 PM	5.7372	-5.8811	-4.69%	0.5896
	9	BC	-6.1658	-4.93%	0.7328	12:13:29 PM	5.4330	-5.5760	-4.45%	0.5898
	8	BC	-6.1296	-4.90%	0.7335	12:13:29 PM	5.3961	-5.5392	-4.43%	0.5904
	10	AB	-5.7447	-4.54%	0.7192	12:07:20 PM	5.0255	-6.3720	-5.03%	0.6273
	12	AB	-5.5473	-4.38%	-0.8302	12:08:32 PM	4.7171	-6.1734	-4.88%	0.6261
5	1	AC	-6.2373	-4.93%	-1.1167	12:00:14 PM	5.1206	-4.7192	-3.73%	1.5181
	3	AC	-5.9365	-4.70%	-0.9846	12:00:14 PM	4.9519	-4.4182	-3.50%	1.5183
	2	AC	-5.9006	-4.68%	-0.9779	12:00:14 PM	4.9226	-4.3805	-3.47%	1.5201
	10	AB	-5.6431	-4.48%	-1.1181	12:04:16 PM	4.5250	-6.3931	-5.08%	0.7500
	12	AB	-5.4444	-4.33%	-1.1267	12:04:16 PM	4.3177	-6.1932	-4.92%	0.7488
6	1	AC	-6.2373	-4.93%	0.7699	12:00:46 PM	5.4674	-4.7192	-3.73%	1.5181
	3	AC	-5.9365	-4.70%	0.7691	12:00:46 PM	5.1674	-4.4182	-3.50%	1.5183
	2	AC	-5.9006	-4.68%	0.7699	12:00:46 PM	5.1307	-4.3805	-3.47%	1.5201
	10	AB	-5.6431	-4.48%	0.7752	12:09:33 PM	4.8679	-6.3931	-5.08%	0.7500
	12	AB	-5.4444	-4.33%	-0.8389	12:08:32 PM	4.6055	-6.1932	-4.92%	0.7488
7	4	AB	-7.4153	-5.94%	-1.0413	12:00:47 PM	6.3740	-7.4153	-5.94%	0.0000
	10	AB	-7.1717	-5.70%	-1.1181	12:04:16 PM	6.0536	-7.1717	-5.70%	0.0000
	6	AB	-7.1071	-5.70%	-0.8976	12:00:47 PM	6.2094	-7.1071	-5.70%	0.0000
	5	AB	-7.0718	-5.68%	-0.9173	12:00:47 PM	6.1545	-7.0718	-5.68%	0.0000
	12	AB	-6.9705	-5.54%	-1.1267	12:04:16 PM	5.8438	-6.9705	-5.54%	0.0000
8	4	AB	-7.4153	-5.94%	-0.7497	12:01:32 PM	6.6656	-7.4153	-5.94%	0.0000
	10	AB	-7.1717	-5.70%	-0.7162	12:08:32 PM	6.4554	-7.1717	-5.70%	0.0000
	6	AB	-7.1071	-5.65%	-0.5829	12:01:32 PM	6.5241	-7.1071	-5.65%	0.0000
	5	AB	-7.0718	-5.68%	-0.6387	12:01:32 PM	6.4331	-7.0718	-5.68%	0.0000
	12	AB	-6.9705	-5.54%	-0.8389	12:08:32 PM	6.1316	-6.9705	-5.54%	0.0000

Table 2.5. Results for scenarios 9-16 for North-to-South cloud motion. Five customer load locations with greatest SS voltage change, their corresponding maximum QSS voltage change, and final QSS voltage change.

Scenario	Location	Phase	SS Voltage Change (V)	SS Voltage Change (%)	Maximum QSS Voltage Change (V)	Time of Maximum QSS Voltage Change	Difference of SS Voltage Change and Max QSS Voltage Change (V)	Final QSS Voltage Change (V)	Final QSS Voltage Change (%)	Difference of SS Voltage Change and Final QSS Voltage Change (V)
9	1	AC	-6.2373	-4.90%	-0.9266	12:04:10 PM	5.3107	-5.4633	-4.29%	0.7740
	3	AC	-5.9365	-4.67%	-0.9091	12:04:09 PM	5.0275	-5.1633	-4.06%	0.7732
	2	AC	-5.9006	-4.65%	-0.8967	12:04:09 PM	5.0038	-5.1265	-4.04%	0.7741
	10	AB	-5.6431	-4.48%	-1.3370	12:00:45 PM	4.3060	-5.6190	-4.46%	0.0240
	12	AB	-5.4444	-4.35%	-1.3627	12:00:45 PM	4.0818	-5.4204	-4.33%	0.0240
10	1	AC	-6.2373	-4.90%	-0.9448	12:08:18 PM	5.2925	-5.4633	-4.29%	0.7740
	3	AC	-5.9365	-4.67%	-0.9934	12:08:16 PM	4.9431	-5.1633	-4.06%	0.7732
	2	AC	-5.9006	-4.65%	-0.9744	12:08:16 PM	4.9261	-5.1265	-4.04%	0.7741
	10	AB	-5.6431	-4.48%	1.1525	12:01:29 PM	4.4905	-5.6190	-4.46%	0.0240
	12	AB	-5.4444	-4.33%	-1.1504	12:01:29 PM	4.2941	-5.4204	-4.31%	0.0240
11	7	BC	-6.4708	-5.16%	-1.2454	12:09:40 PM	5.2254	-5.8811	-4.69%	0.5896
	9	BC	-6.1658	-4.93%	-1.2573	12:09:40 PM	4.9085	-5.5760	-4.45%	0.5898
	8	BC	-6.1296	-4.90%	-1.2144	12:09:40 PM	4.9152	-5.5392	-4.43%	0.5904
	10	AB	-5.7447	-4.54%	-1.3313	12:00:45 PM	4.4134	-6.3720	-5.03%	0.6273
	12	AB	-5.5473	-4.38%	-1.3568	12:00:45 PM	4.1905	-6.1734	-4.88%	0.6261
12	7	BC	-6.4708	-5.16%	-1.0305	12:19:19 PM	7.5013	-5.8811	-4.69%	0.5896
	9	BC	-6.1658	-4.93%	-1.0469	12:19:19 PM	7.2126	-5.5760	-4.45%	0.5898
	8	BC	-6.1296	-4.90%	-0.9723	12:19:19 PM	7.1020	-5.5392	-4.43%	0.5904
	10	AB	-5.7447	-4.54%	-1.1412	12:01:29 PM	6.8860	-6.3720	-5.03%	0.6273
	12	AB	-5.5473	-4.38%	-1.1392	12:01:29 PM	4.4082	-6.1734	-4.88%	0.6261
13	1	AC	-6.2373	-4.93%	-0.9315	12:04:10 PM	5.3057	-4.7188	-3.73%	1.5185
	3	AC	-5.9365	-4.70%	-0.9137	12:04:09 PM	5.0228	-4.4178	-3.50%	1.5187
	2	AC	-5.9006	-4.68%	-0.9014	12:04:09 PM	4.9992	-4.3801	-3.47%	1.5205
	10	AB	-5.6431	-4.48%	-1.3369	12:00:45 PM	4.3061	-5.6314	-4.47%	0.0117
	12	AB	-5.4444	-4.33%	-1.3626	12:00:45 PM	4.0818	-5.4327	-4.32%	0.0117
14	1	AC	-6.2373	-4.93%	-0.9499	12:08:18 PM	7.1872	-4.7186	-3.73%	1.5187
	3	AC	-5.9365	-4.70%	-0.9985	12:08:16 PM	6.9350	-4.4176	-3.50%	1.5189
	2	AC	-5.9006	-4.68%	-0.9794	12:08:16 PM	6.8799	-4.3799	-3.47%	1.5207
	10	AB	-5.6431	-4.48%	-1.1525	12:01:29 PM	6.7956	-5.6295	-4.47%	0.0135
	12	AB	-5.4444	-4.33%	-1.1504	12:01:29 PM	4.2940	-5.4309	-4.31%	0.0135
15	4	AB	-7.4153	-5.94%	-1.0684	12:07:14 PM	6.3469	-7.4153	-5.94%	0.0000
	10	AB	-7.1717	-5.70%	-1.3370	12:00:45 PM	5.8347	-7.1717	-5.70%	0.0000
	6	AB	-7.1071	-5.70%	-0.9334	12:07:14 PM	6.1737	-7.1071	-5.70%	0.0000
	5	AB	-7.0718	-5.68%	-0.9277	12:07:14 PM	6.1441	-7.0718	-5.68%	0.0000
	12	AB	-6.9705	-5.54%	-1.3627	12:00:45 PM	5.6079	-6.9705	-5.54%	0.0000
16	4	AB	-7.4153	-5.94%	-0.9779	12:14:27 PM	6.4374	-7.4153	-5.94%	0.0000
	10	AB	-7.1717	-5.70%	-1.1525	12:01:29 PM	6.0192	-7.1717	-5.70%	0.0000
	6	AB	-7.1071	-5.70%	-0.8681	12:14:27 PM	6.2390	-7.1071	-5.70%	0.0000
	5	AB	-7.0718	-5.68%	-0.8622	12:14:27 PM	6.2097	-7.0718	-5.68%	0.0000
	12	AB	-6.9705	-5.54%	-1.1504	12:01:29 PM	5.8202	-6.9705	-5.54%	0.0000

Table 2.6. Results for scenarios 1-8 for West-to-East cloud motion. Five customer load locations with the greatest QSS voltage increase (left side of table) and the greatest QSS voltage decrease (right side of table).

Maximum QSS Voltage Increase						Maximum QSS Voltage Decrease					
Scenario	Location	Phase	Maximum QSS Voltage Increase (V)	Time of Maximum QSS Voltage Increase	Final QSS Voltage Change (V)	Scenario	Location	Phase	Maximum QSS Voltage Decrease (V)	Time of Maximum QSS Voltage Decrease	Final QSS Voltage Change (V)
1	15	AB	1.2297	12:01:13 PM	2.3251	1	20	BC	-1.1613	12:05:50 PM	4.4163
	13	AB	1.2286	12:01:13 PM	3.0836		16	AC	-1.1387	12:00:47 PM	3.8878
	14	AB	1.2285	12:01:13 PM	2.7297		18	AB	-1.1320	12:01:01 PM	3.8136
	26	AB	1.2165	12:01:13 PM	0.4340		12	AB	-1.1267	12:04:16 PM	6.1834
	25	AB	1.2159	12:01:13 PM	0.7411		10	AB	-1.1181	12:04:16 PM	6.3832
2	15	AB	1.2235	12:02:43 PM	2.3251	2	16	AC	-1.1039	12:01:33 PM	3.8878
	13	AB	1.2223	12:02:43 PM	3.0836		20	BC	-1.0708	12:11:39 PM	4.4163
	14	AB	1.2223	12:02:43 PM	2.7297		18	AB	-0.9882	12:02:01 PM	3.8136
	26	AB	1.2103	12:02:43 PM	0.4340		21	AB	-0.9225	12:07:18 PM	4.3895
	25	AB	1.2097	12:02:43 PM	0.7411		12	AB	-0.8389	12:08:32 PM	6.1834
3	24	AB	0.7695	12:03:56 PM	0.3661	3	20	BC	-1.1600	12:05:50 PM	4.2772
	30	AB	0.7691	12:03:56 PM	1.0486		16	AC	-1.1451	12:00:47 PM	3.9088
	33	A	0.7689	12:03:56 PM	-0.3514		18	AB	-1.1228	12:01:01 PM	5.0168
	31	A	0.7682	12:03:56 PM	0.0389		1	AC	-1.1166	12:00:14 PM	5.4930
	32	ABC	0.7679	12:03:56 PM	0.3488		12	AB	-1.1157	12:04:16 PM	6.1734
4	22	AB	0.7816	12:00:41 PM	0.9801	4	16	AC	-1.1071	12:01:33 PM	3.9088
	17	AB	0.7814	12:00:41 PM	1.0105		20	BC	-1.0697	12:11:39 PM	4.2772
	26	AB	0.7812	12:00:41 PM	1.6703		18	AB	-0.9856	12:02:01 PM	5.0168
	25	AB	0.7789	12:00:41 PM	1.9756		21	AB	-0.9182	12:07:18 PM	4.3879
	39	AB	0.7783	12:00:41 PM	0.9756		12	AB	-0.8302	12:08:32 PM	6.1734
5	29	BC	2.1908	12:00:46 PM	-1.7934	5	20	BC	-1.1613	12:05:50 PM	1.5970
	23	BC	2.1872	12:00:46 PM	-2.5438		16	AC	-1.1387	12:00:47 PM	3.1468
	19	BC	2.1864	12:00:46 PM	-2.5126		12	AB	-1.1267	12:04:16 PM	6.1932
	28	BC	2.1841	12:00:46 PM	-1.4806		18	AB	-1.1257	12:01:01 PM	3.8118
	27	BC	2.1812	12:00:46 PM	-2.3950		10	AB	-1.1181	12:04:16 PM	6.3931
6	29	BC	2.1917	12:00:46 PM	-1.0549	6	16	AC	-1.1010	12:01:33 PM	3.1467
	23	BC	2.1880	12:00:46 PM	-1.8109		20	BC	-1.0708	12:11:39 PM	2.3213
	19	BC	2.1872	12:00:46 PM	-1.7798		18	AB	-0.9882	12:02:01 PM	3.8111
	28	BC	2.1850	12:00:46 PM	-0.7424		21	AB	-0.9225	12:07:18 PM	4.3976
	27	BC	2.1821	12:00:46 PM	-1.6631		12	AB	-0.8389	12:08:32 PM	6.1914
7	NA	NA	NA	NA	NA	7	20	BC	-1.1613	12:05:50 PM	5.2802
	NA	NA	NA	NA	NA		16	AC	-1.1387	12:00:47 PM	3.8835
	NA	NA	NA	NA	NA		18	AB	-1.1320	12:01:01 PM	5.7813
	NA	NA	NA	NA	NA		12	AB	-1.1267	12:04:16 PM	6.9705
	NA	NA	NA	NA	NA		10	AB	-1.1181	12:04:16 PM	7.1717
8	NA	NA	NA	NA	NA	8	16	AC	-1.1010	12:01:33 PM	3.8835
	NA	NA	NA	NA	NA		20	BC	-1.0709	12:11:39 PM	5.2802
	NA	NA	NA	NA	NA		18	AB	-0.9938	12:02:01 PM	5.7813
	NA	NA	NA	NA	NA		21	AB	-0.9225	12:07:18 PM	5.1671
	NA	NA	NA	NA	NA		12	AB	-0.8389	12:08:32 PM	6.9705

Table 2.7. Results for scenarios 9-16 for North-to-South cloud motion. Five customer load locations with the greatest QSS voltage increase (left side of table) and greatest QSS voltage decrease (right side of table).

Maximum QSS Voltage Increase						Maximum QSS Voltage Decrease					
Scenario	Location	Phase	Maximum QSS Voltage Increase (V)	Time of Maximum QSS Voltage Increase	Final QSS Voltage Change (V)	Scenario	Location	Phase	Maximum QSS Voltage Decrease (V)	Time of Maximum QSS Voltage Decrease	Final QSS Voltage Change (V)
9	15	AB	1.2302	12:08:21 PM	2.3251	9	12	AB	-1.3627	12:00:45 PM	5.4204
	13	AB	1.2290	12:08:21 PM	3.0836		11	AB	-1.3442	12:00:45 PM	5.2785
	14	AB	1.2290	12:08:21 PM	2.7297		10	AB	-1.3370	12:00:45 PM	5.6190
	26	AB	1.2169	12:08:21 PM	0.4340		9	BC	-1.2525	12:09:40 PM	5.7155
	25	AB	1.2163	12:08:21 PM	0.7411		7	BC	-1.2407	12:09:40 PM	6.0205
10	15	AB	1.2295	12:16:10 PM	2.3251	10	11	AB	-1.1565	12:01:29 PM	5.2785
	13	AB	1.2283	12:16:10 PM	3.0836		10	AB	-1.1525	12:01:29 PM	5.6190
	14	AB	1.2283	12:16:10 PM	2.7297		12	AB	-1.1504	12:01:29 PM	5.4204
	26	AB	1.2162	12:16:10 PM	0.4340		9	BC	-1.0429	12:19:19 PM	5.7155
	25	AB	1.2156	12:16:10 PM	0.7411		7	BC	-1.0266	12:19:19 PM	6.0205
11	22	AB	0.7877	12:01:12 PM	0.9801	11	12	AB	-1.3568	12:00:45 PM	6.1734
	30	AB	0.7877	12:00:56 PM	1.0486		11	AB	-1.3384	12:00:45 PM	6.0334
	17	AB	0.7875	12:01:12 PM	1.0105		10	AB	-1.3313	12:00:45 PM	6.3720
	35	AB	0.7873	12:00:56 PM	1.3524		9	BC	-1.2573	12:09:40 PM	5.5760
	26	AB	0.7873	12:01:12 PM	1.6703		7	BC	-1.2454	12:09:40 PM	5.8811
12	22	AB	0.7877	12:01:54 PM	0.9801	12	11	AB	-1.1452	12:01:29 PM	6.0334
	17	AB	0.7875	12:01:54 PM	1.0105		10	AB	-1.1412	12:01:29 PM	6.3720
	26	AB	0.7873	12:01:54 PM	1.6703		12	AB	-1.1392	12:01:29 PM	6.1734
	25	AB	0.7850	12:01:54 PM	1.9756		9	BC	-1.0469	12:19:19 PM	5.5760
	34	AB	0.7843	12:01:54 PM	0.9756		7	BC	-1.0305	12:19:19 PM	5.8811
13	29	BC	2.3776	12:00:50 PM	-1.2290	13	12	AB	-1.3626	12:00:45 PM	5.4327
	23	BC	2.3736	12:00:50 PM	-1.9841		11	AB	-1.3441	12:00:45 PM	5.2909
	19	BC	2.3727	12:00:50 PM	-1.9529		10	AB	-1.3369	12:00:45 PM	5.6314
	28	BC	2.3703	12:00:50 PM	-0.9166		9	BC	-1.2573	12:09:40 PM	3.4347
	27	BC	2.3671	12:00:50 PM	-1.8361		7	BC	-1.2453	12:09:40 PM	3.7424
14	29	BC	2.3815	12:00:54 PM	-1.2351	14	11	AB	-1.1565	12:01:29 PM	5.2890
	23	BC	2.3775	12:00:54 PM	-1.9897		10	AB	-1.1525	12:01:29 PM	5.6295
	19	BC	2.3766	12:00:54 PM	-1.9585		12	AB	-1.1504	12:01:29 PM	5.4309
	28	BC	2.3742	12:00:54 PM	-0.9226		9	BC	-1.0418	12:19:19 PM	3.4291
	27	BC	2.3711	12:00:54 PM	-1.8416		7	BC	-1.0256	12:19:19 PM	3.7367
15	NA	NA	NA	NA	NA	15	12	AB	-1.3627	12:00:45 PM	6.9705
	NA	NA	NA	NA	NA		11	AB	-1.3442	12:00:45 PM	6.8311
	NA	NA	NA	NA	NA		10	AB	-1.3370	12:00:45 PM	7.1717
	NA	NA	NA	NA	NA		9	BC	-1.2584	12:09:40 PM	6.5923
	NA	NA	NA	NA	NA		7	BC	-1.2465	12:09:40 PM	6.8983
16	NA	NA	NA	NA	NA	16	11	AB	-1.1565	12:01:29 PM	6.8311
	NA	NA	NA	NA	NA		10	AB	-1.1525	12:01:29 PM	7.1717
	NA	NA	NA	NA	NA		12	AB	-1.1504	12:01:29 PM	6.9705
	NA	NA	NA	NA	NA		9	BC	-1.0480	12:19:19 PM	6.5923
	NA	NA	NA	NA	NA		7	BC	-1.0316	12:19:19 PM	6.8983

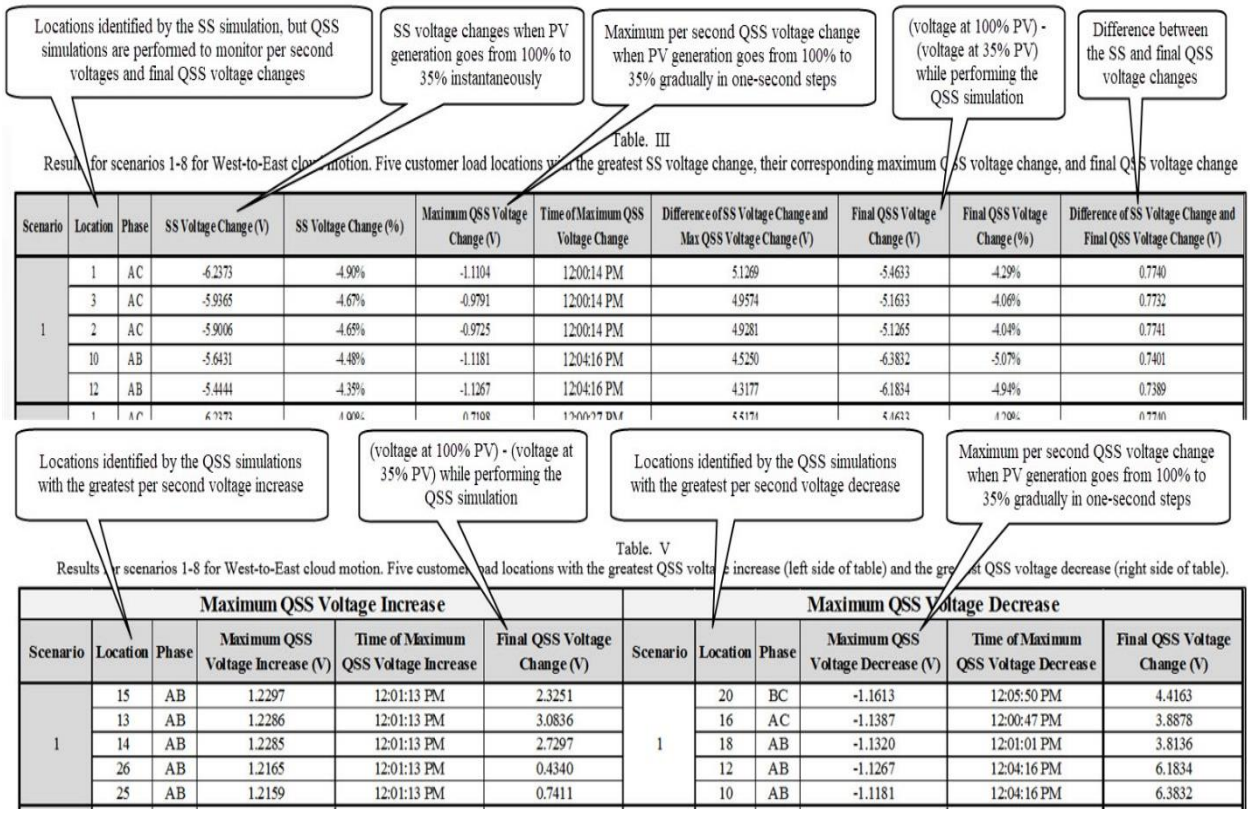

Figure 2.11. Description of the quantities computed by the SS and QSS simulations presented in Tables 2.4-2.7.

In the first scenario, location 1 has the greatest SS voltage change, which is a 6.24 V decrease. However, its maximum per second QSS voltage change, occurring at 12:00:14 PM, is only 1.11 V. Note that the SS approach cannot provide any information about rate of change, or per-second voltage changes. On the other hand, using QSS analysis, per-second voltage changes can be calculated, where high voltage changes can indicate flicker issues.

From Table 2.4, it may also be seen from Scenario 1 that the final QSS voltage change, 5.46 V, is also different than the SS voltage change, 6.24 V. This illustrates that the final states of SS and QSS simulations at location 1 are different even though both simulations start at the same initial condition and have the same final condition in terms of load and generation. The same pattern can be seen for the other locations except when controllers are frozen.

For the first set of scenarios, with West-to-East cloud motion, the five locations with the greatest voltage change from the QSS simulations are identified and presented in Table 2.6 for each scenario. The identified locations for Scenario 1 are also shown in Figure 2.12. The maximum QSS voltage change belongs to location 15, which is 1.23 V occurring at 12:01:13 PM. However, its final QSS voltage change is 2.32 V, which is only 37 % of the SS voltage change at location 1. Therefore, SS and QSS simulations can identify different locations with the greatest voltage change, which, if mitigation solutions are being considered, could result in an ineffective design based on the SS analysis. Note that Figure 2.12 illustrates that the five locations identified by SS simulations (in red) are different than the five locations identified by QSS simulations (in blue), as well as the voltage changes computed by SS and QSS simulations are different.

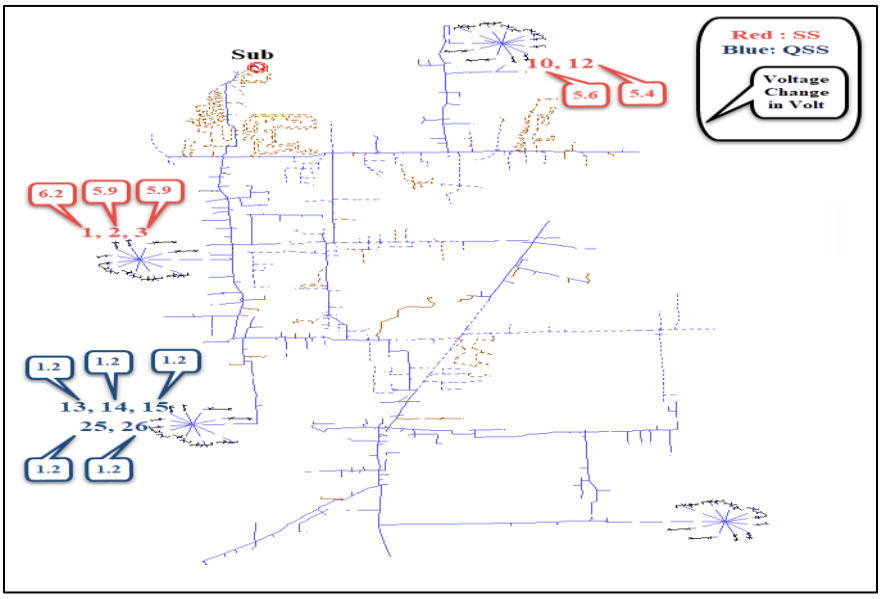

Figure 2.12. Locations that have maximum voltage changes identified by QSS and SS approaches for Scenario 1. Note that the two approaches identify very different locations.

Figure 2.13 illustrates the voltage variations from the QSS approach for locations identified by the SS approach in scenario 1. That is, the locations are selected by the SS approach, but QSS results for those locations are presented. It can be seen that the cloud shadow, which is moving from West-to-East, first covers locations 1, 2, and 3, and shortly thereafter covers locations 10 and

12. Again the effect of cloud shadow on the voltages of locations 10 and 12 can be observed around 12:04:20 PM as well as controller actions around 12:04:55 PM in Figure 2.13.

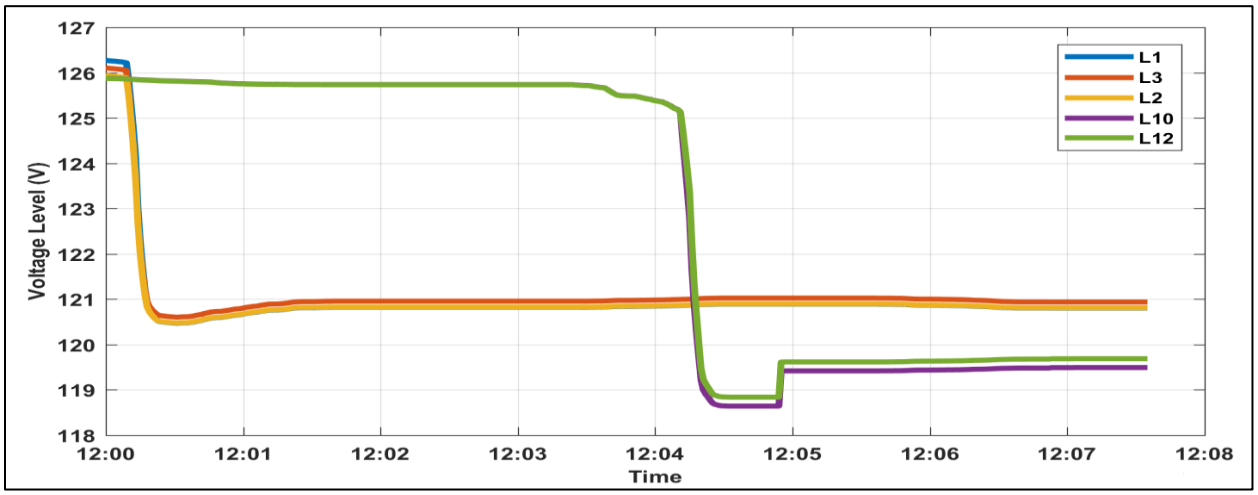

Figure 2.13. Voltage variations from the QSS approach at locations identified by the SS approach with the greatest SS voltage change for Scenario 1.

Voltage variations for locations which have the greatest QSS voltage changes for scenario 1 are shown in Figures 2.14 and 2.15. Figure 2.14 corresponds to the locations which have the greatest QSS voltage increase (left section of Tables 2.6 and 2.7), and Figure 2.15 corresponds to the locations which have the greatest QSS voltage decrease (right section of Tables 2.6 and 2.7).

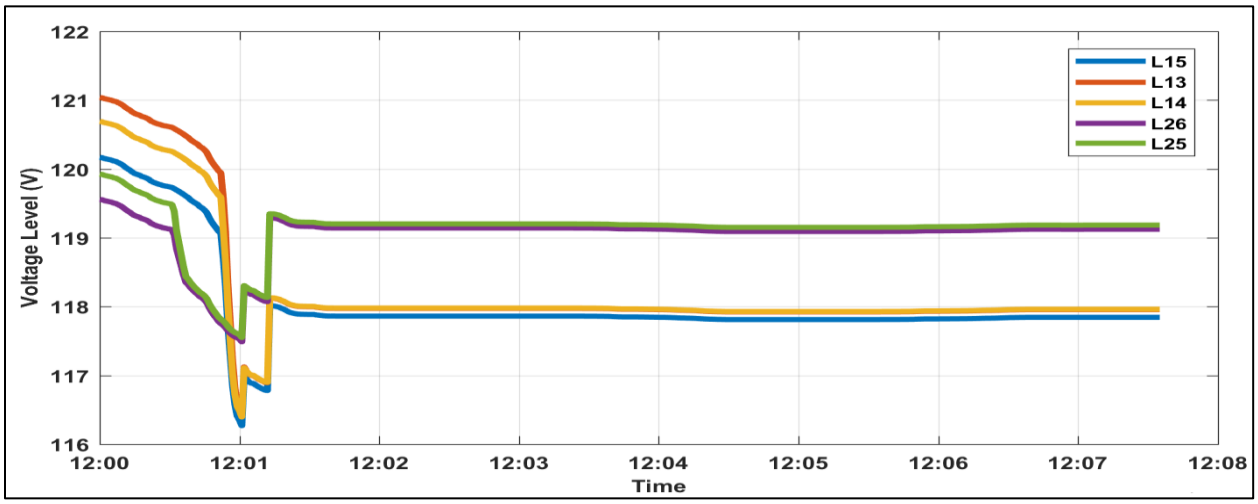

Figure 2.14. Voltage variations at locations identified by the QSS approach with greatest voltage increase for Scenario 1.

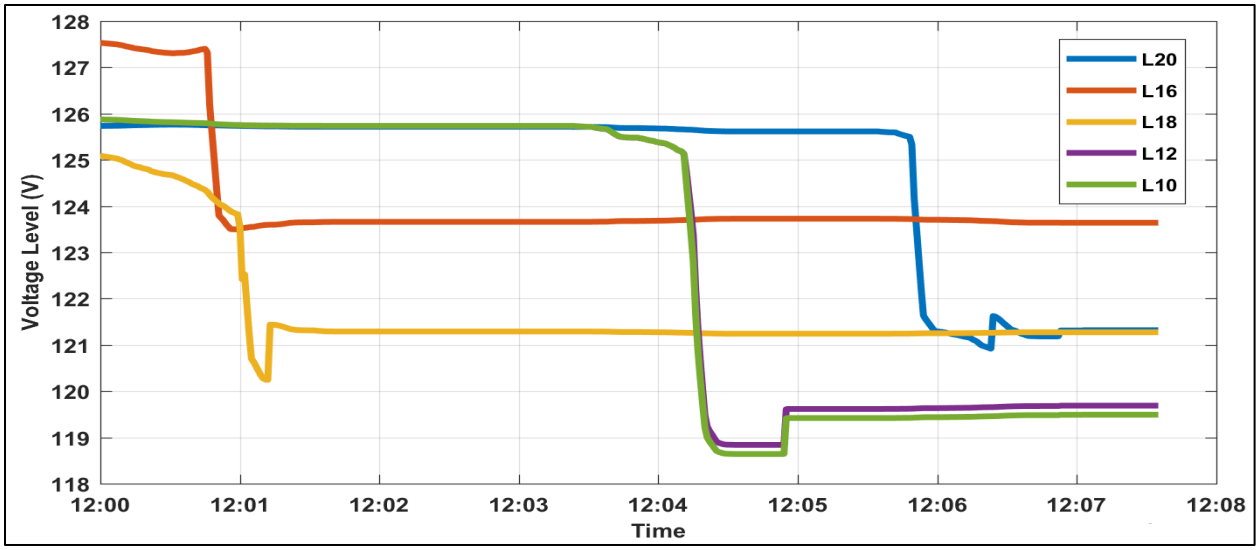

Figure 2.15. Voltage variations at locations identified by the QSS approach with greatest voltage decrease for Scenario 1.

Observations and discussions

The following observations regarding control dead-bands, control time-delays, cloud speed, and cloud motion direction are derived from the results of the 16 scenarios:

- Increasing the control dead-band increases the maximum SS voltage change.
- Increasing the control dead-band decreases the maximum QSS voltage increase, and can change where the maximum QSS voltage increase occurs.
- Increasing the control delay increased the maximum QSS voltage increase, and can also change where it occurs.
- The maximum SS voltage change occurs when controllers are frozen.
- Reducing the cloud speed decreases the maximum QSS voltage decrease.
- The direction of cloud motion affects both the maximum QSS voltage change and where it occurs. However, the impact is more significant on the maximum QSS voltage decrease.
- Locations where the maximum QSS voltage decrease occurs generally have significant SS voltage changes.

- For a given location the maximum QSS voltage increase occurs when the controller dead-band is a minimum, the controller delay is a maximum, and the cloud speed is a maximum.
- Controller actions are major contributors to the maximum QSS voltage change. The magnitude of the maximum QSS voltage increase (which is primarily due to controller action) is about 146% of the maximum QSS voltage decrease.

Due to the non-linear nature of the control devices, the final state computed by the QSS approach is generally different than the final steady state computed by the SS approach, even though the load and generation are the same for the initial and final states. The maximum difference, approximately 1.5V, occurs in scenarios 5, 6, 13, and 14. Figure 2.16 shows the differences for all of the scenarios. When controllers are frozen in scenarios 7, 8, 15, and 16, the SS and QSS results are the same.

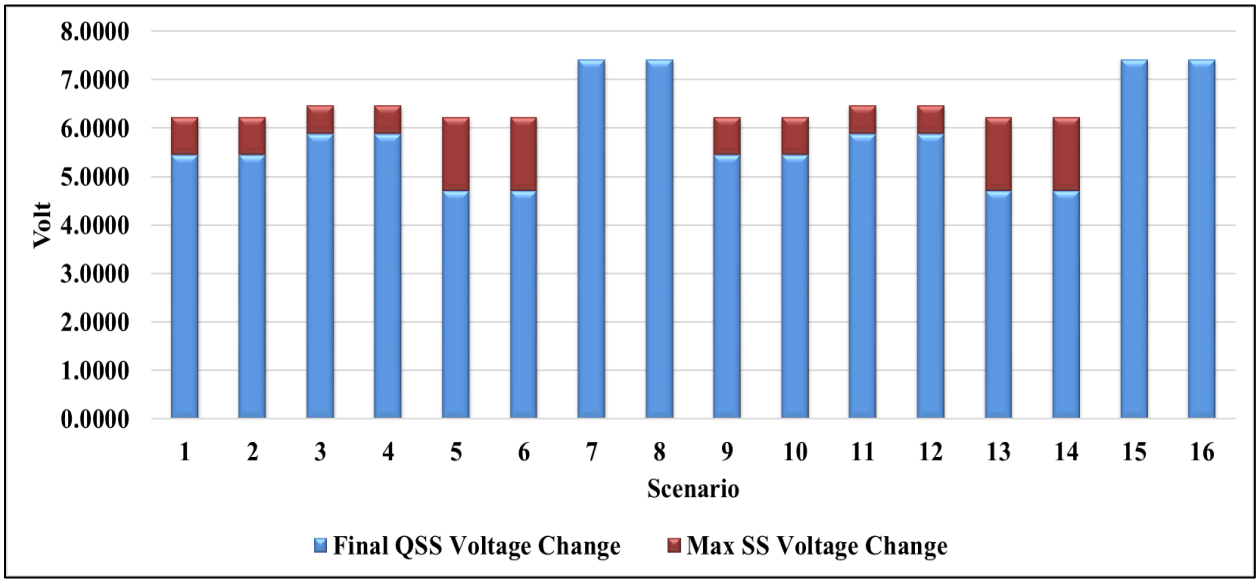

Figure 2.16. Maximum SS voltage change computed by the SS approach versus maximum QSS final voltage change (regardless of decrease or increase) computed by the QSS approach.

Different controller settings also lead to different final states for QSS simulations. For example, location 1 had a 5.46 V final voltage decrease in Scenario 2, where as Scenario 5 with a different cloud direction the same location had a final voltage decrease of 4.7 V. Figure 2.17 illustrates how

the non-linearity of the controllers, due to the dead-band and the sequence of control actions, either due to time delay or sequence of disturbances, can affect the final QSS state. It results in different final states even though all final states have the same load and generation. For instance, in Path i controller X operates before controller Y, while in Path j controller X operates after controller Y. The different sequence of controller operations can be driven by the direction of cloud motion. Therefore, some controllers can operate before other controllers in scenarios 1-8 when the motion direction is from West-to-East, while in scenarios 9-16, other controllers can operate first when the cloud motion direction is from North-to-South.

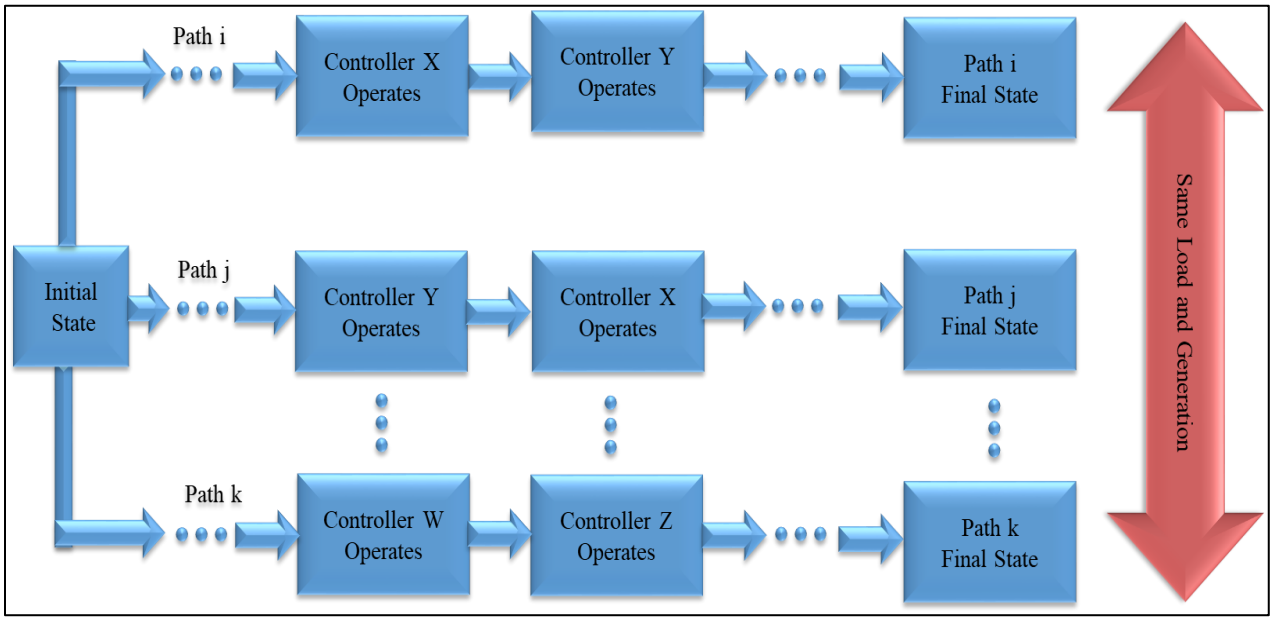

Figure 2.17. How controller settings can lead to different final states in QSS simulations.

One advantage of QSS approach over SS approach is the ability to track and observe all intermediate states during a system disturbance. Specifically, effects of controller actions on voltage variations cannot be observed with SS simulations. Figure 2.18 shows an example where voltage changes of over 2V occurred for location 28 in Scenario 6 (the fourth top QSS voltage increase). However, if only the initial and final states of location 28 were considered, as in the SS analysis, the voltage change is only 0.74V.

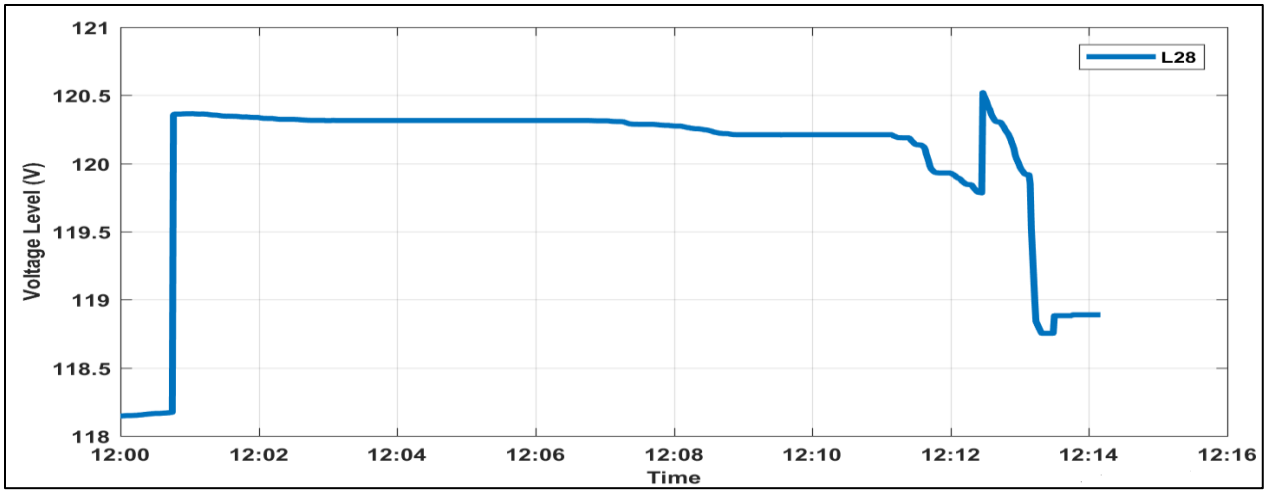

Figure 2.18. Voltage variation at location 28 in Scenario 6.

The QSS approach can significantly improve the identification of locations where mitigation may be needed. The magnitude of the maximum voltage changes, and the locations of those changes computed by the QSS, are generally very different than the locations identified by the SS approach. Figure 2.19 illustrates significant differences between the maximum SS voltage changes and the corresponding maximum QSS voltage changes at the same locations. It also shows that if SS voltage changes, or maximum QSS voltage changes are considered for identifying flicker issues, there will be different interpretations in terms of severity.

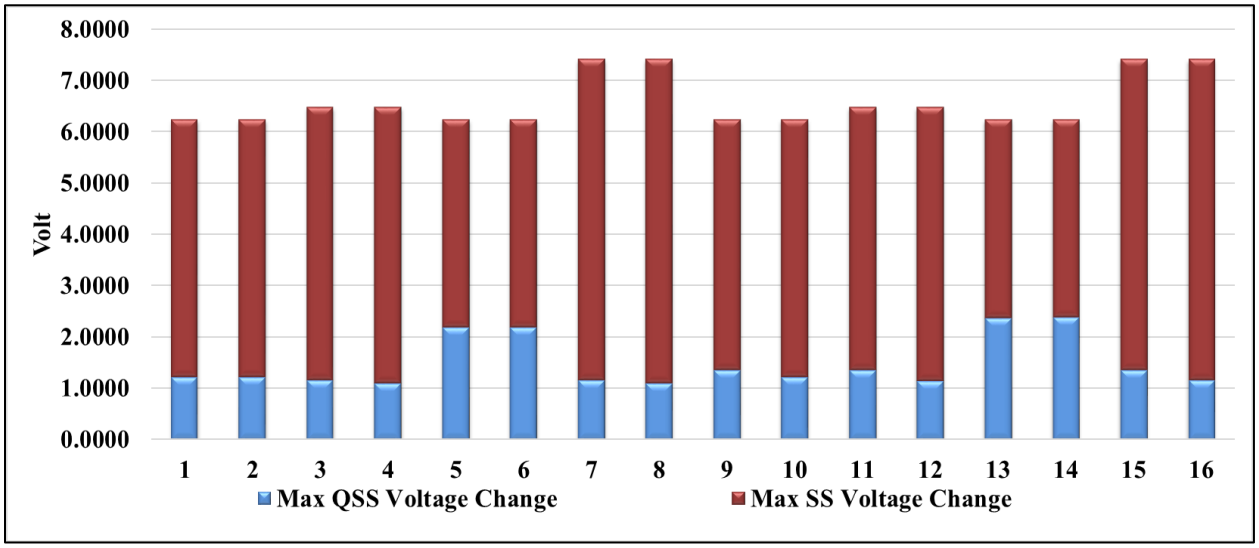

Figure 2.19. Maximum SS voltage change and their corresponding maximum QSS voltage change.

Figures 2.20 and 2.21 compare the locations of the greatest voltage changes identified by the SS and QSS approaches across the scenarios. From Table 2.8, it may be seen that the number of locations with large voltage changes that are common to both SS and QSS simulations are relatively small.

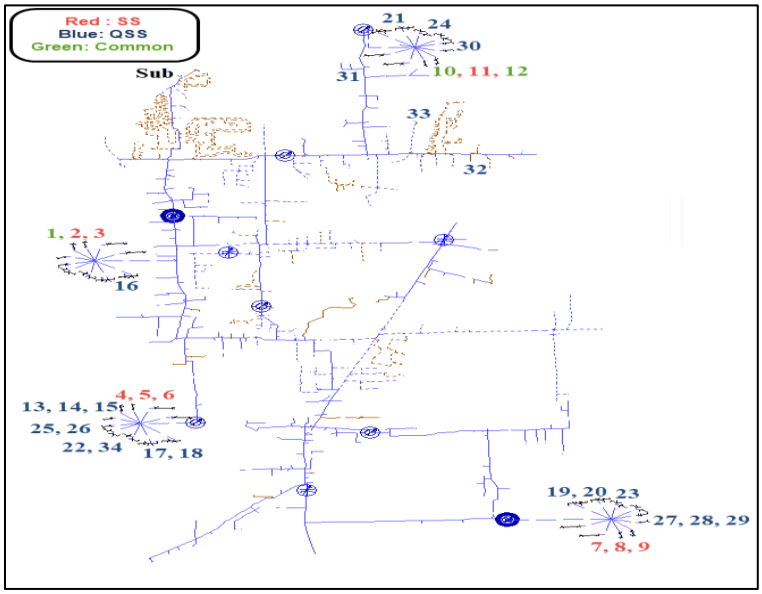

Figure 2.20. Comparing locations with large voltage changes identified by QSS and SS simulations for Scenarios 1-8, West-to-East cloud motion.

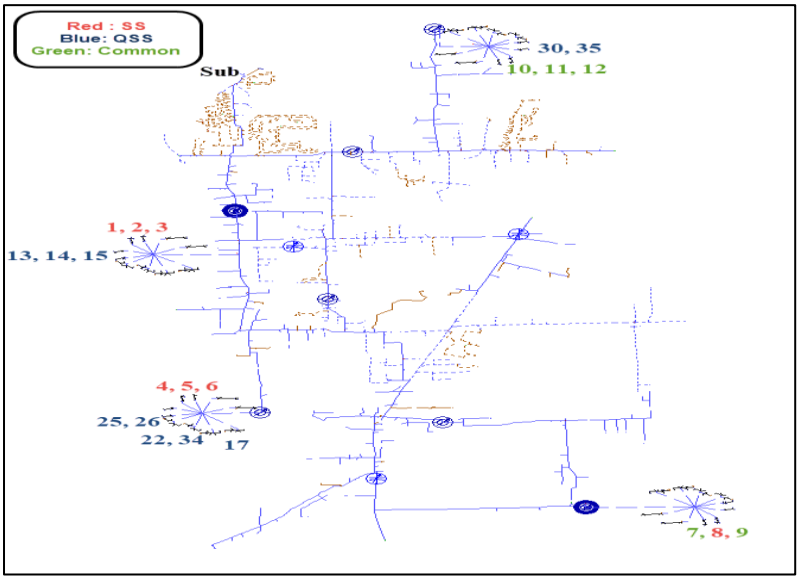

Figure 2.21. Comparing locations with large voltage changes identified by QSS and SS simulations for Scenarios 9-16, North-to-South cloud motion.

Table 2.8. For all scenarios, locations identified with large voltage changes that were identified by SS or QSS, or were common to both.

Scenario Set	Simulation Type	Identified Locations
1 (West-East)	SS	1, 2, 3, 4, 5, 6, 7, 8, 9, 10, 11, 12
	QQ	1, 10, 12, 13, 14, 15, 16, 17, 18, 19, 20, 21, 22, 23, 24, 25, 26, 27, 28, 29, 30, 31, 32, 33, 34
	Common to SS and QSS	1, 10, 12
2 (North-South)	SS	1, 2, 3, 4, 5, 6, 7, 8, 9, 10, 11, 12
	QQ	7, 9, 10, 11, 12, 13, 14, 15, 17, 22, 25, 26, 30, 34, 35
	Common to SS and QSS	7, 9, 10, 11, 12

Figure 2.22 illustrates the number of load busses that had a one-volt-or-more change, and this amount of change is sufficient to cause utility control devices to operate. A count of the number of one-volt changes is used here to rank the severity of the scenarios considered. The most dramatic difference occurs for Scenario 8, where SS identifies 291 customer loads with one volt or greater change, but where QSS only identifies 2 customer loads with a one volt change per second or greater. However, sometimes QSS identifies more customer loads with large voltage changes than SS, as seen in Scenarios 5, 6, 13, and 14. It is observed that by increasing the control time delay, the number of one volt or greater changes increases significantly, and by increasing the controller dead-band, the number of changes decreases. The least number of one volt or more changes was

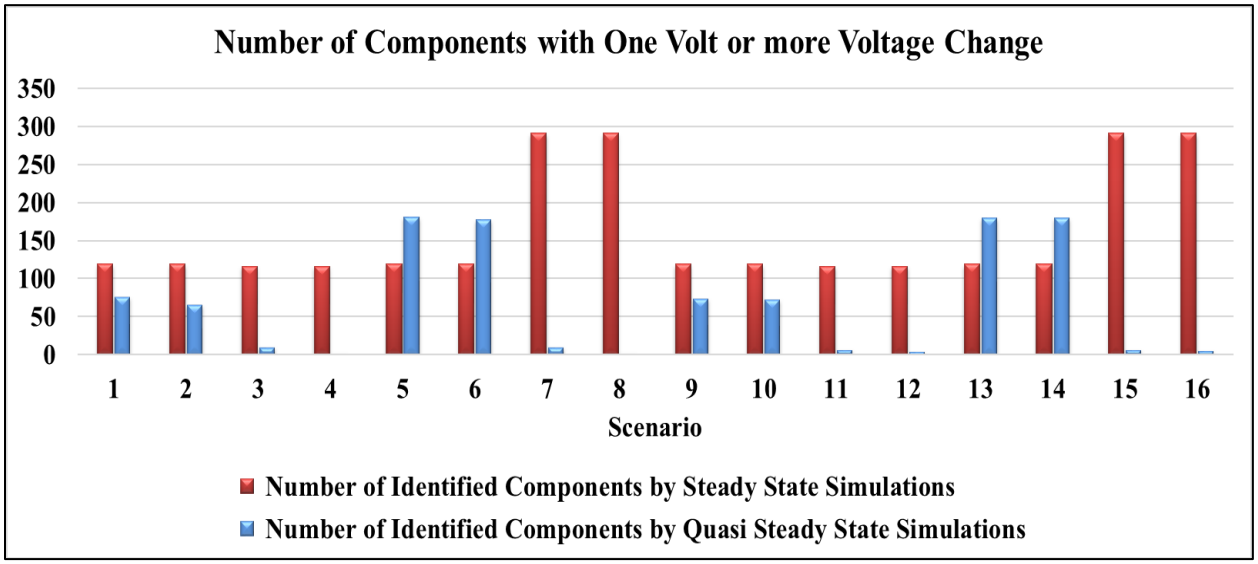

Figure 2.22. The number of components with one volt or more change for SS and QSS simulations for each scenario.

observed when the smallest delay and the greatest dead-band are applied. This points out the impact that controller settings have on voltage changes. In specific cases, voltage control devices can be significant contributors to voltage changes.Using 16 different scenarios and employing a realistic distribution feeder, it has been shown that the results obtained from the SS approach can be significantly different from the results obtained from the QSS approach. The magnitude of the maximum voltage changes and the locations of those changes calculated using the QSS approach are regularly very different than those computed by the SS approach. The QSS and SS simulations do not even reach the same final steady state condition, even though the PV generation and loading at the final steady state is the same. This difference is in part due to the nonlinearity of the control devices and the path taken by the system to reach its final state. It is also observed that the final steady state condition of QSS simulations can depend upon the speed and direction of cloud motion. Controller settings also affect the final state and the maximum QSS voltage changes.

2.4 Employing new standards and grid codes

In this section the flicker standards used in industry are introduced. Then implementation of the flickermeter method, used in the IEEE 1453-2015 [42], by the CMS is discussed. The impacts of CMS parameters on short-term flicker severity are then investigated. Finally, PV penetration levels identified by the flicker curves are compared with the penetration levels determined by the flickermeter method of the IEEE 1453-2015.

A portion of [69] is re-formatted and reused in this section. The first author of [69] is the author of this dissertation and the reuse is in compliance with IEEE policy at the time of writing this dissertation. The policy can be found in the appendix. Note that IEEE holds the copyright of [69], whose citation is provided in the bibliography.

2.4.1 Voltage flicker standards

Voltage fluctuations on power systems can give rise to noticeable, and sometimes irritating, illumination changes from lighting equipment. This phenomenon is referred to as voltage flicker, or just flicker. The IEEE 1547.7-2013 standard [77], Guide for Conducting Distribution Impact Studies for Distributed Resource Interconnection, has referred to "Flicker Curves" illustrated in IEEE 141-1993 [40] and IEEE 519-1992 [41] standards to identify observable or objectionable flicker levels. The flicker curves from these standards, also known as "GE Curves", have been utilized by a large number of electric utilities in the US due to the ease of use. These flickers curves are useful for dealing with rectangular voltage changes with a known frequency. However, PV resources produce random voltage fluctuations, which are slower-ramping in nature, and thus do not fit the assumptions of the traditional flicker analysis.

The IEEE 1547.7-2013 standard has also referred to the IEEE 1453-2004 standard, Recommended Practice for the Analysis of Fluctuating Installations on Power Systems, for flicker computation. The newer version of the IEEE 1453, which superseded the 2004 version in 2015, adopted the flicker evaluation and measurement methods from the IEC 61000-4-15 [78]. The IEEE 1453 standard was in response to the advent of power electronics equipment and complex voltage fluctuations, which are not handled appropriately by the GE flicker curves.

While the IEEE 1453-2013 is the most applicable and updated practice to evaluate voltage flicker from such sources as PV generation, many electric utilities still utilize the GE flicker curves. Computing short-term flicker based on the IEEE 1453-2015, also known as the flickermeter method, needs at least 10 minutes of voltage measurements/values, and involves a significant amount of computation, such as developing probability and cumulative density functions. Electric utilities currently do not have computations in place for performing this analysis, and thus continue

to use the GE flicker curves while performing PV interconnection studies and assessing possible flicker issues. Figure 2.23 demonstrates the borderlines of visibility and irrigation.

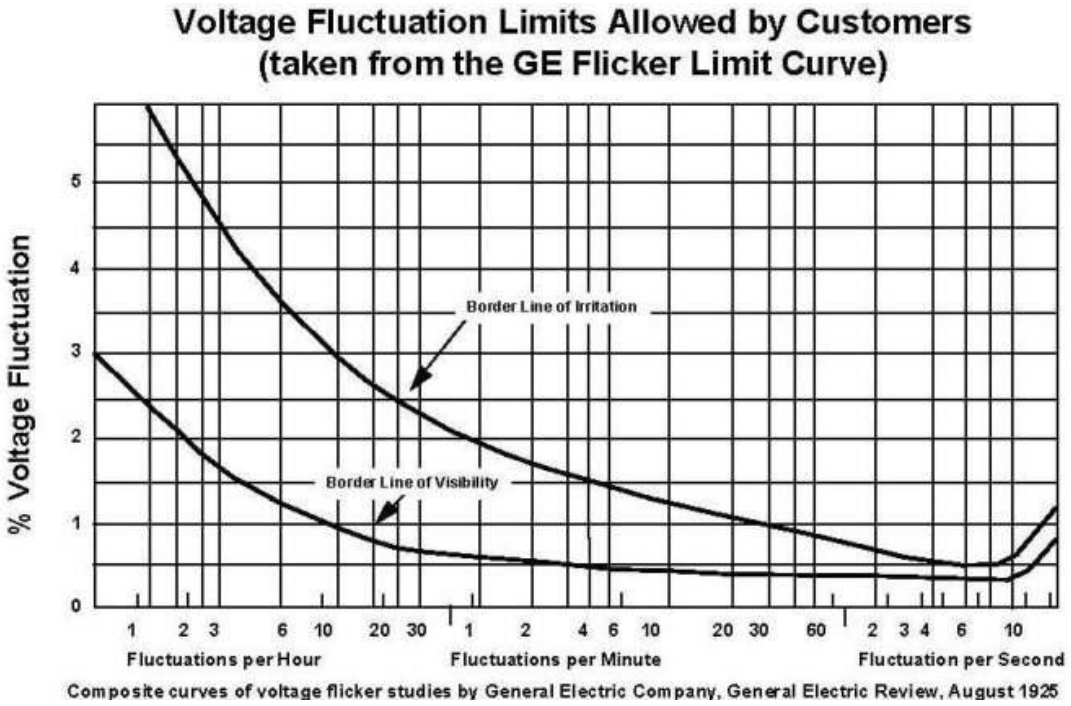

Figure 2.23. GE flicker limit curves presented in [40] and [41].

To perform voltage flicker studies, induced by PV resources, the PV system under investigation is placed at the appropriate location in a circuit model and its power output is adjusted to represent how the system will behave when clouds pass over the PV arrays. The resulting changes in voltage are then measured to determine if that location will experience irritating levels of voltage flicker.

The IEEE 1453-2015 standard, IEEE Recommended Practice for the Analysis of Fluctuating Installations on Power systems, adapted the flicker computation from the IEC 61000-4-15 [78] standard. The measurement method is the result of years of research by scientists and engineering in ocular systems, brain response, and lamp response. Figure 2.24 presents the process of the flicker computation with a flickermeter [42]. The blocks shown are briefly described below.

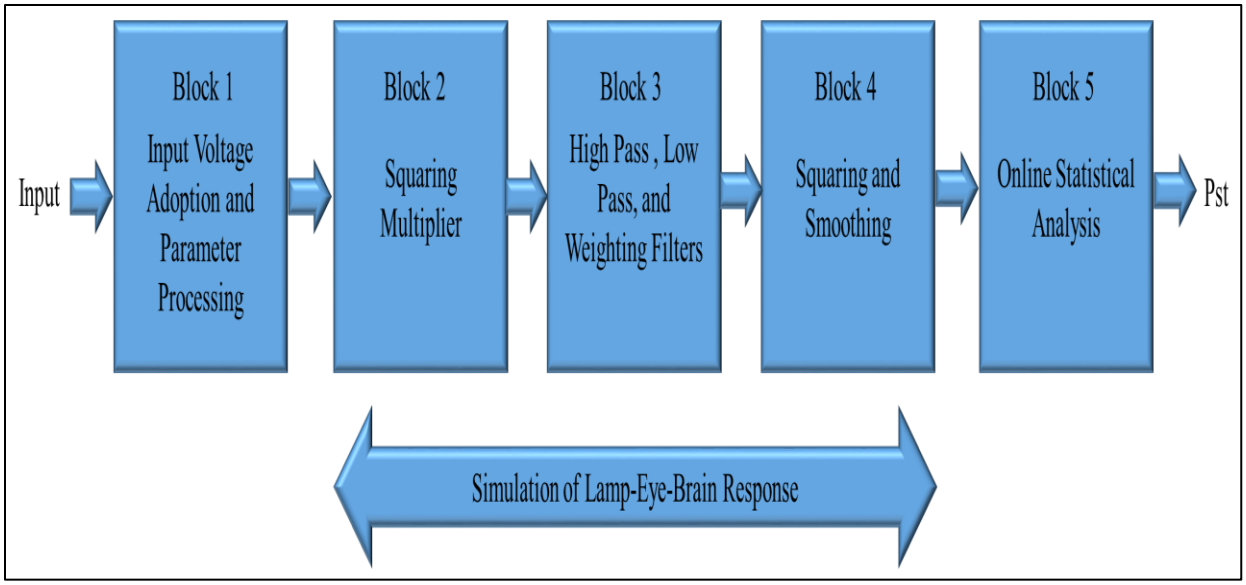

Figure 2.24. Block diagram of flicker computation [69]. © 2018 IEEE

Block 1 converts the exact values to a percent ratio, which removes the flicker measurement dependence upon the input carrier voltage level. Blocks 2-4 simulate lamp-eye-brain response. Block 2 separates the low frequency voltage oscillations from the main voltage signal (carrier signal) through a squaring demodulator, simulating the behavior of the incandescent lamp. Block 3 utilizes multiple filters to filter out unwanted frequencies produced by the demodulator. Moreover, it weighs the input signal according to the incandescent lamp eye-brain response. In Block 4 a squaring multiplier and sliding mean filter are used to simulate nonlinear eye-brain response as well as the short-term storage effect of the brain. In Block 5 the output of Block 4 is statistically processed. A histogram based on suitable classes is created. From the classes a Probability Density Function (PDF) is created, and based on the PDF, a Cumulative Distribution Function (CDF) is formed as illustrated in Figure 2.25. The CDF can be considered as the probability that the instantaneous flicker sensation does not exceed a specific level [42].

Short-term flicker severity (Pst) is of interest here and is computed over a window of 10 minutes. Pst is computed based on equation 2.17.

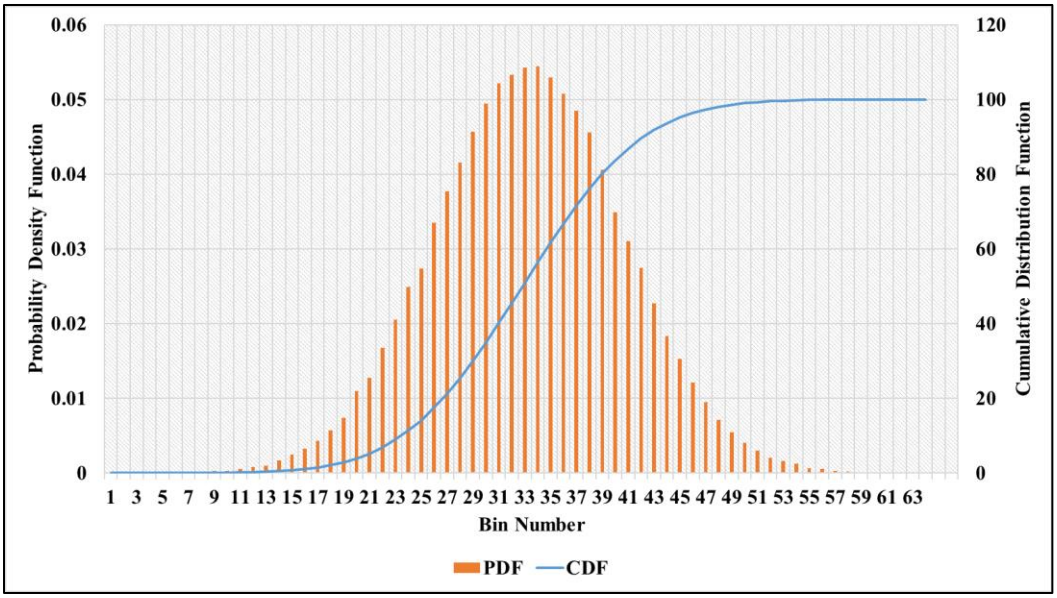

Figure 2.25. Sample PDF and CDF curves used for Pst calculation [69]. © 2018 IEEE

$$P_{st} = \sqrt{0.0314P_{0.1} + 0.0525P_{1s} + 0.0657P_{3s} + 0.28P_{10s} + 0.08P_{50s}} \quad (2.17)$$

where $P_{0.1}$, P_{1s}, P_{3s}, P_{10s} and P_{50s} represent flicker levels that are exceeded 0.1, 1.0, 3.0, 10.0, and 50.0 percent of the time, respectively, and are obtained from the CDF curve of Figure 2.25. The suffix "s" used on the variables P_{1s}, P_{3s}, P_{10s} and P_{50s} represents smoothed values, which are obtained from equations 2.18 to 2.21. The P_x terms in equations 2.18 to 2.21 represent the flicker levels that are exceeded X percent of the time. For instance, P_1 of equation 2.18 represents the flicker level that is exceeded 1% of the time.

$$P_{1s} = \frac{P_{0.7} + P_1 + P_{1.5}}{3} \quad (2.18)$$

$$P_{3s} = \frac{P_{2.2} + P_3 + P_4}{3} \quad (2.19)$$

$$P_{10s} = \frac{P_6 + P_8 + P_{10} + P_{14} + P_{17}}{5} \quad (2.20)$$

$$P_{50s} = \frac{P_{30} + P_{50} + P_{80}}{3} \quad (2.21)$$

The IEEE 1547 standard limits the P_{st} values for low voltage systems to 1.0, and it should not be exceeded more than 5% of the time. Table 2.9 presents the flicker severity limits for low voltage, medium voltage, and high/extra high voltage systems [77]. For medium and high voltage systems the limits of 0.9 should not be exceeded more than 1 % of the time.

Table 2.9. Flicker severity levels for different voltage levels [77]

Flicker Severity level	Low Voltage level	Medium Voltage Level	High Voltage and Extra High Voltage Levels
P_{st} [10-min]	1.0	0.9	0.8

2.4.2 CMS and flicker computation

So far, short-term flicker computation and the standards defining allowed flicker levels have been discussed. In the next section, computation of the short-term flicker severity by the cloud motion simulator is presented.

To compute the short-term flicker a 600-second (10 minutes) monitoring interval is required. Therefore, the cloud motion simulator, which produces QSS analysis results once per second, requires 600 simulations to calculate one P_{st} value. After the 600th step in the simulation, the cloud motion simulator computes the first value of P_{st}. In doing this, the CMS calculates the percentage voltage changes for the first 600 seconds, creating a histogram. Based on the histogram, the CDF, and the smoothed flicker levels (equations 2.18-2.21), the P_{st} can be calculated using (2.17). After computing the first value of P_{st}, each new one second step of the simulation delivers a new voltage change, and consequently a new P_{st} value. As illustrated in Figure 2.26, the process can be thought of as a moving window of 600 values, where each window of 600 values provides a single P_{st} value.

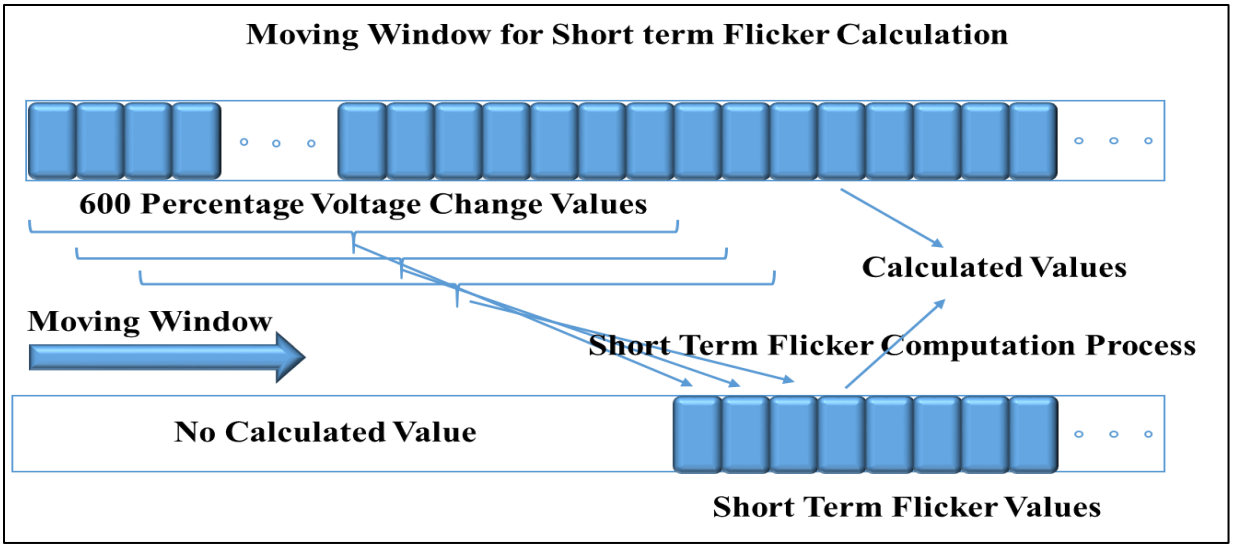

Figure 2.26. CMS Pst computation based on the concept of a moving window [69]. © 2018 IEEE

2.4.3 Effect of cloud motion simulator parameters on flicker severity

This section examines the impact of the CMS parameters, such as, cloud speed, number of clouds, width of clouds, and time interval between clouds, on the short-term flicker with two case studies. The first case study uses a simple model, which has a PV generator. Having only one PV generator allows observing the effect of the CMS parameters without being worried about the impact of neighboring PV generators. Figure 2.27 shows the circuit model for case study one.

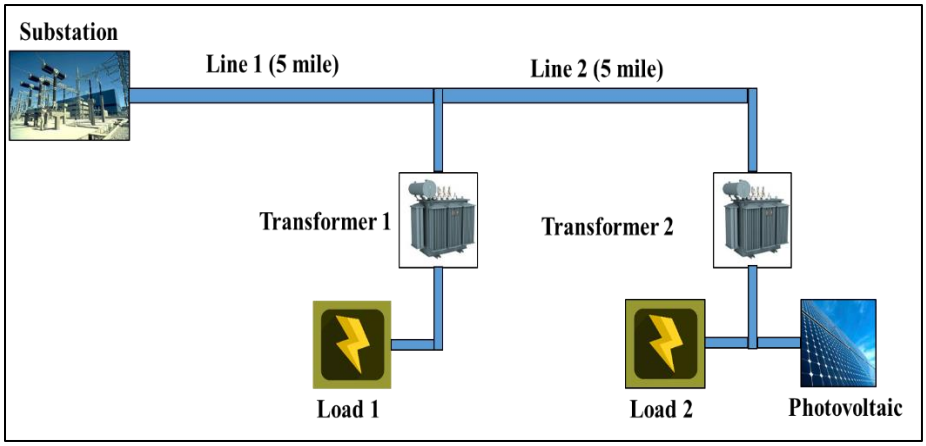

Figure 2.27. Circuit for first case study, which has one PV generator [69]. © 2018 IEEE

The distance between the substation and the first load is 5 miles, and the distance between load 1 and load 2 is also 5 miles. The PV generator is located at load 2 and has a rated capacity of 500

kVA, operating at unity power factor. It is assumed that the cloud motion direction is West-to-East. Thus, there is a 10-mile distance from the substation to load 2 which the clouds pass over. The second case study utilizes the circuit model, shown in Figure 2.10. All PV generators are operating under unity power factor.

Different scenarios are utilized to investigate the effects of the CMS parameters on P_{st}. In each scenario, one parameter of the CMS is investigated. Table 2.10 presents the employed CMS parameters as well as the P_{st} values of the first case study. Detailed results for the second case study include clouds moving from North-to-South and clouds moving from West-to-East. In the second case study, the maximum Pst value for each scenario is reported. Tables 2.11 and 2.12 provide the results when the motion direction is West-to-East and North-to-South, respectively.

Coverage time is defined as the time a cloud covers a PV generator. For the PV systems considered here coverage time is calculated by dividing the width of a cloud by its speed. In all scenarios considered the output of PV systems is modeled as decreasing from 100% to 20%, requiring 10 seconds to reach the 20% generation level. If the coverage time is more than the decay time, then the PV generator will reach its lower generation limit of 20%. However, if the coverage time is less than the decay time, then the PV generator will not reach its lowest generation value, which is 20% for the simulations considered here. Note that the time to reach the final state can be modified based on the available meteorological data. The inverse of the decay curve is used as the recovery curve. Hence, the decay time is equal to the recovery time.

Two directions are considered to evaluate the impact of cloud movement direction on the simulation results. The maximum Pst value for each scenario is reported. Figure 2.28 presents the voltage changes and computed Pst values for the scenarios assessed in the second case study where the cloud speed is 20 miles/hour, the number of clouds is 10, the width of the clouds is 1000 ft,

Table 2.10. Detailed results of the first case study, where Pst values are evaluated with just one cms parameter varying for each scenario [69].

Cloud Speed (mile/hour)	Number of Clouds	Width of Clouds (ft)	Intervals (s)	Pst	Coverage Time (s)
10	10	1000	20	0.4461	68.18
15	10	1000	20	0.4761	45.45
20	10	1000	20	0.4809	34.09
25	10	1000	20	0.4814	27.27
30	10	1000	20	0.4814	22.73
10	10	300	20	0.4807	20.45
15	10	300	20	0.4814	13.64
20	10	300	20	0.4816	10.23
25	10	300	20	0.4702	8.18
30	10	300	20	0.4672	6.82
Cloud Speed (mile/hour)	**Number of Clouds**	**Width of Clouds (ft)**	**Intervals (s)**	**Pst**	**Coverage Time (s)**
20	10	100	20	0.4010	3.41
20	10	300	20	0.4816	10.23
20	10	600	20	0.4807	20.45
20	10	1000	20	0.4809	34.09
20	10	1500	20	0.4729	51.14
Cloud Speed (mile/hour)	**Number of Clouds**	**Width of Clouds (ft)**	**Intervals (s)**	**Pst**	**Coverage Time (s)**
20	1	1000	20	0.2530	34.09
20	6	1000	20	0.4318	34.09
20	10	1000	20	0.4809	34.09
20	20	1000	20	0.4962	34.09
20	30	1000	20	0.4963	34.09
Cloud Speed (mile/hour)	**Number of Clouds**	**Width of Clouds (ft)**	**Intervals (s)**	**Pst**	**Coverage Time (s)**
20	10	1000	2	0.4032	34.09
20	10	1000	5	0.4775	34.09
20	10	1000	7	0.4807	34.09
20	10	1000	10	0.4793	34.09
20	10	1000	15	0.4809	34.09
20	10	1000	20	0.4809	34.09

Table 2.11. Detailed results of the second case study. The cloud motion direction is West-to-East [69].

Case Study	Group	Scenario	Motion Direction	Cloud Speed (mile/hour)	Number of Clouds	Width of Clouds (ft)	Intervals (s)	Pst	Coverage Time (s)
2	1	1	W-E	10	10	1000	20	0.5155	68.18
2	1	2	W-E	15	10	1000	20	0.5620	45.45
2	1	3	W-E	20	10	1000	20	0.5751	34.09
2	1	4	W-E	25	10	1000	20	0.6059	27.27
2	1	5	W-E	30	10	1000	20	0.6158	22.73
2	2	1	W-E	10	10	300	20	0.5461	20.45
2	2	2	W-E	15	10	300	20	0.5581	13.64
2	2	3	W-E	20	10	300	20	0.5758	10.23
2	2	4	W-E	25	10	300	20	0.5752	8.18
2	2	5	W-E	30	10	300	20	0.5749	6.82
Case Study	**Group**	**Scenario**	**Motion Direction**	**Cloud Speed (mile/hour)**	**Number of Clouds**	**Width of Clouds (ft)**	**Intervals (s)**	**Pst**	**Coverage Time (s)**
2	3	1	W-E	20	10	100	20	0.4502	3.41
2	3	2	W-E	20	10	300	20	0.5758	10.23
2	3	3	W-E	20	10	600	20	0.5753	20.45
2	3	4	W-E	20	10	1000	20	0.5751	34.09
2	3	5	W-E	20	10	1500	20	0.5746	51.14
Case Study	**Group**	**Scenario**	**Motion Direction**	**Cloud Speed (mile/hour)**	**Number of Clouds**	**Width of Clouds (ft)**	**Intervals (s)**	**Pst**	**Coverage Time (s)**
2	4	1	W-E	20	1	1000	20	0.3022	34.09
2	4	2	W-E	20	6	1000	20	0.5119	34.09
2	4	3	W-E	20	10	1000	20	0.5751	34.09
2	4	4	W-E	20	20	1000	20	0.5990	34.09
2	4	5	W-E	20	30	1000	20	0.5995	34.09
Case Study	**Group**	**Scenario**	**Motion Direction**	**Cloud Speed (mile/hour)**	**Number of Clouds**	**Width of Clouds (ft)**	**Intervals (s)**	**Pst**	**Coverage Time (s)**
2	5	1	W-E	20	10	1000	2	0.4473	34.09
2	5	2	W-E	20	10	1000	5	0.5580	34.09
2	5	3	W-E	20	10	1000	7	0.5695	34.09
2	5	4	W-E	20	10	1000	10	0.5743	34.09
2	5	5	W-E	20	10	1000	15	0.5748	34.09
2	5	6	W-E	20	10	1000	20	0.5751	34.09

Table 2.12. Detailed results of the second case study. The cloud motion direction is North-to-South [69].

Case Study	Group	Scenario	Motion Direction	Cloud Speed (mile/hour)	Number of Clouds	Width of Clouds (ft)	Intervals (s)	Pst	Coverage Time (s)
2	1	1	N-S	10	10	1000	20	0.4886	68.18
2	1	2	N-S	15	10	1000	20	0.5229	45.45
2	1	3	N-S	20	10	1000	20	0.5241	34.09
2	1	4	N-S	25	10	1000	20	0.5379	27.27
2	1	5	N-S	30	10	1000	20	0.5548	22.73
2	2	1	N-S	10	10	300	20	0.5196	20.45
2	2	2	N-S	15	10	300	20	0.5279	13.64
2	2	3	N-S	20	10	300	20	0.5246	10.23
2	2	4	N-S	25	10	300	20	0.5202	8.18
2	2	5	N-S	30	10	300	20	0.5167	6.82
Case Study	**Group**	**Scenario**	**Motion Direction**	**Cloud Speed (mile/hour)**	**Number of Clouds**	**Width of Clouds (ft)**	**Intervals (s)**	**Pst**	**Coverage Time (s)**
2	3	1	N-S	20	10	100	20	0.4600	3.41
2	3	2	N-S	20	10	300	20	0.5246	10.23
2	3	3	N-S	20	10	600	20	0.5244	20.45
2	3	4	N-S	20	10	1000	20	0.5241	34.09
2	3	5	N-S	20	10	1500	20	0.5135	51.14
Case Study	**Group**	**Scenario**	**Motion Direction**	**Cloud Speed (mile/hour)**	**Number of Clouds**	**Width of Clouds (ft)**	**Intervals (s)**	**Pst**	**Coverage Time (s)**
2	4	1	N-S	20	1	1000	20	0.2854	34.09
2	4	2	N-S	20	6	1000	20	0.4740	34.09
2	4	3	N-S	20	10	1000	20	0.5241	34.09
2	4	4	N-S	20	20	1000	20	0.5417	34.09
2	4	5	N-S	20	30	1000	20	0.5417	34.09
Case Study	**Group**	**Scenario**	**Motion Direction**	**Cloud Speed (mile/hour)**	**Number of Clouds**	**Width of Clouds (ft)**	**Intervals (s)**	**Pst**	**Coverage Time (s)**
2	5	1	N-S	20	10	1000	2	0.4321	34.09
2	5	2	N-S	20	10	1000	5	0.5143	34.09
2	5	3	N-S	20	10	1000	7	0.5185	34.09
2	5	4	N-S	20	10	1000	10	0.5238	34.09
2	5	5	N-S	20	10	1000	15	0.5240	34.09
2	5	6	N-S	20	10	1000	20	0.5241	34.09

and the time interval between clouds is 20 seconds. It can be seen that for the first 10 minutes no Pst value is calculated. However, after 10 minutes of the simulation, Pst values are computed.

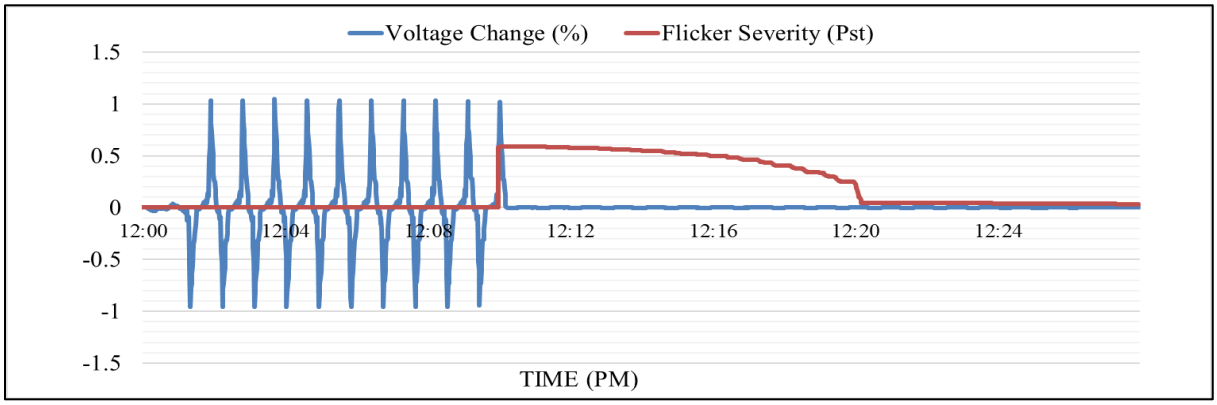

Figure 2.28. Voltage changes and computed Pst values for the second case study, group 1, scenario 3 [69]. © 2018 IEEE

Observations from the case studies are discussed in the following. Figures 2.29-2.32 are based on the first case study, where only one parameter is assessed per figure. However, generally the same trends are recognized for the second case study.

Cloud Speed: For Case Study 1 two groups of scenarios are considered, as shown in Table 2.10. For Group 1 the coverage time is always larger than the decay time, 10 seconds in this study, and for Group 2 the coverage time can be smaller than the decay time.

With increasing cloud speed P_{st} increases as long as the coverage time is greater than the decay time. If the cloud speed results in the coverage time being less than the decay time, increasing the cloud speed can decrease P_{st} slightly. Figure 2.29a demonstrates the impact of cloud speed on P_{st} when the coverage time is always greater than the decay time. Figure 2.29b presents the cloud speed impact when the coverage time can be less than the decay time.

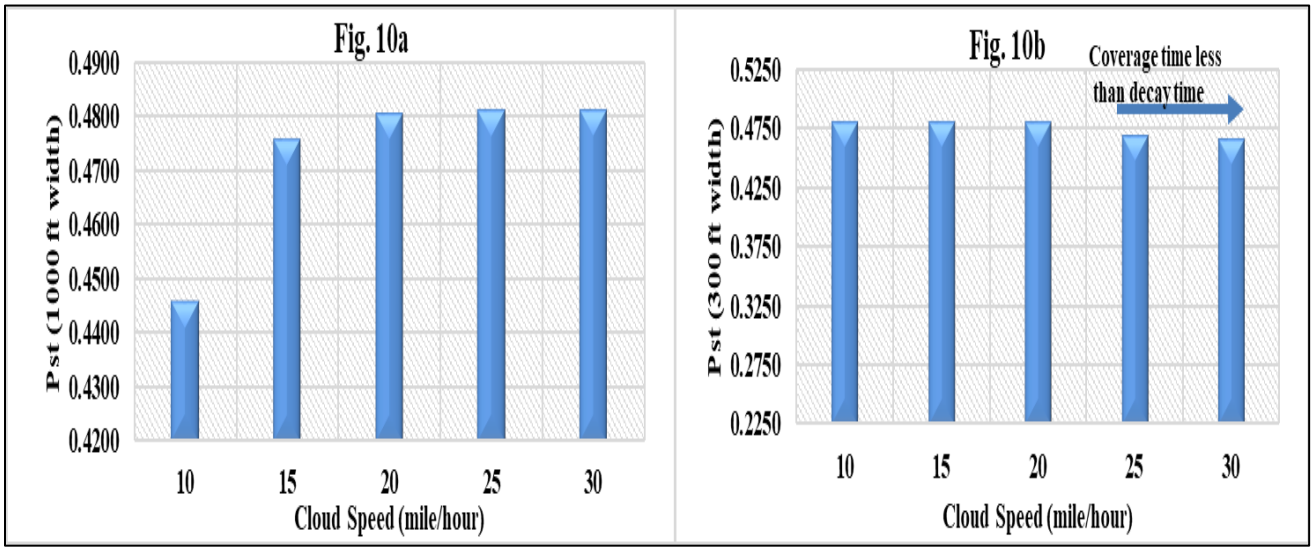

Figure 2.29. Effect of cloud speed on Pst. Fig 12a. Coverage time is always more than the decay time. Fig 12b. Coverage time can be less than the decay time [69]. © 2018 IEEE

Width of Clouds: With increasing width of clouds, Pst increases as long as the coverage time is less than the decay time. When the coverage time is greater than the decay time, increasing the

cloud width results in decreasing Pst slightly. Figure 2.30 shows the effect of cloud width on Pst based on the results of the first case study.

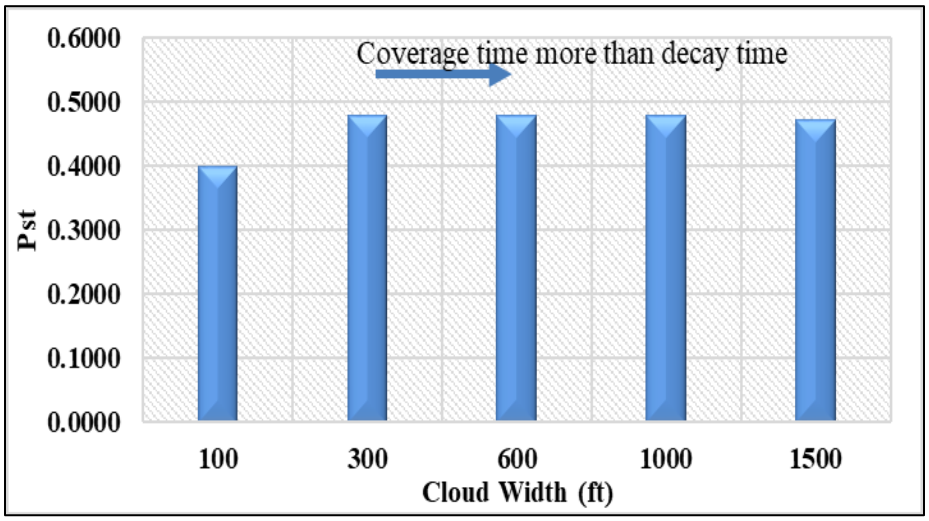

Figure 2.30. Effect of cloud width on Pst from first case study results [69]. © 2018 IEEE

Number of clouds: Generally, increasing the number of clouds results in increasing the number of voltage fluctuations in the 600- second window, resulting in an increasing Pst. However, as shown in Figure 2.31, after the 600-second window is full with voltage changes, increasing the number of clouds does not change Pst values, since it is not going to increase the number of voltage changes inside the 600-second window.

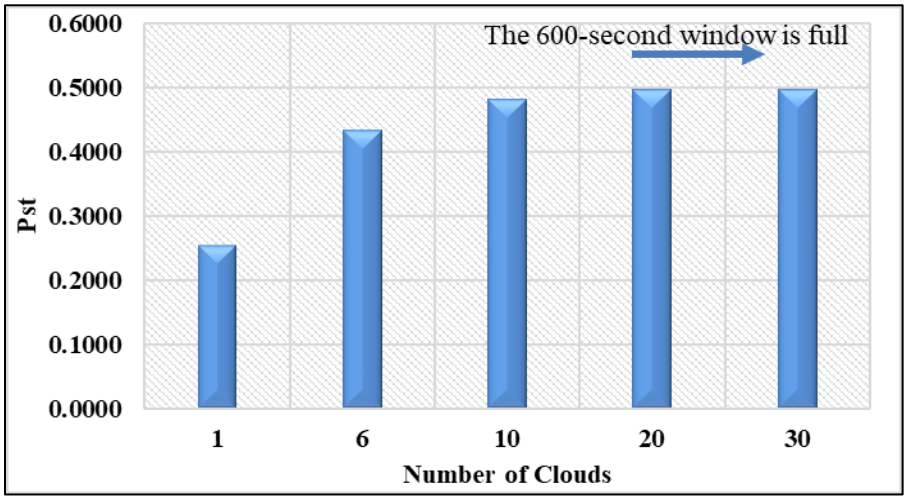

Figure 2.31. Effect of number of clouds on Pst from first case study results [69]. © 2018 IEEE

Time Interval between two successive clouds: By increasing the time interval between clouds to be close to the decay time, Pst increases. However, increasing the interval greater than the decay time does not affect Pst too much as long as all fluctuations are happening inside the 600-second widow of the Pst calculation. Figure 2.32 presents the Pst values versus the time interval between successive clouds.

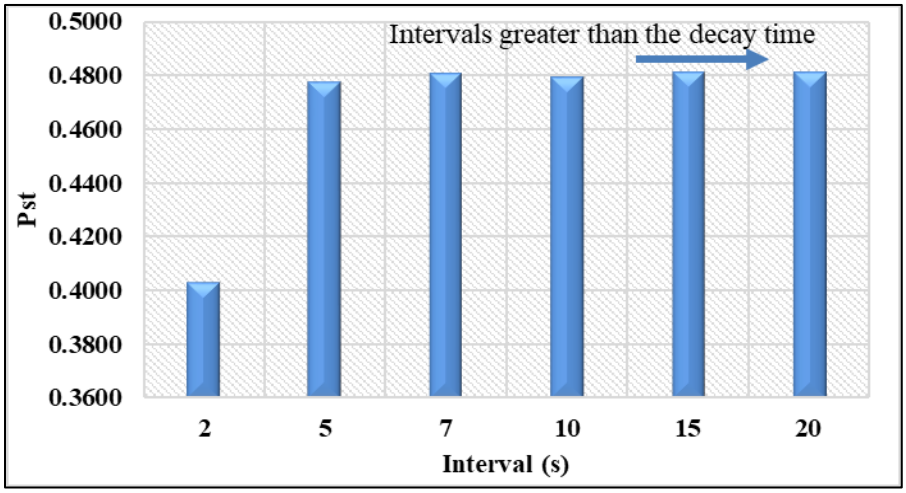

Figure 2.32. Effect of time interval between clouds on Pst from first case study results [69]. © 2018 IEEE

An important takeaway is the impact of cloud motion direction on P_{st}. P_{st} values presented in Tables 2.11 and 2.12, the second case study, which are the maximum P_{st} values calculated in each scenario, show that the direction of cloud motion can affect the maximum value of P_{st}. The difference is due to the fact that for different cloud motion directions different PV generators are affected in the time sequence, and this results in different voltage changes, and consequently different P_{st} values. Such results could not be obtained without the QSS analysis.

2.4.4 Identifying penetration levels using the flicker curve versus employing the flickermeter

In this section, a more realistic distribution feeder is used to compare the penetration levels identified by the flicker borderline of irritation presented in [40] and [41] and flickermeter method employed in [42]. The case study shown in Figure 2.10 is used, but some load values are modified,

and all small-scale PV generators are removed. The main goal of this study is to determine the maximum allowable PV generation connected to the primary side of the feeder based on the aforementioned criteria. Figure 2.33 presents the location of the large-scale PV system used in this study.

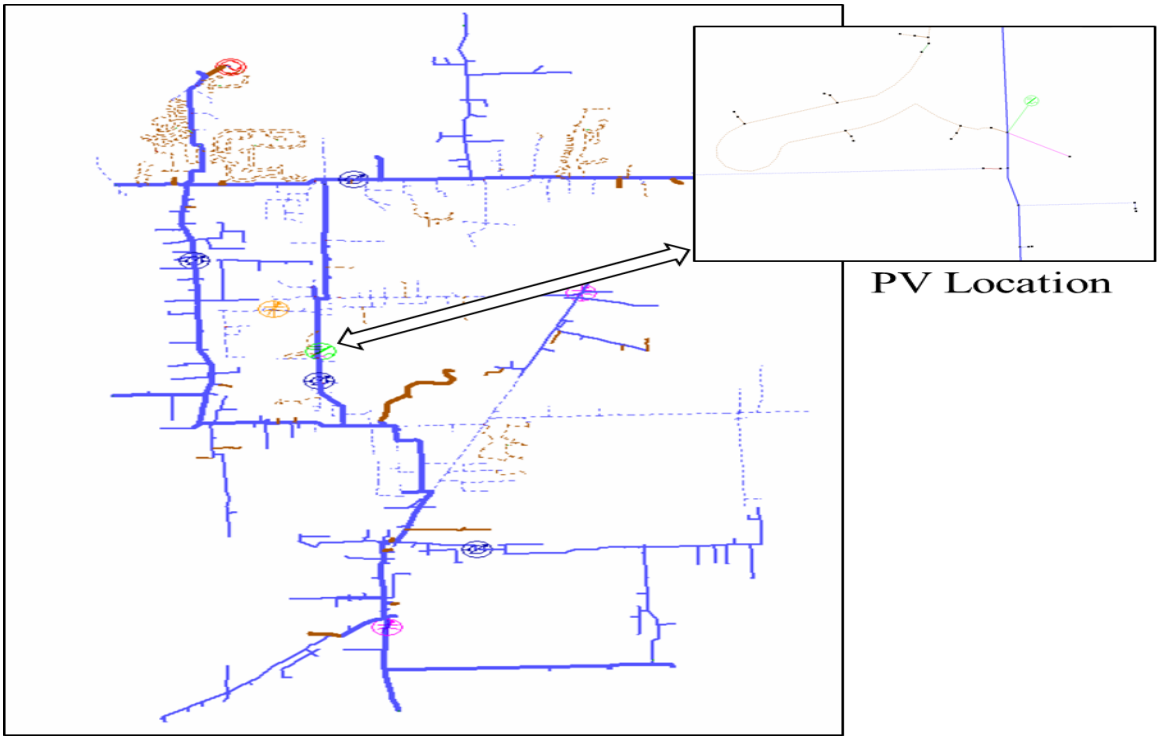

Figure 2.33. Location of the PV system employed to identify penetration levels

Based on the insight provided by previous sections, a set of the CMS parameters is selected to provide the greatest P_{st} values given a specific PV generation size. In other words, the worst case scenario is considered to allow a fair comparison with the flicker curve method. The applied CMS parameters and the P_{st} values at the PV location are presented in Table 2.13. The employed set of CMS parameters results in 30 fluctuations in 10 minutes, which means 3 fluctuations per minute. The corresponding allowable voltage variations based on the borderline of irradiation is 1.5% voltage change per minute. Different generation levels are examined to find which generation level provides 1.5% voltage changes when that specific generation level goes through an 80% decrease,

mimicking the 80% decrease simulated by the CMS. The results show that a 3 MW unit can cause such a voltage change. However, when the penetration level of 32% is considered, and the short-term flicker severity is computed by the CMS, the P_{st} value is 0.323, far away from the 0.9 limit for the medium voltage systems defined by [77] and shown in Table 2.9. Note that here and in the rest of the dissertation, penetration levels are computed based on the load level of the feeders at the time of analysis. Noontime is usually selected for the analysis since the PV generation is at maximum.

Table 2.13.The CMS parameters and penetration levels identified by the flickermeter and flicker curve method

Case	PV Size (kW)	PV Penetration	Cloud Speed (mph)	Number of Clouds	Width of Clouds (ft.)	Intervals (S)	Final Generation Level (%)	Coverage Time (S)	Time Interval	Direction	Pst	Flicker Curve Limit	Observation
1	3000	32%	20	30	300	10	20	10.23	10	W-E	0.323	1.5% per minute limit violated	No overloading or overvoltage
2	15000	160%	20	30	300	10	20	10.23	10	W-E	0.603	1.5% per minute limit violated	Overvoltage issues started to be observed
3	17000	182%	20	30	300	10	20	10.23	10	W-E	0.632	1.5% per minute limit violated	Overloading issues started to be observed

To investigate other penetration limiting criteria, such as ANSI voltage range [79] and overloading of the components, PV size, and consequently the penetration level is increased to determine those limits. As shown in Table 2.13, the system started to encounter over-voltages at the 160% penetration level, and overloading issues at 182% penetration level. However, still, P_{st} values are not close to the 0.9 limit. This case study demonstrates that the flicker curve method can restrict the penetration levels significantly and unnecessarily. On the other hand, the flickermeter method can handle the random nature of the voltage variations induced by PV resources perfectly. It can also prevent such unnecessary limitations on PV penetration levels.

2.5 Conclusion remarks

This chapter introduced a new analysis approach to investigate integration of solar PV resources and addressed flaws of the current PV integration analysis practice.

Currently, steady state step-change analysis is widely applied to probe the impact of the fluctuations of PV resources induced by cloud shadows on voltage. With the step-change method, it is assumed that the irradiance discretely varies from the initial state to the final state, mimicking no cloud coverage and full cloud coverage of solar arrays. Moreover, it is assumed that all PV arrays are affected at once. Both assumptions are unrealistic. Furthermore, cloud motion direction, speed, and the effect of Volt-var control device dead band and delay cannot be simulated precisely with the SS step-change approach.

In this chapter, the QSS analysis approach was introduced, and differences with the current PV steady state analysis were explored through simulations. A cloud motion simulator, which is in charge of performing the QSS simulations, was described, and how the CMS parameters can be estimated from the available meteorological data was discussed.

In addition, this chapter investigated state-of-the-art flicker standards and compared them in terms of identifying maximum allowable PV penetration levels. It was observed that the GE flicker curves, which are currently extensively used in industry, were restricting the penetration levels significantly and unnecessarily. However, when the flickermeter method was implemented by the CMS, and penetration limits were determined and compared with the IEEE 1547.7-2013 limits, it was observed that utilizing the flickermeter method increased the penetration levels considerably.

A case study demonstrated that the proposed analysis approach could increase the penetration level of a realistic distribution feeder by 400% without violating the ANSI voltage limits or overloading the system components.

Chapter 3: Accurate Modeling of Photovoltaic Resources and Secondary Circuits

3.1 Introduction and chapter objective

This chapter investigates the current practices in modeling secondary connections and circuits and discusses their flaws. To address the flaws of current models, a new approach of modeling detailed secondary circuits is presented. Then the proposed secondary models are added to their primary systems and, changes in voltage and voltage flicker values are compared to the case with simplified secondary models.

In the second part of this chapter, the inaccuracy of using point sensor data to model the output of large PV systems is examined. Then a new approach of modeling large PV resources is introduced and several case studies, simulated by the CMS, illustrate its effectiveness to increase the penetration level of PV resources.

The main objective of this chapter is to improve the accuracy of the state of art models in current PV integration analysis. This chapter proposes the use of detailed secondary circuit models to precisely identify voltage issues as well as the utilization of distributed models for large PV resources to expand penetration levels.

3.2 Detailed secondary models

While actual distribution feeders have both primary and secondary circuits, the utilities corresponding circuit models typically only contain the primary components. The models usually exclude the secondary circuits and connections downstream of distribution service transformers, and connect the loads and/or generators to the primary system by using aggregate models.

Sometimes, the distribution service transformers are neglected in the model, and load and/or generation are connected directly to the primary system.

In practice there is usually a secondary conductor between a distribution service transformer and a utility pole. Then a service drop, in case of overhead systems or service lateral, in case of underground distribution systems, completes the path between the service transformer and a customer. Figure 3.1 presents a secondary system with its components. A service drop may have two conductors for 1-phase systems, or three conductors for 3-phase systems, and a neutral conductor. When these conductors are insulated and twisted together, they are referred to as a triplex cable.

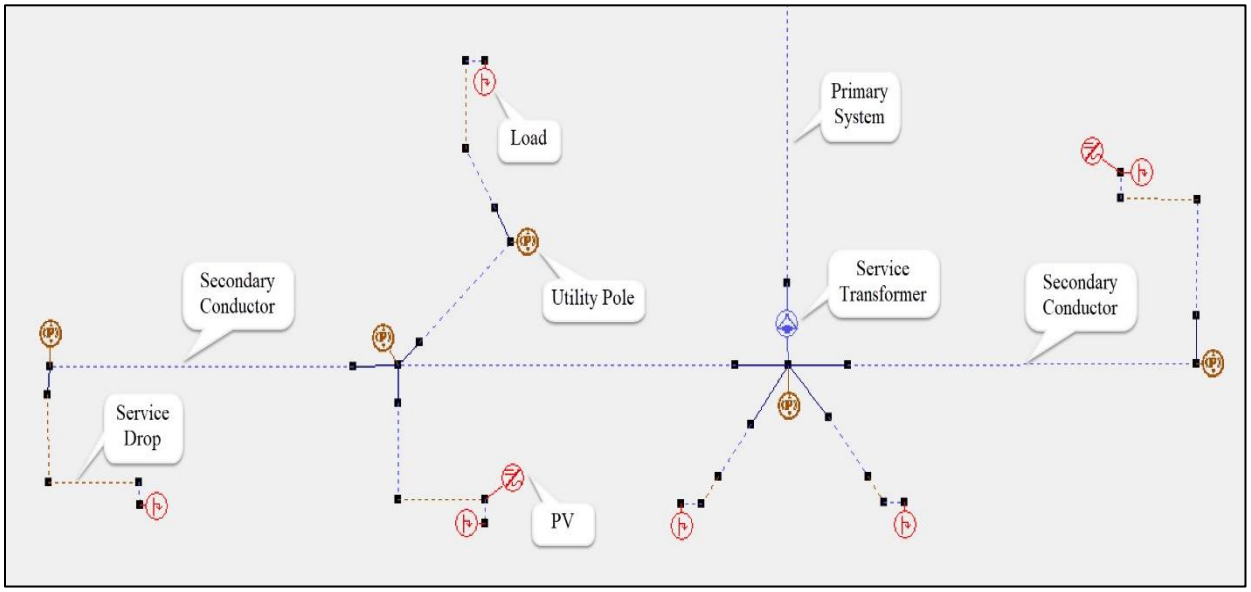

Figure 3.1. A typical secondary system with load and PV generation

Currently all components downstream of distribution transformers are ignored and lumped models of loads and generators are employed as shown in Figure 3.2. In some cases, even the service transformers are ignored, and aggregate load and generation are directly connected to the primary systems [12], [48]-[52]. Some studies have tried to improve the model accuracy by adding an impedance between the service transformer and lumped loads and/or generators [80]-[83].

However, estimating the voltage drop between service transformers and loads on real circuit models, which may have different load types, as well as estimating the impedance for different secondary configurations, requires a lot of assumptions and simplifications, which makes such secondary models ultimately inaccurate.

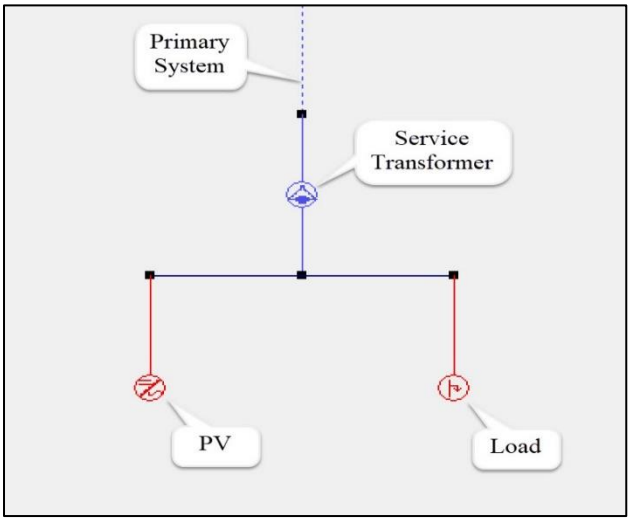

Figure 3.2. A simplified secondary model with aggregate load and generation

Modeling all secondary components and adding them to primary models of distribution systems, which already have a large number of components, created computer memory and divergence issues in the past due to the large size of the problem. However, due to the increased computational power of computers today, the aforementioned issues can be overcome. In addition, considering high growth rate of small-scale distributed PV resources, which are connected to the secondary side of distribution systems, modeling of secondary circuits has turned into a necessity to accurately analyze voltage variations of PV resources. It is obvious that without modeling the electrical circuits to which the PV resources are connected, accurate analysis of voltage issues is not possible. This section investigates the importance of modeling secondary circuits and proposes a new approach to model detailed secondary circuits, which can identify potential voltage problems of PV resource interconnection.

3.2.1 Importance of detailed secondary models to the analysis accuracy

To illustrate the importance of modeling secondary circuits, a simple example is used which considers the impacts of service transformer and secondary conductor impedances on voltage analysis. Figure 3.3 presents the employed 3-phase system, consisting of a 1-mile primary conductor, a 150 ft. secondary conductor, and a 20 kVA load with 0.95 power factor. No PV generation is considered in this case. The goal is to investigate the voltage drop over the secondary system. The following are the three assessed cases:

Case 1: Service transformer and secondary conductor are modeled.

Case 2: Only service transformer is modeled.

Case 3: Load is directly connected to the primary system.

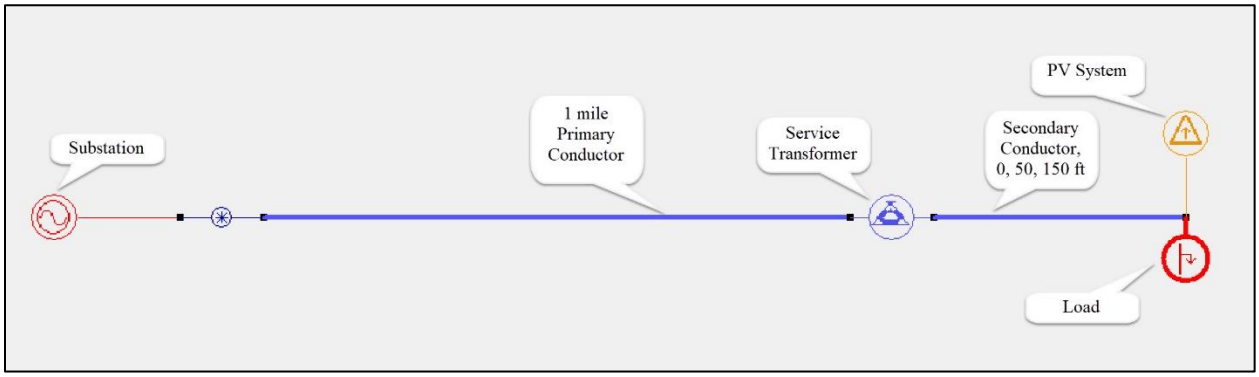

Figure 3.3. Simple circuit model to study importance of secondary circuits

Voltages at the load location are provided in Table 3.1 for the three cases. Table 3.1 shows that ignoring the impedance of service transformer, which is a 30 kVA transformer, imposes some error. However, ignoring the secondary conductor causes a significant voltage error. In this example, not modeling the secondary circuits hides the under-voltage issue happening at the load location. However, in the case of ignoring the secondary circuit, a 119.4 V, a reasonable voltage level, is observed at the load location. Therefore, for accurate analysis of the voltage drop, between service transformers and loads, detailed secondary models are essential.

Table 3.1 Voltages at load location of figure 3.3 while using the same load

Phase A Voltage (V)	Phase B Voltage (V)	Phase C Voltage (V)	Modeled Secondary Components
113.81	114.11	114.01	Transformer and Secondary Conductor (150 ft)
119.36	119.37	119.37	Transformer
119.98	119.98	119.98	None

The impedance of secondary conductors and service drops are dependent on their lengths. The impedance of distribution service transformers can also be different. Table 3.2 provides the range of impedance values based on the capacity of service transformers [84].

Table 3.2. Percent impedance range of service transformers [84]

kVA Rating	Percent Impedance
75	1.00-5.00
112.5-300	s1.20-6.00
500	1.50-7.00
700-2500	5.75

Another aspect of ignoring secondary circuits is the inaccuracy it introduces in voltage sensitivity to real and reactive power variations. To investigate the impact of secondary circuit impedances on the voltage sensitivity, three lengths of 0, 50, and 150 ft. are selected for the secondary conductor of Figure 3.3. For each secondary conductor length, a PV system injects either 10 kW or 10 kvar to compute the voltage sensitivity to real and reactive powers, respectively. Results of the analysis are presented in Table 3.3 and Figure 3.4. It is observed that with the 0 ft. secondary conductor, the sensitivity of the voltage to reactive power is approximately five times that of the sensitivity of the voltage to real power. With the 50 ft. secondary conductor, the sensitivity values are close to each other, noting that the sensitivity to real power is slightly higher. However, in the case of the 150 ft. secondary conductor, the sensitivity of the voltage to real power is more than twice the sensitivity of the voltage to reactive power.

Table 3.3 Results of sensitivity analysis to real and reactive power injections at the load location of Figure 3.3

Secondary Length (ft)	Voltage (V) (No Injection)	Voltage (V) (After injection)	Voltage Change (V)	Voltage Change (%)	ΔP (kW)	ΔQ (kvar)	ΔV/ΔP	ΔV/ΔQ	R1 (Ohm)	X1 (Ohm)	R1/X1
0	119.36	119.49	0.127	0.106%	10	0	0.0127	0.0000	0.0043	0.0230	0.19
50	117.57	118.58	1.004	0.854%	10	0	0.1004	0.0000	0.0339	0.0310	1.09
150	113.81	116.70	2.890	2.539%	10	0	0.2890	0.0000	0.0930	0.0471	1.98
0	119.36	120.01	0.640	0.536%	0	10	0.0000	0.0640	0.0043	0.0230	0.19
50	117.57	118.45	0.880	0.748%	0	10	0.0000	0.0880	0.0339	0.0310	1.09
150	113.81	115.20	1.389	1.221%	0	10	0.0000	0.1389	0.0930	0.0471	1.98

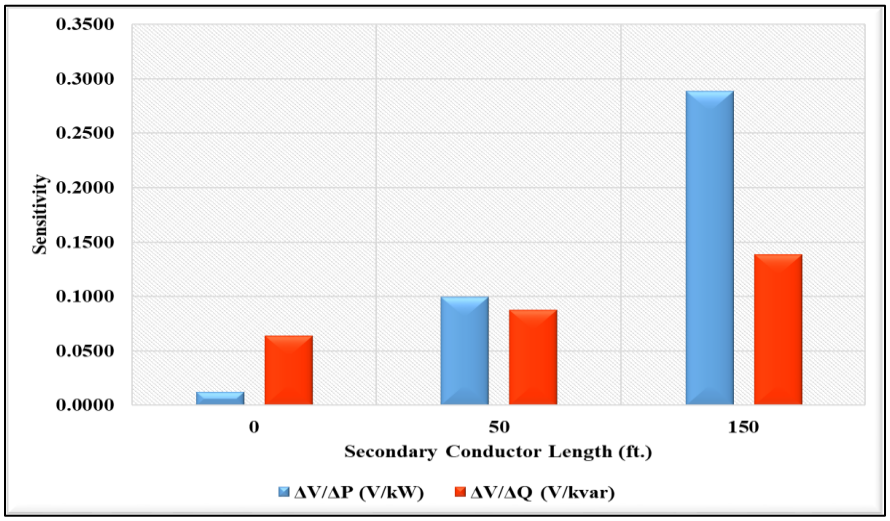

Figure 3.4. Results of sensitivity analysis to real and reactive power with different secondary conductor lengths

Several studies have investigated the sensitivity of voltage to real and reactive power, mainly to develop Volt-var control schemes to achieve effective voltage control [13], [85]-[88]. The following provides the main logic behind those voltage sensitivity studies.

In a balanced circuit model, represented by an equivalent per-phase resistance R_{eq} and reactance X_{eq} between the source and bus i, the voltage of bus i can be estimated by equation 3.1 [86].

$$V_i = V_0 + \frac{R_{eq} * P_i + X_{eq} * Q_i}{V_i} \qquad (3.1)$$

where, P_i, Q_i are the active and reactive powers, respectively, injected/absorbed at bus i. Therefore, the sensitivity of voltage at bus i due to variations of P_i, Q_i can be computed by equation 3.2.

$$\frac{\partial V_i}{\partial_{P_i}} = \frac{R_{eq}}{V_i}, \quad \frac{\partial V_i}{\partial_{Q_i}} = \frac{X_{eq}}{V_i} \qquad (3.2)$$

Equation (3.2) shows that the resistance and reactance between bus i and the source/substation define the voltage sensitivities to real and reactive powers, respectively.

Most above-mentioned voltage sensitivity studies have assumed that the studied system was balanced and have not considered the unbalance imposed by the conductors. However, the case study used in this section for voltage sensitivity analysis is not balanced. Table 3.3 demonstrates that, by increasing the length of the secondary conductor, the ratio of R1 over X1 is increasing, and that is why the sensitivity of voltage to real power is less than reactive power with no secondary conductor. However, with the 150 ft. secondary conductor, the sensitivity of voltage to real power is twice that of the reactive power. Note that the conductors used in distribution have higher R/X ratios than the conductors used in transmission.

In addition, the analysis in [12] shows that, in some cases, the customers without PV generation, but sharing a secondary with a customer with PV, may encounter higher voltage changes compared to the customers with PV generation, but electrically closer to the substation, due to irradiance fluctuations. The mentioned case study of [12] also proves the falsehood of the assumption that locations with PV generation have the greatest voltage changes, and locations without PV generation are safe from drastic voltage changes and flicker issues. By considering the importance of modeling secondary circuits, the next section provides a practical way of modeling detailed secondary circuits.

3.2.2 Developing secondary models based on customer information

The proposed method in this section aims to provide a practical method to model detailed secondary circuits, which are customized for each distribution system/utility, and employ them

instead of simplified secondary circuits. In the first step the most common secondary configurations need to be identified and modeled. Most utilities do not have detailed information of every customer and its corresponding secondary system, but they have information regarding the number of customers connected a distribution service transformers, as well as billing information of those customers. In the case of existence of Automatic Meter Reading (AMR) and Advanced Metering Infrastructure (AMI) systems, time-stamped data of service transformers may also be available. Figure 3.5 shows 38 secondary configurations, which are developed based on the most common secondary configurations of multiple distribution feeders in California, including up to 38 customers connected to a service transformer. These secondary configurations can be selected according to the number of customers and automatically be added to the corresponding primary system models.

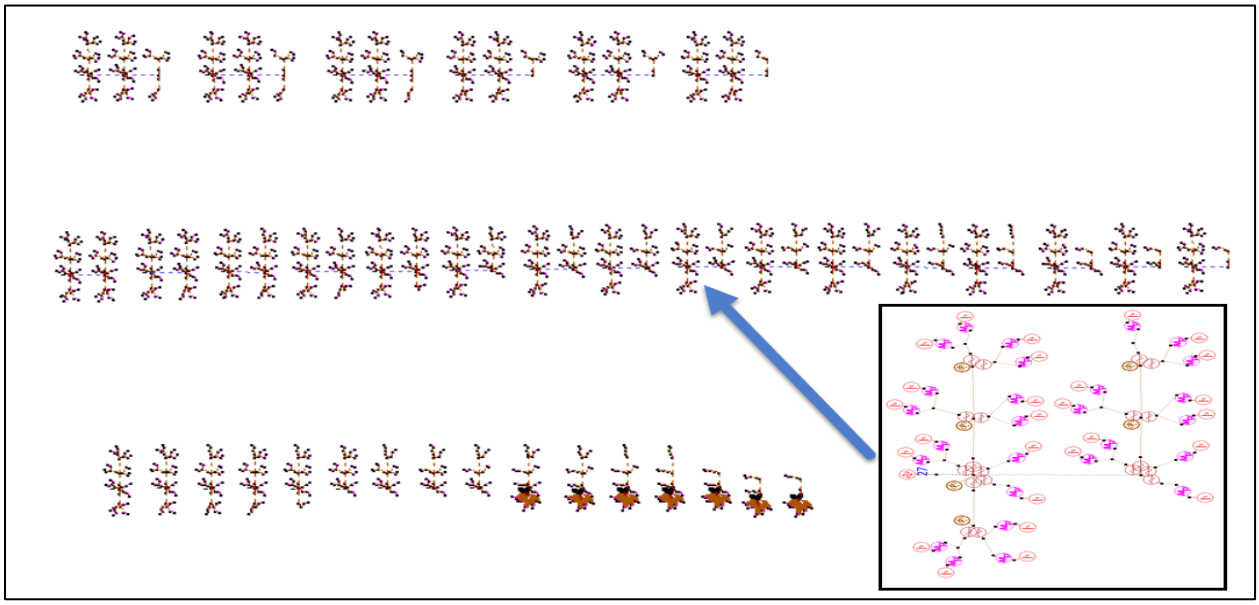

Figure 3.5. Developed secondary circuits based on the most common secondary configurations

3.2.3 Effect of detailed secondary models on identifying PV penetration levels

Previously, a comparison is performed between the flicker curve and flickermeter methods in terms of determining maximum PV penetration levels. This section investigates the impacts of

secondary circuits on identifying penetrations levels combined with the aforementioned flicker limits. This section also probes the impact of modeling secondary circuits on QSS voltage changes and flicker values.

The circuit model shown in Figure 3.6 is used as the case study. The secondary voltage is 240/120 V. On the circuit model there are 16 secondary circuit models, where eight are simplified secondary models and eight are corresponding detailed secondary models. The simplified secondary models are obtained by neglecting the secondary conductors and service drops, and aggregating the load and generation. Since the secondary circuits are all fed from the same point on the primary system, comparing the voltage changes observed in the simplified secondary circuit models with their corresponding detailed models is straightforward.

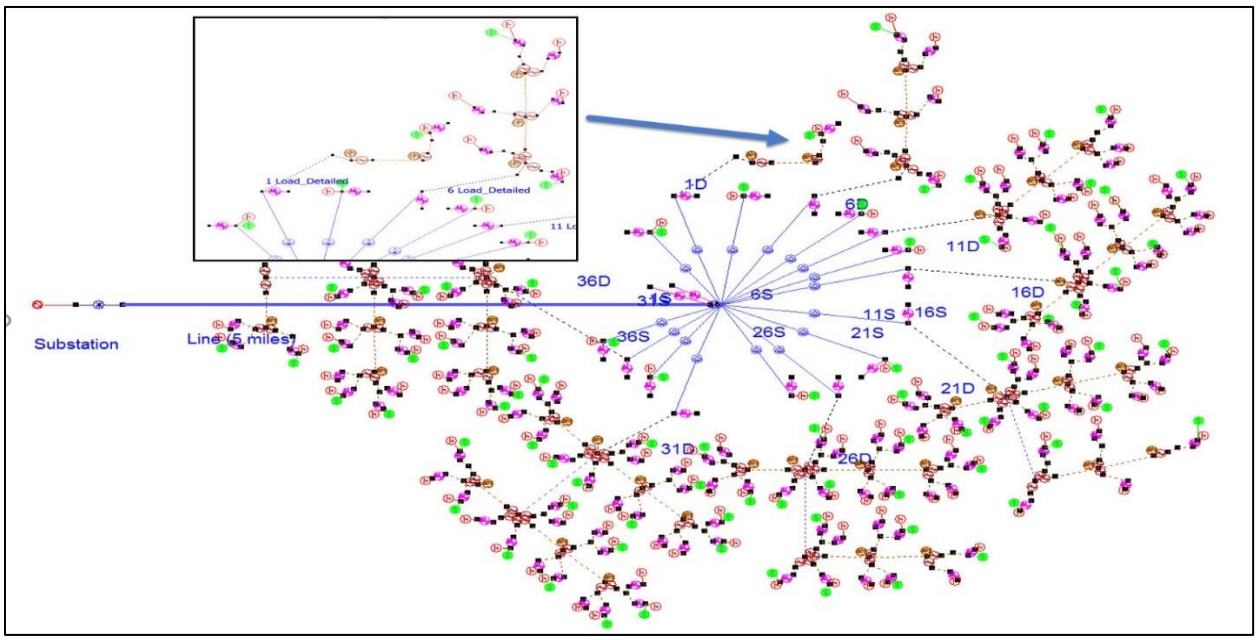

Figure 3.6. Test circuit model with detailed secondary circuit models and their corresponding simplified secondary models.

The detailed secondary models of the test circuit varies from one customer with one PV generator to 36 customers with 20 PV generators. The simulations all started at 12:00 pm when the total load on the feeder was 1280 kW. Given that the load is from an hourly profile, the load

remained constant in the second-by-second simulations. If high-resolution load data is available it can be incorporated into the analysis. However, given that PV and load fluctuations are typically uncorrelated, using static load data should have minimal impact on the results. Table 3.4 presents the number of customers and PV generators for each detailed secondary model, including the maximum length of conductor run for each secondary model.

Table 3.4. Characteristics of detailed secondary circuits

Secondary model	Number of customers	Number of PV generators	Maximum length of secondary path from distribution transformer to the furthest load (ft.)
1D	1	1	145
6D	6	2	315
11D	11	5	315
16D	16	8	315
21D	21	11	365
26D	26	14	365
31D	31	17	365
36D	36	20	365

Impact of secondary circuit models on maximum PV penetration levels

Four analysis approaches to determining the maximum allowable levels of PV penetration are compared. From this the effects of using different standards and secondary models can be observed. The first approach, referred to as the **S**implified **S**econdary **S**teady **S**tate (**SS^2**) approach, employs the following in PV generation simulations:

- Secondary systems are modeled with a distribution transformer and an equivalent lumped load and generator.
- Changes in PV generation are simulated with a step change.
- Border of irritation flicker, as defined in the IEEE 1453-1992 standard, is used to determine the maximum allowable limit of PV generation penetration.

In the second approach, referred to as the Detailed Secondary Steady State (DSSS) approach, the maximum allowable level of PV penetration is determined based on the followings:

- Secondary systems are modeled in detail included secondary and service conductors, where each individual customer is represented by a separate load bus.
- Changes in PV generation are simulated with a step change.
- Border of irritation flicker, as defined in the IEEE 1453-1992 standard, is used to determine the maximum allowable limit of PV generation penetration.

The third employed approach, referred as the Simple Secondary Quasi-Steady State (SSQS) approach, uses the following in calculating maximum allowable PV penetration level:

- Secondary systems are modeled with a distribution transformer and an equivalent lumped load and generator.
- Changes in PV generation due to changing cloud cover are modeled with a piece-wise linear curve.
- The P_{st} is used to identify the maximum allowable limit of PV generation penetration.

The fourth approach, referred to as the Detailed Secondary Quasi-Steady State (DSQS) approach, to determining the maximum allowable level of PV penetration employs the following:

- Secondary systems are modeled in detail included secondary and service conductors, where each individual customer is represented by a separate load bus.
- Changes in PV generation due to changing cloud cover are modeled with a piece-wise linear curve

The P_{st} is used to determine the maximum allowable limit of PV generation penetration.

Table 3.5 presents the assumptions used in the four aforementioned analysis approaches.

Table 3.5. Summary of the analysis approaches

Analysis Approach	Secondary Model	PV Generation Simulation	Flicker Standard Used
SS^2	Simplified	Step Change Steady State	Flicker Curve
DSSS	Detailed	Step Change Steady State	Flicker Curve
SSQS	Simplified	Quasi Steady State	Flickermeter
DSQS	Detailed	Quasi Steady State	Flickermeter

For the SSQS and DSQS simulations, the maximum level of PV penetration is determined by the flickermeter calculations computed by the CMS and the limits presented in Table 2.9 [77]. Table 3.6 shows the employed CMS parameters in the SSQS and DSQS simulations.

Table 3.6. Employed CMS parameters

Parameter	Parameter Description	Parameter Value
p_1	Number of clouds	40
p_2	Direction of the cloud motion	west-to-east
p_3	Speed of cloud shadows	30 miles/hour (44 ft/sec)
p_4	Time between successive clouds	5 seconds
p_5	Width of clouds	440 feet
p_6	Rate of change of PV generation	20% change in generation by end of second 1 60% change in generation by end of second 5 80% change in generation by end of second 10

The above CMS settings result in four voltage fluctuations per minute, since four clouds pass over a specific point in the system per minute. Based on the borderline of irritation presented in [40], [41], four voltage fluctuations per minute correspond to an irritation boundary voltage change of 1.4%. The 1.4% value is thus to be used to determine the maximum level of PV penetration in the SS^2 and DSSS approaches. With the SS^2 and DSSS approaches, which use the steady state step-change method, the maximum level of allowable PV penetration is determined when a violation occurs above the threshold of irritability when PV generation decreases from 100% to 20%. Table 3.7 summarizes the results from applying the four analysis approaches to the test circuit.

Table 3.7. Comparison of maximum voltage changes and maximum allowable PV penetration levels for SSSS, DSSS, SSQS, and DSQS approaches for the test circuit

Analysis Approach	Threshold of Irritability ($\Delta V\%$)	Secondary P_{st}	Maximum Allowable PV Penetration (% of load)
SS^2	1.4%	N/A	41
DSSS	1.4%	N/A	31
SSQS	N/A	1.007	500
DSQS	N/A	1.008	365

For the SS^2 case that used simplified secondary models and the flicker curve voltage limit of 1.4%, a 41% PV penetration is the maximum allowable level. PV penetration is computed based

on the current load of the system, which is 1280 kW. For the DSSS case, using detailed secondary models and the flicker curve voltage change limit of 1.4%, the maximum PV penetration allowed is 31% (397 kW). Comparing the two secondary models using the flicker curve method, it is observed that the detailed secondary models have voltage flicker violations at lower penetrations.

For the SSQS case, where simplified secondary models and the flickermeter method are used, a P_{st} flicker violation, based on the IEEE 1547.7-2013 [77], in the second decimal place occurred at a 500% PV penetration level (6.4MW). When analyzing the allowable PV penetration on the simplified secondary models, the flicker curve method allows 459% (5.9MW) PV penetration. Thus, use of the flicker curve method limits PV penetration. However, a PV penetration of 365% is likely unattainable due to other limiting factors, such as thermal overloads or ANSI voltage limits.

For the DSQS case, where the flickermeter method and detailed secondary models are used, a P_{st} violation in the second decimal place resulted at a 365% penetration (4.7MW). When comparing both methods that utilized the flickermeter method, voltage violations occurred at lower penetrations with the detailed secondary circuits (365%) compared to the simplified secondary models (500%).

When comparing the flicker curve and flickermeter results of the detailed secondary studies, the allowable penetration levels are significantly higher for the flickermeter analysis, as observed in the previous chapter. For the DSSS, the allowable PV penetration is just 31%. When the same detailed secondary models are studied again with the flickermeter, the allowable PV penetration increased by 334% (from 31% to 365%) when compared to the analysis with the flicker curve method.

Impact of secondary circuits on maximum QSS voltage changes and flicker values

To show the difference of QSS voltage changes and P_{st} values computed using detailed and simplified secondary models, comparing SSQS and DSQS approaches, a 50 % PV penetration is considered. The same cloud pattern shown in Table 3.6 is employed. Table 3.8 and Figure 3.7 compare the differences in results of maximum QSS voltage increases, QSS voltage decreases, and P_{st} values between the detailed models and their corresponding simplified secondary models. Negative values mean that the magnitudes of maximum quantities from the detailed models are greater. Positive values mean simplified secondary models quantities have greater magnitudes. From Table 3.7, maximum QSS voltage increase, QSS voltage decrease, and short-term flicker values between the SSQS and DSQS approaches have error ranges from -54% to +33%, from -45% to +13%, and from -20% to 15%, respectively. Such error ranges indicate that the simplified models cannot provide accurate results for voltage issues analysis, and detailed secondary models are required for precise identification of voltage problems.

Table 3.8. Errors of maximum voltage increases, voltage drops, and P_{st} values between the SSQS and DSQS approaches performed on the feeder shown in Figure 8 when PV penetration is 50%.

Number of Customer(s)	Maximum Difference of Voltage Increase	Maximum Difference of Voltage Drop	Maximum Difference of P_{st} Values
1	-3.23%	-4.01%	-2.48%
6	0.05%	10.90%	12.15%
11	31.58%	-31.43%	-6.59%
16	33.46%	-44.91%	-5.36%
21	24.36%	-14.87%	14.53%
26	-11.36%	-24.55%	-5.19%
31	12.67%	13.24%	-7.07%
36	-53.67%	-31.37%	-20.28%

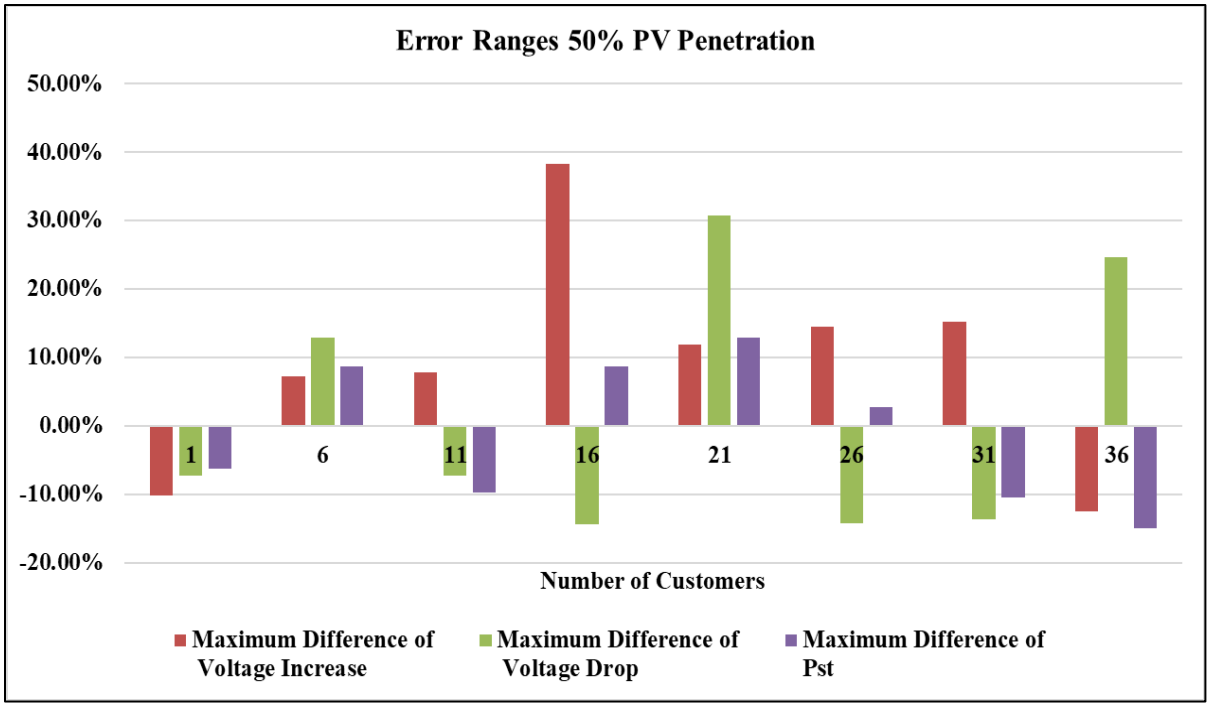

Figure 3.7. Maximum error in the QSS voltage increases, QSS voltage decreases, and Pst values between the SSQS and DSQS approaches

3.3 Distributed models of large photovoltaic systems

Currently, point sensor data is used to estimate the generation of PV resources, regardless of their size, as there are many public databases that contain these datasets. For small-scale PV systems, point models are useful and accurate enough. However, for large PV systems that span over acres of land, employing a pyranometer measurements cannot be an accurate representation of the whole PV system generation as well as its fluctuations. It is because point sensors can over-represent the variability in generation output caused by cloud shadows. A partially covered PV system is a good example to use to understand the inefficiency of point sensor data to model the generation of large PV resources. Note that no matter how fast a cloud is moving, it takes the cloud some time to cover/uncover a PV system spread over a large geospatial area.

This section proposes a new method to model large PV resource using distributed models. Developing the CMS allows validating the proposed method easily. Through several case studies,

differences of voltage changes and flicker values computed by the point and distributed models are compared. Moreover, the impact of the distributed model of large PV systems on maximum allowable PV penetration level is also examined.

A portion of [69] is re-formatted and reused in this section. The first author of [69] is the author of this dissertation and the reuse is in compliance with IEEE policy at the time of writing this dissertation. The policy can be found in the appendix. Note that IEEE holds the copyright of [69], whose citation is provided in the bibliography.

3.3.1 Case studies of employing the PV distributed model to investigate voltage changes and flicker values of large PV resources

Two model types are considered for modeling large PV resources in the case studies presented in this section, point and distributed models. With a point model the CMS treats the large PV unit just like a single, smaller PV generator, similar to rooftop PV systems of a few kW. With the point model, when a cloud initially covers the PV unit, the total PV generation immediately decays according to the decay curve discussed in the previous chapter. In the distributed model the large PV system is modeled by breaking it into a number of point PV generators spread over the associated geographical area. Each individual point PV generator in the distributed generator model reacts independently to the cloud cover(s).

Case study 1

This case study employs the circuit model used in section 3.2.3 and presented in Figure 3.6. However, since large PV systems are connected to the primary side of power systems, all PV generators in the secondary circuits are turned off, and one central generator is attached to the primary side of the system. Again the four analysis approaches used in section 3.2.3 are used to

identify maximum allowable PV penetration levels with the point model used. Results of the analysis are provided in Table 3.9.

Table 3.9. Comparison of maximum allowable primary PV penetration for SSSS, DSSS, SSQS, and DSQS analysis approaches, using a point model

Analysis Approach	Threshold of Irritability	Primary P_{st}	Secondary P_{st}	Maximum PV Penetration (% of load)
SSSS	1.4%	N/A	N/A	56
DSSS	1.4%	N/A	N/A	56
SSQS	-	0.90	0.94	490
DSQS	-	0.90	0.94	490

After assessing the point model, a distributed PV model with the size of 6.3 MW is considered, which corresponds to the 490% maximum PV penetration level with the point model. A square area of 38 acres was used for the 6.3 MW distributed generator. Note that each MW of PV generation typically requires 5-7 acres of land [88]. The PV generation was distributed as shown in Figure 3.8. Nine PV generators, each with a capacity of 700 kW, were modeled over a geospatial area corresponding to 38 acres. Only the DSQS and SSQS cases were considered for the distributed generator model, as the Flicker curve does not directly address this type of geospatial analysis. The cloud parameters from Table 3.6 are used again. With a cloud speed of 30 mph (44 ft/s), once the first cloud comes to the edge of the generator, it takes the cloud approximately 29 seconds to move over the entire area of the distributed generator. Sometimes in the simulation there are two clouds partially covering the distributed generator at the same time. Previously, with the point model, the P_{st} on the primary exceeds 0.9 at the 490% PV penetration level. However, when the PV unit is distributed, the maximum value computed for P_{st} is 0.56 on the primary and 0.58 on the secondary side, far away from 0.9 and 1.0 limits. With the distributed model, the clouds cover the distributed

PV generator gradually (in this case nine point PV generators). Therefore, the per-second voltage changes are smaller, which results in smaller values of P_{st}.

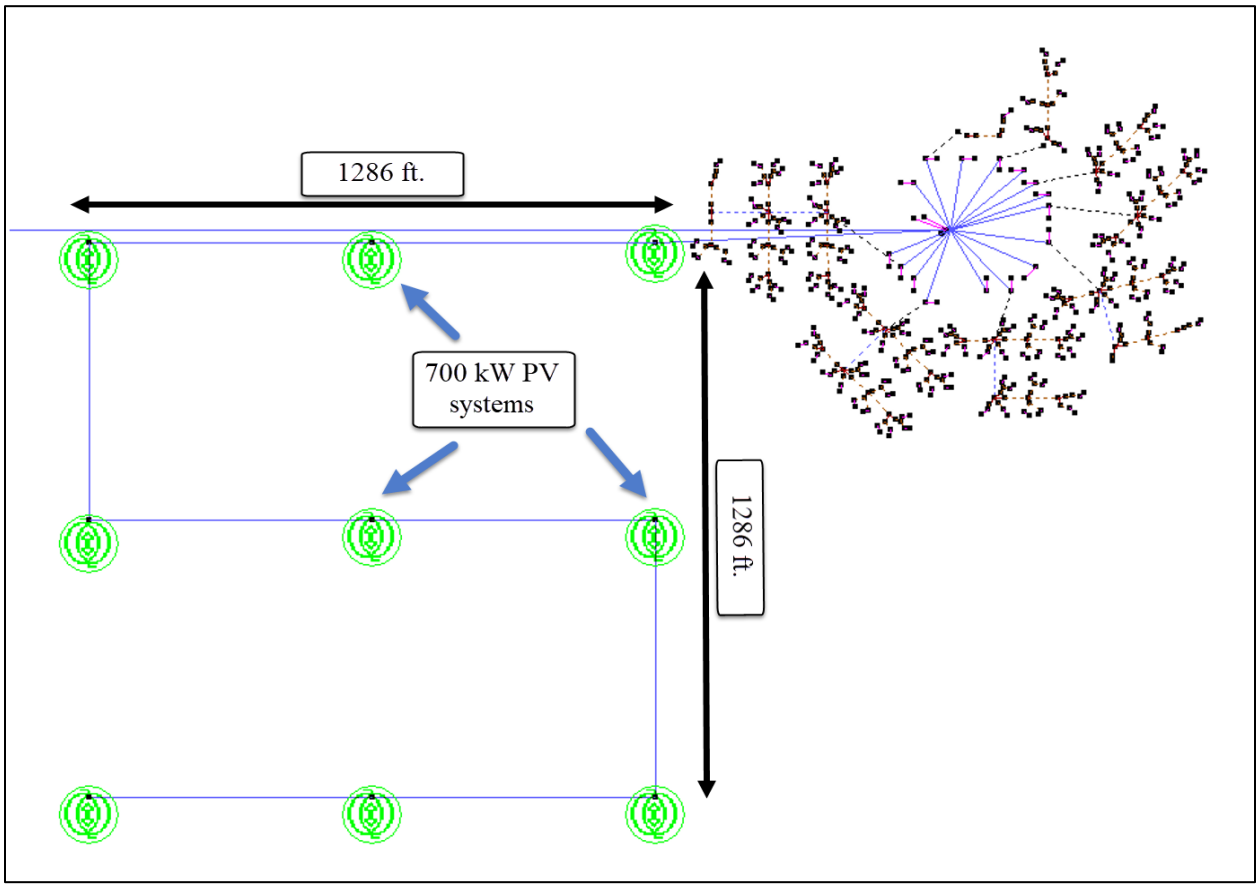

Figure 3.8. Modeling of 6.3 MW generator with nine point generators

Table 3.10 presents the maximum PV penetration levels when the P_{st} limit of 0.9 is violated for both the point and distributed PV models. Relative to flicker violations, the distributed PV model allows a PV unit approximately three times larger than the point model. This analysis shows that using distributed models, which are more realistic, results in smaller QSS voltage changes and consequently, smaller flicker severities. Therefore, using the distributed model increases PV penetration levels as long as other limiting factors, such as overloading and over-voltages, have not restricted the penetration levels already.

Table 3.10. Comparison of PV penetration levels when evaluating the Point and Distributed PV Model

PV Model Type	Analysis Approach	PV Penetration (% of load)	Max Primary P_{st}	Max Secondary P_{st}
Point	SSQS/DSQS	490	0.90	0.94
Distributed	SSQS/DSQS	490	0.56	0.58
Distributed	SSQS/DSQS	1600	0.90	0.93

Case study 2

The second case study is the realistic circuit model, which was presented in section 2.4.3 and is shown in Figure 2.33. In section 2.4.3, a comparison between maximum allowable penetration levels identified by the flickermeter and flicker curve methods is performed by employing a point model of the PV system. This section applies a distributed model, including five smaller PV systems, and compares the computed P_{st} values by the CMS.

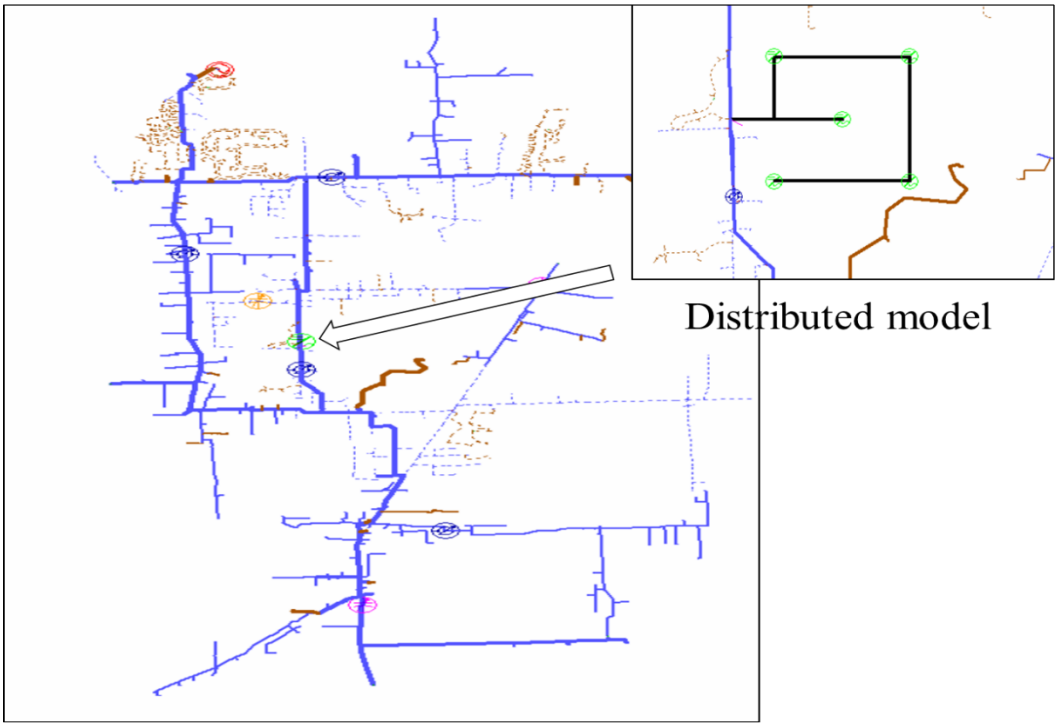

Figure 3.9. Modeling the case study of section 2.4.3 with a distributed PV model

The employed CMS parameters in the analysis and computed P_{st} values are provided in Table 3.11. Table 3.11 demonstrates that using the distributed PV model decreases the short-term flicker values approximately 30% for both PV penetration levels examined. This case study also emphasizes the importance of using distributed models for large PV resources to obtain realistic results.

Table 3.11. Employed CMS parameter and computed P_{st} values of point and distributed models

PV Size (kW)	PV Penetration	Cloud Speed (mph)	Number of Clouds	Width of Clouds (ft.)	Intervals (S)	Final Generation Level (%)	Coverage Time (S)	Time Interval	Direction	PV Model	Pst
15000	160%	20	30	300	10	20	10.23	10	W-E	Point	0.603
17000	182%	20	30	300	10	20	10.23	10	W-E	Point	0.632
15000	160%	20	30	300	10	20	10.23	10	W-E	Distribued	0.421
17000	182%	20	30	300	10	20	10.23	10	W-E	Distribued	0.439

Case study 3

The third case study of this section is the circuit model which was used in section 3.4.4 and is shown in Figure 2.27. The same analysis approach, similar to the previous case studies, is applied, and P_{st} values are compared by the CMS when point and distributed models are utilized.

In order to perform the comparison, the 500 kVA PV system is broken into four smaller 125 kVA PV generators, where a square area of 2.5 acres is considered for the 500 KVA distributed generator. Therefore, each 125 kVA generator is placed 330 ft. away from other generators, covering 2.5 acres. The distance between PV generator 1 and PV generators 2 and 3 of Figure 3.10 is 330 ft. Similar to section 3.4.4, all scenarios are simulated and the resulting P_{st} values are computed. Table 3.12 presents the maximum flicker decrease in each group. It can be seen that in some cases P_{st} values decreased by 48% by using the distributed model.

Table 3.12. Comparison of P_{st} values, while using point and distributed models. In each group, the scenario with the greatest decrease is selected [69].

Case Study	Group	Scenario	Pst (Point Model)	Pst (Distributed Model)	Percentage Decrease
1	1	2	0.4761	0.2757	42%
1	2	1	0.4807	0.2649	45%
1	3	2	0.4816	0.2911	40%
1	4	4	0.4962	0.3046	39%
1	5	3	0.4807	0.2499	48%

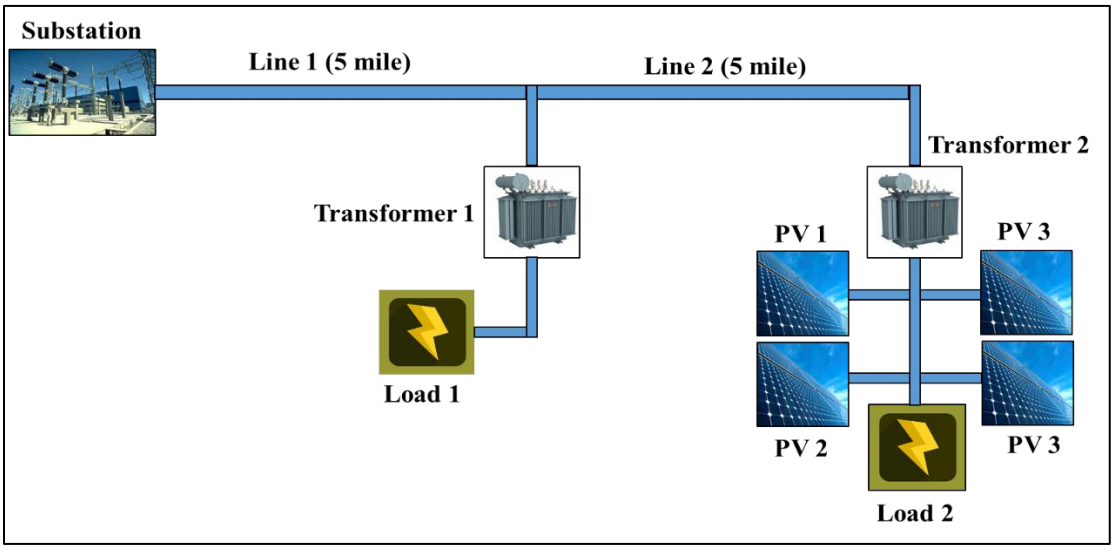

Figure 3.10. Circuit of the first case study with the large PV generator modeled with four smaller point PV generators [69]. © 2018 IEEE

3.4 Conclusion remarks

This chapter investigated flaws of models employed in current PV integration analysis practice. Then it addressed these flaws by proposing more accurate models, which improved the accuracy of the analysis by identifying the locations with voltage problems more precisely.

This chapter first probed the analysis inaccuracy imposed by ignoring secondary circuits or oversimplifying them by investigating voltage drops, voltage changes, and flicker values of simplified secondary circuits and detailed secondary circuits. Then it proposed a method to add detailed secondary models to the primary models to provide a complete circuit model. Finally, the

impact of secondary circuits on allowable PV penetration levels was examined. It was observed that, to identify accurate penetration levels, detailed secondary models are essential.

This chapter also probed the inaccuracy imposed by using point sensor data to model the output of large PV resources. In addition, distributed models of large PV systems were introduced and compared with their corresponding point models through three case studies. Being equipped with the CMS, and distributed models of large PV systems, more accurate analysis of voltage changes of PV systems and flicker severity was achieved. Simulation results demonstrated that PV penetration level could increase three times if distributed models were employed. Moreover, another case study indicated that flicker severity could decrease by 30% by employing distributed models of large PV systems.

This chapter combined the accurate analysis, presented in the previous chapter, with accurate models of secondary circuits, and distributed models of large PV systems, to provide a new and more comprehensive analysis approach of studying PV penetration. The proposed analysis approach can increase the allowable penetration levels of PV resources significantly, while providing a voltage analysis that can be used for more accurate mitigation of problems.

Chapter 4: Effective Control Strategy

4.1 Introduction and chapter objectives

The main objectives of Volt-Var Control (VVC) are maintaining acceptable utilization voltage levels and power factors close to unity in distribution systems. The VVC can be also applied to reduce losses, energy consumption, peak demand, and tear and wear on control devices. Typically, switched capacitor banks, substation load tap changing transformers (LTCs) and On-Load Voltage Regulators (OLVRs) are the devices used to perform the classic VVC.

However, with high and constant growth of distributed RERs, it appears distributed VVC schemes are more effective in voltage regulation by addressing the issues at their locations. In this chapter the performance of distributed VVC schemes is compared with a traditional VVC configuration in voltage regulation to accomplish energy saving goals from Conservation Voltage Reduction (CVR). The goal is to improve the CVR performance of distribution feeders by employing improved VVC schemes.

This chapter also compares the voltage regulation performance of unity power factor, which is the current practice, with the performance of Volt-var and Volt-Watt controls of smart inverters. The goal is to quantify the performance of those control methods over time with an index, which eventually allows evaluating their performance in encountering fast and frequent irradiance fluctuations, and not at just one snapshot of the system.

This chapter's objectives are investigating effectiveness of distributed VVC schemes and comparing the voltage regulation performance of Volt-var and Volt-Watt control strategies of smart inverters with unity power factor, which both result in better handling of large PV penetration levels.

4.2 Distributed Volt-var control devices

In this section the performance of distributed Volt-var control devices in voltage control is compared with traditional VVC devices and configurations. The goal is to achieve an effective voltage regulation strategy, which is necessary for accomplishing CVR goals.

4.2.1 Effectiveness of distributed Volt-var control schemes, a case study

A portion of [90] is re-formatted and reused in this section. The first author of [90] is the author of this dissertation and the reuse is in compliance with GJ policy at the time of writing this dissertation. The policy can be found in the appendix.

In this case study first the characteristics of the best CVR performing feeders, among approximately 1100 distribution feeders, are investigated. Then by employing the insight obtained from the performed analysis, a poor performing CVR feeder is altered into an efficient CVR performer using a more distributed VVC configuration.

Conservation Voltage Reduction (CVR)

Conservation Voltage Reduction has been used as a cost-effective approach to achieve energy savings, peak demand reduction, and feeder loss reduction [91]-[93]. The main objective of CVR is to reduce the real power, and eventually energy, consumed by loads. If loads are voltage-dependent, this goal is achieved by lowering customer utilization voltage. As shown in figure 4.1, CVR can be applied only during specific hours, usually peak hours, or can be applied throughout the whole day. The effect of voltage reduction on energy consumption is quantified using the energy Conservation Voltage Regulation Factor (CVRF) as presented in equation 4.1.

$$CVRF = \frac{Percentage\ change\ in\ energy}{Percentage\ change\ in\ voltage} \qquad (4.1)$$

CVR factors for both real and reactive power can be defined.

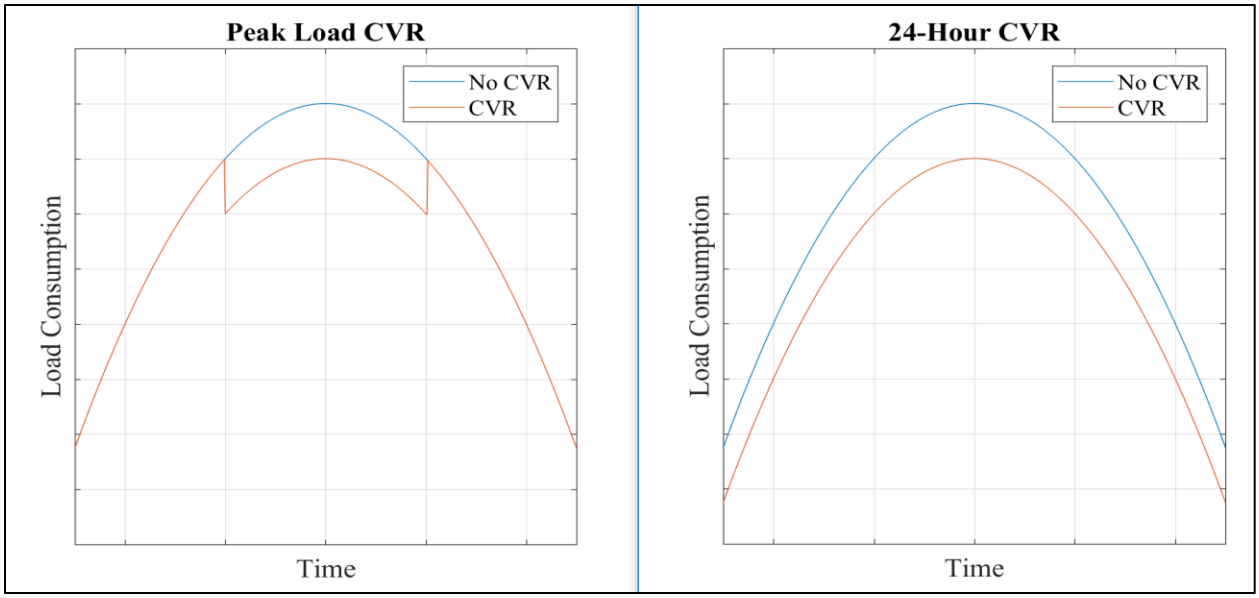

Figure 4.1. CVR implementation during either specific hours or the whole day

Characteristics of the Best CVR Performers

The objective of this section is to identify the characteristics of the best CVR performing feeders. Using experimentally determined summer and winter CVRFs, the CVR performance of approximately 1100 urban and urban-rural distribution feeders under a VVC scheme is evaluated. The energy savings for each feeder are computed, and then top CVR performing feeders are selected. Power flow calculations based on SCADA measurements are used in the evaluations of the top performing feeders, where the power flow calculations are run for each hour of a year, or 8760 times, for each feeder to calculate the energy supplied and feeder losses. Table 4.1 provides the estimated annual energy savings, energy consumption reduction, length and category of the best CVR performing feeders. Studying the topology and voltage profiles of the best CVR performers, it is observed that a good CVR performer has a flat voltage profile due to either the topology/loading conditions or sufficient Volt/VAR control devices to create a flat voltage profile. Figure 4.2 shows a relatively flat voltage profile, in terms of customer level voltage, for a top CVR performing feeder at peak load (Feeder 9 in Table 4.1 - a short feeder without VVC).

Table 4.1. Characteristics and saving of the selected feeders for CVR implementation [90]

Feeder Number	Type	Annual MWh (Base Case)	Annual MWh with CVR (Coordinated Control)	Percentage Improvement	Saving (MWh)	Feeder Length (Mile)	Control Category
1	Urban-Rural	23728	22609	4.72%	1119	18.4	VVC Devices
2	Urban-Rural	23885	22794	4.57%	1091	22.9	VVC Devices
3	Urban	20567	19493	5.22%	1074	13.5	Flat VP
4	Urban	18336	17350	5.38%	986	9.4	Flat VP
5	Urban	18668	17690	5.24%	977	9.4	Flat VP
6	Urban-Rural	20245	19291	4.71%	954	11.1	VVC Devices
7	Urban	17931	16979	5.31%	953	14.5	Flat VP
8	Urban-Rural	20365	19433	4.58%	932	18.7	VVC Devices
9	Urban-Rural	17402	16614	4.53%	788	15.6	Flat VP
10	Urban-Rural	14279	13615	4.65%	664	13.0	Flat VP
11	Urban-Rural	13498	12840	4.87%	658	4.1	Flat VP

The percentage voltage deviation versus distance from the substation is also illustrated for Feeder 9. The voltage drop for Feeder 9 is approximately 1.7V from an initial 125V at the substation.

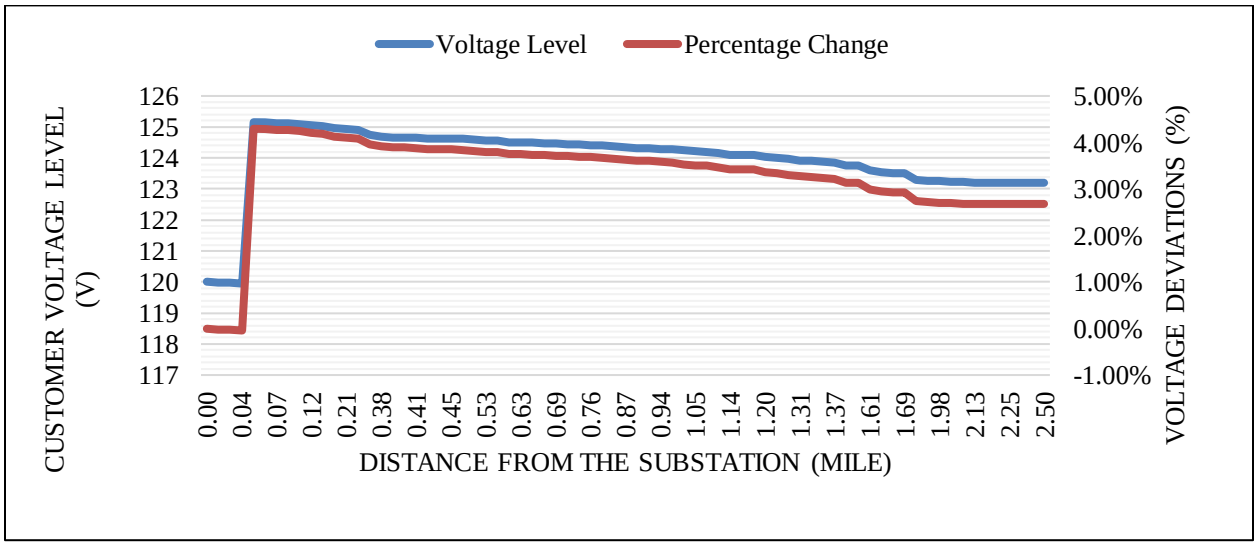

Figure 4.2. Voltage drop versus distance for Feeder 9, a short feeder without VVC devices [90]

Figure 4.3 presents the voltage drop for an efficient CVR performer with VVC devices, Feeder 2. It can be seen that the voltage level is boosted 4 times by voltage regulators. Figure 4.3 also

shows the percent voltage deviation versus distance for Feeder 2. As shown in Table 4.1, Feeder 2 is the second top CVR performer in terms of energy savings.

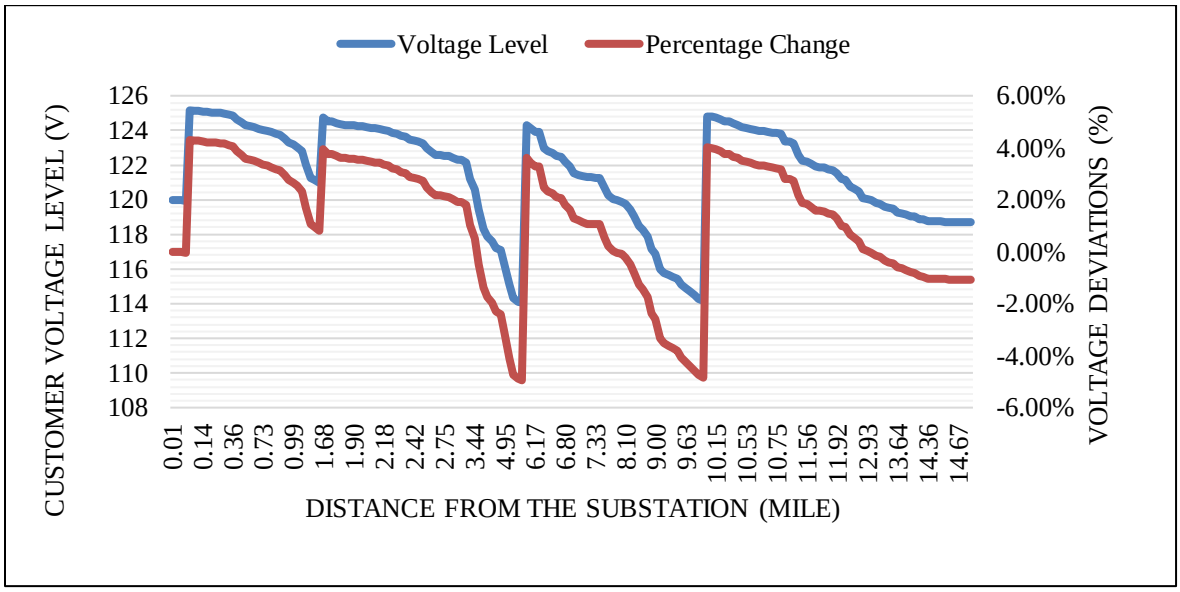

Figure 4.3. Voltage drop versus distance for Feeder 2 with VVC devices. [90]

Figure 4.4 shows results for Feeder 8, a relatively short feeder with VVC. The effect of the capacitor banks on Feeder 8 can be seen around 1.9 miles from the substation. Note that Figure 4.2-4.4 are plotted for the phase that has the smallest voltage at the end of the feeder.

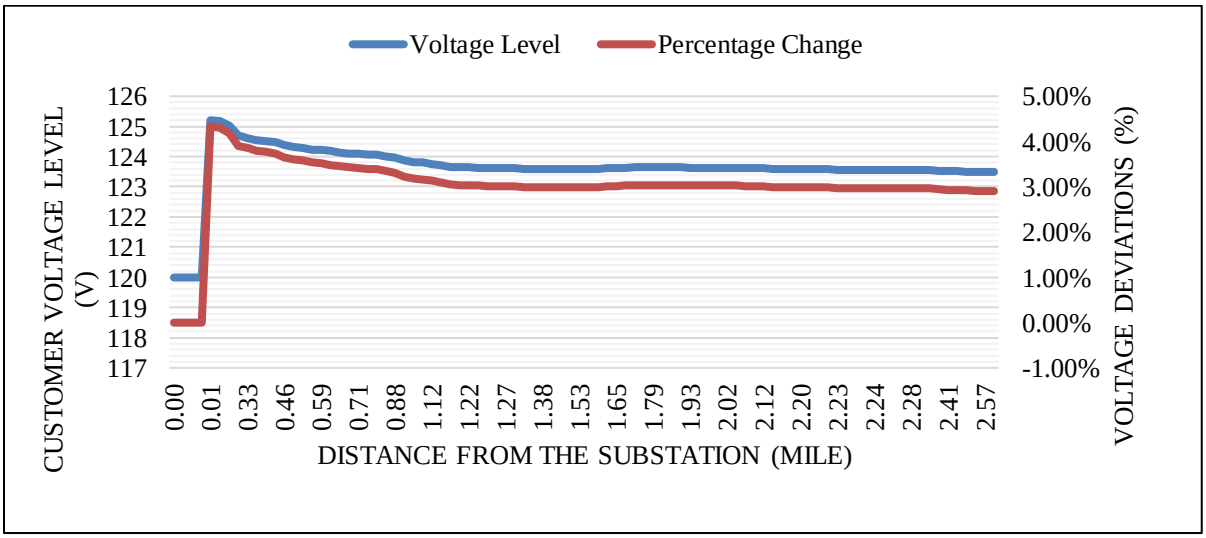

Figure 4.4. Voltage drop versus distance for Feeder 8, a feeder with VVC devices and a relatively flat voltage profile [90]

A scatter plot of feeder annual MWh consumption versus annual MWh savings is plotted in Figure 4.5 for the top eleven CVR performing feeders. When the top CVR performers are categorized according to their characteristics, a natural flat voltage profile or VVC devices, a more precise correlation is found among the feeders. This is illustrated in Figures 4.6 and 4.7, where the R2 correlation criterion increases from 0.848 in Figure 4.5 to 0.919 and 0.898 for Figures 4.6 and 4.7, respectively.

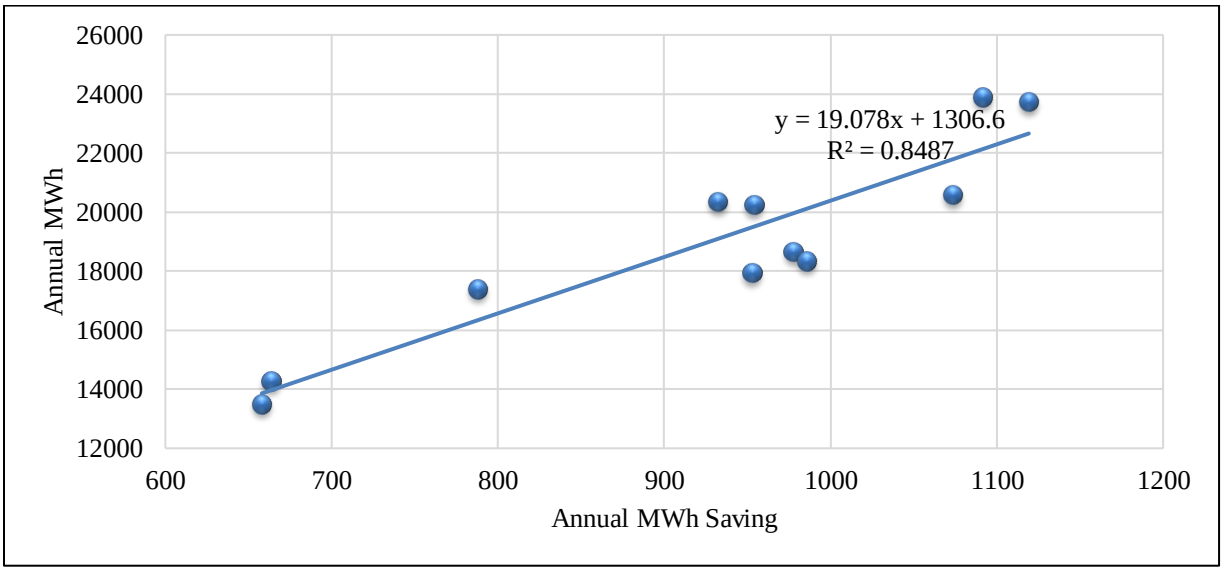

Figure 4.5. Correlation between annual saving and feeder annual consumption for the eleven top CVR performing feeders. [90]

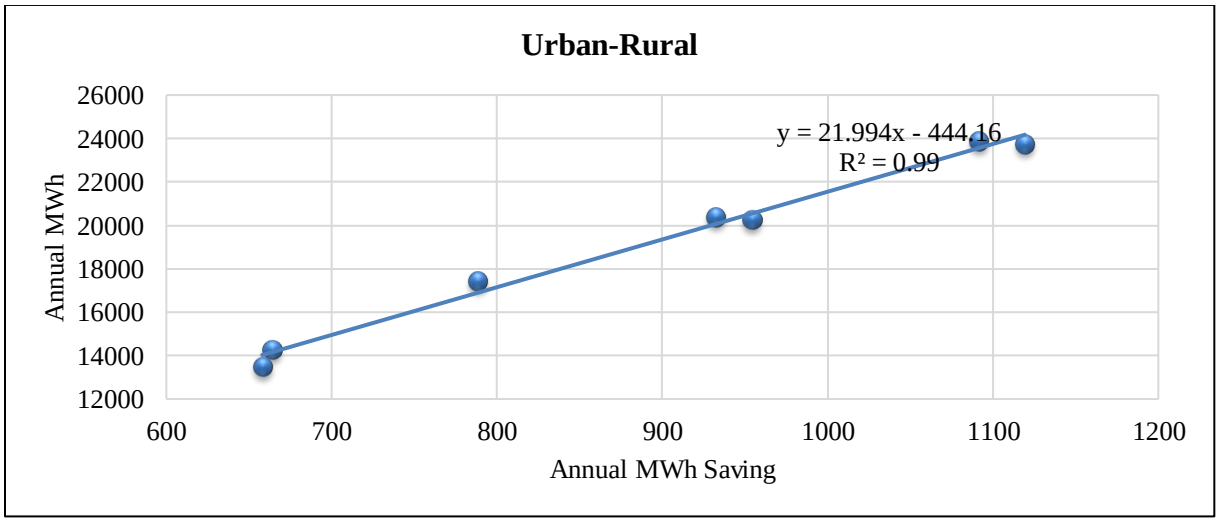

Figure 4.6. Correlation between annual MWh savings and MWh consumption for top CVR performing feeders with relatively flat voltage profiles. [90]

In addition, Figures 4.6 and 4.7 illustrate that when a selection is to be made as to whether CVR should be implemented on one feeder or another, where both feeders have a flat voltage profile, the feeder with the higher energy consumption can provide more energy and dollar savings.

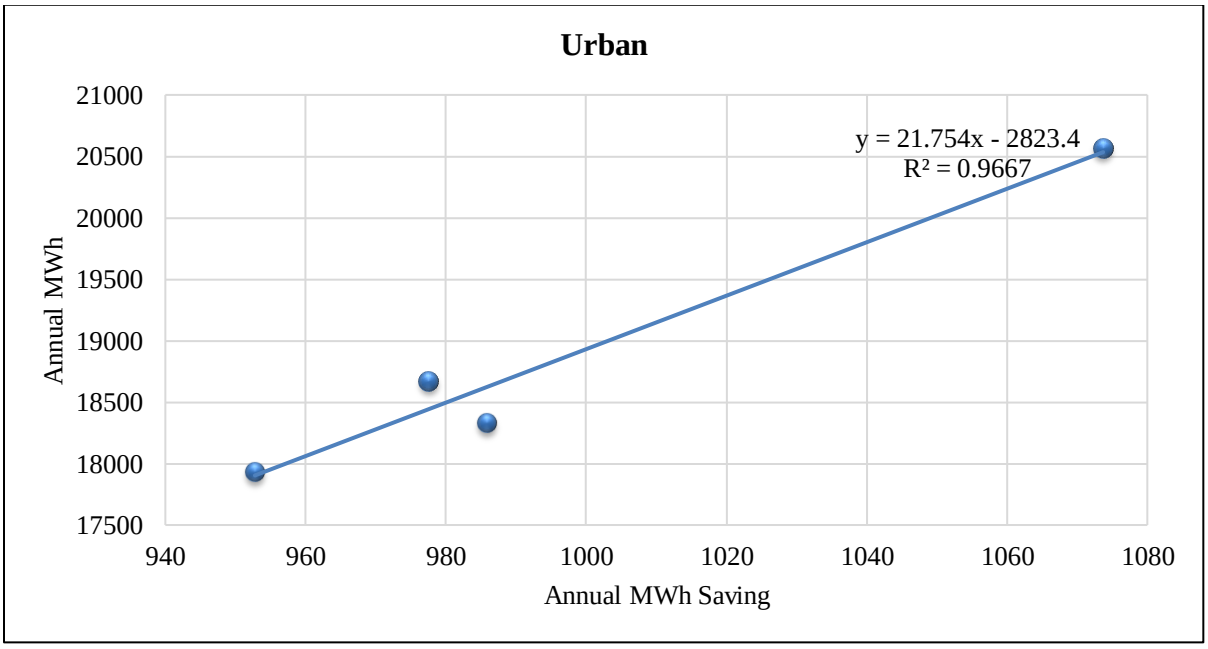

Figure 4.7. Correlation between annual MWh savings and annual MWh consumption for top CVR performing feeders with VVC devices [90].

Modifying a poor CVR performer into a top performer

In this section a poor CVR performing feeder is selected and its VVC scheme is redesigned. The goal is to create a flat voltage profile to achieve better CVR performance. Voltage dependency factors of -0.1 and -0.6, as defined by equation 4.1, are employed for summer and winter, respectively.

The selected feeder originally had two voltage regulators (one at the substation), four 3-phase fixed capacitors, and one 3-phase switched capacitor, where the capacitors all together represented 3450 kvar. The existing standards require the service voltage to be between 114 and 126 V. The goal for the redesigned VVC is to maintain the primary system voltage, in terms of customer level voltage, to be greater than 116 V. This would allow for a 2V drop over the secondary circuits.

Figure 4.8 and 4.9 show the percent voltage drops before and after redesigning the VVC system and applying the CVR control for summer and winter conditions, respectively.

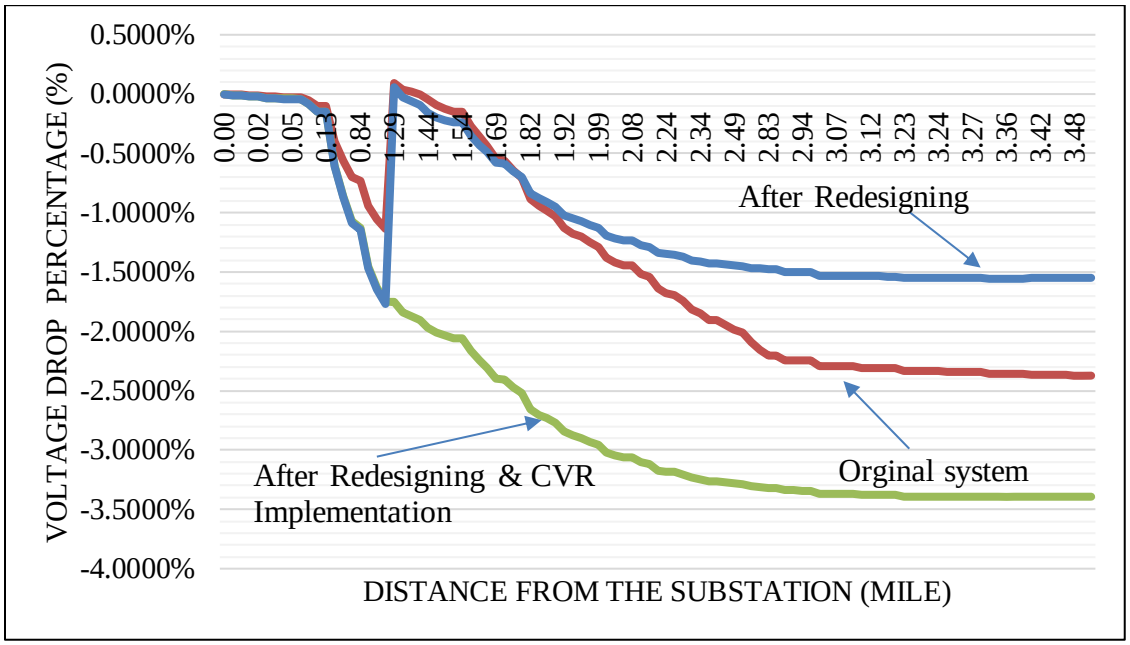

Figure 4.8. Percent voltage drop before and after redesigning the VVC system for the selected poor performing feeder during summer [90]

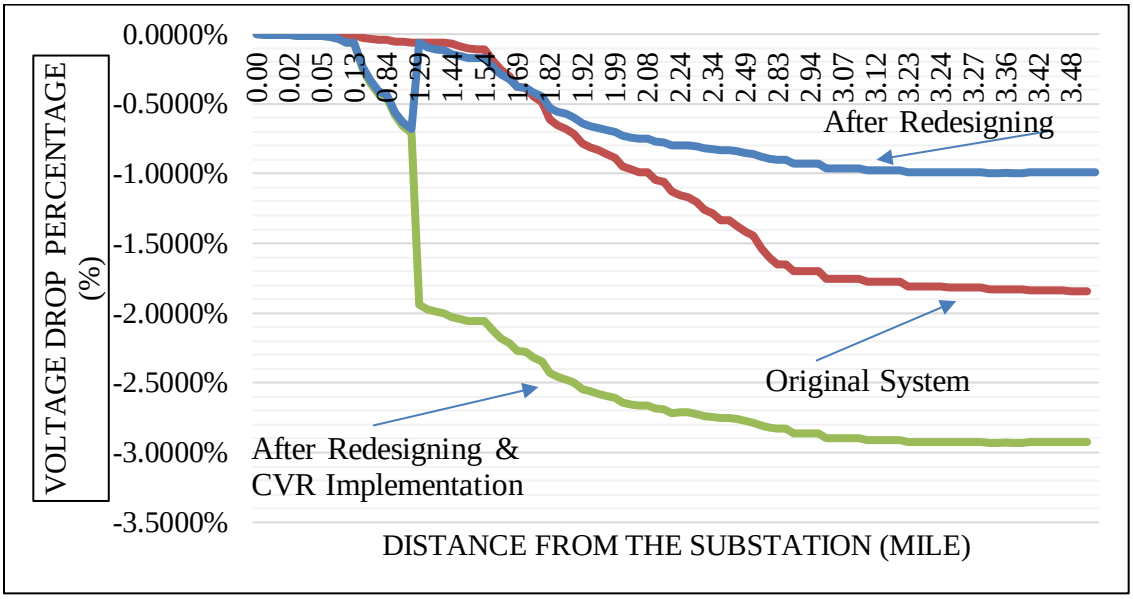

Figure 4.9. . Percent voltage drop before and after redesigning the VVC system for the selected poor performing feeder during winter [90]

Nine single-phase, small switched capacitors are employed in the new VVC scheme, representing a total of 1500 kvar, which is less than half of the original VAR support. Discrete

Ascent Optimal Programming (DAOP) is employed to place the switched capacitors [94]. Table 4.2 presents the capacitor types and reactive power values employed in the feeder before and after redesigning the VCC scheme.

Table 4.2. VVC devices before and after redesign [90]

Before		
Phase	**Capacitor Type**	**Capacity (kvar)**
3 (ABC)	Fixed	1200
3 (ABC)	Fixed	900
3 (ABC)	Fixed	600
3 (ABC)	Fixed	450
3 (ABC)	Switched	300
	Total	3450
After		
Phase	**Capacitor Type**	**Capacity (kvar)**
1 (A)	Switched	200
1 (A)	Switched	200
1 (A)	Switched	100
1 (A)	Switched	150
1 (B)	Switched	200
1 (B)	Switched	200
1 (B)	Switched	200
1 (C)	Switched	150
1 (C)	Switched	100
	Total	1500

The new VVC system improved the voltage profile such that CVR can be implemented with 120V at the substation and 118 V at the second regulator. In summer, the maximum voltage drop before the redesign is approximately 2.5%. The maximum voltage drop after the VVC redesign is 1.5% and after CVR implementation is about 3.5%. In winter, before redesigning the VVC system, the maximum percent voltage drop is about 2%. However, after redesigning the VVC scheme, the maximum percent voltage drop is approximately 1% and after CVR implementation is about 3%. The configuration of the feeder's VVC devices before and after the VVC scheme redesign is shown in figures 10a and 10b, respectively.

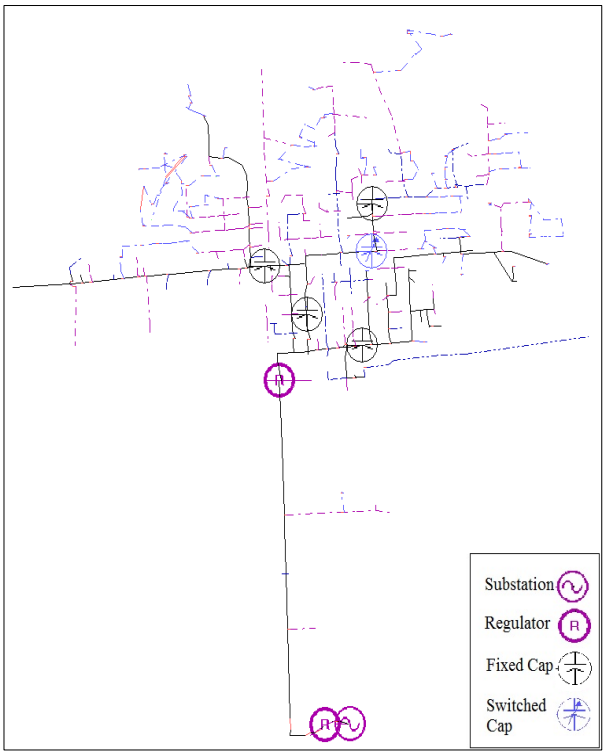

Figure 4.10a. VVC scheme of the original feeder

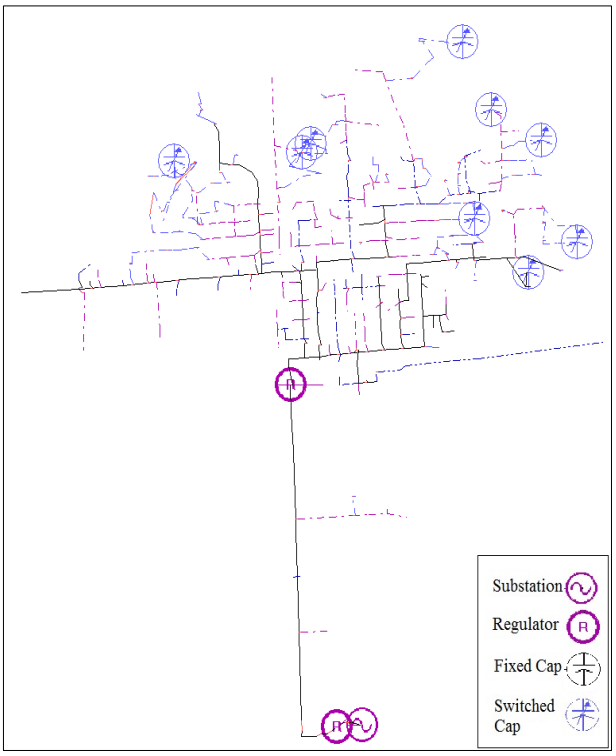

Figure 4.10b. VVC scheme after the redesign [90]

Table 4.3 presents the characteristics of the selected poor CVR performing feeder before and after the VVC redesign. Annual consumption before redesigning the VVC system is 27130 MWh. After the VVC redesign the annual consumption decreases to 26148 MWh, which provided a savings of 983 MWh per year. This corresponds to a 3.62% increase in energy savings. Note that the modified poor performing feeder now ranks in the top five performers shown in Table 4.1.

Table 4.3. Characteristics and saving of the modified feeder after CVR implementation [90]

Feeder Number	Type	Annual MWh (Base Case)	Annual MWh with CVR (Coordinated Control)	Percentage Improvement	Saving (MWh)	Feeder Length (Mile)	Control Category
12	Urban-Rural	27130	26148	3.62%	983	25.2	VVC Devices

Takeaway

This VVC redesign case study shows that traditional VCC configurations cannot address new challenges, such as energy saving initiatives efficiently. However, more distributed VVC

configurations, using more devices, but with smaller capacities, can provide effective voltage regulation, and consequently a flat voltage profile, which is essential for energy saving programs. Although in the redesigned VVC scheme switched capacitors were used, they can be substituted with smart inverters with reactive power control and supply the same reactive power support with even higher resolution, compared to the discrete operation of large switched capacitors. Moreover, this cases study demonstrates that by using a more distributed VVC configuration, less reactive power support is required to achieve the desired objective of good CVR performance.

4.3 Application of smart inverters in voltage regulation

Due to the steady growth of RERs, participation of distributed resources in voltage/frequency regulation was revisited in in the early 2000s. By officially authorizing the participation of distributed resources in voltage regulation, the first amendment of the IEEE 1547 standard in 2013 [65], and due to the emergence of power quality issues, investigating different smart inverter controls has become a necessity.

In this section voltage regulation performance of unity power factor control, which is the current practice, is compared with the performance of Volt-var and Volt-Watt control strategies. The IEEE 13-bus and 123-bus feeders [95] are used to perform the comparisons. To be able to quantify the performance, a Voltage Regulation Index (VRI) is employed. Using the VRI allows evaluating the performance of the mentioned controls while facing irradiance fluctuations through employing the QSS analysis approach.

4.3.1 Smart inverter controls

Smart inverters may monitor different quantities, such as voltage, frequency, or power factor, and employ real and/or reactive powers to regulate these quantities. Fixed Power Factor (FPF), Volt-var (VV), Volt-Watt (VW), frequency-Watt and Watt-power factor are examples of smart

inverters controls [96]. FPF, VV, and VW controls are considered in the following sections. Hence, they are briefly introduced here.

A portion of [28] is re-formatted and reused in this subsection. The first author of [28] is the author of this dissertation and the reuse is in compliance with IEEE policy at the time of writing this dissertation. The policy can be found in the appendix. Note that IEEE holds the copyright of [28], whose citation is expressed in the bibliography.

Fixed Power Factor (FPF) Control

With FPF control the power factor at the location of the inverter is kept constant. The power factor range is between -1 and 1. Both -1 and +1 lead to the same result, generating no reactive power. A positive power factor, or leading power factor, indicates generating reactive power. A negative power factor, or lagging power factor, indicates absorbing reactive power. The regulation of power factor is usually performed by producing/curtailing reactive power [96]. However, it can be performed by regulation of real power. Different power factor quadrants and the states of real and reactive power injection/absorption are illustrated in Figure 4.11 [28].

Volt-VAR (VV) Control

The VV control strategy is utilized to control the injection or absorption of reactive power based on the voltage level at the inverter terminals. The principle underlying VV control is to inject reactive power when the voltage falls below a specified level, and to absorb reactive power when the voltage exceeds a specified level. A voltage dead-band may also be used, and as long as the voltage falls inside of the dead-band, no reactive power injection/absorption occurs [96]. A typical VV control characteristic is illustrated in Figure 4.12 [28]. The voltage range between V2 and V3, shown in Figure 4.12, represents the dead-band.

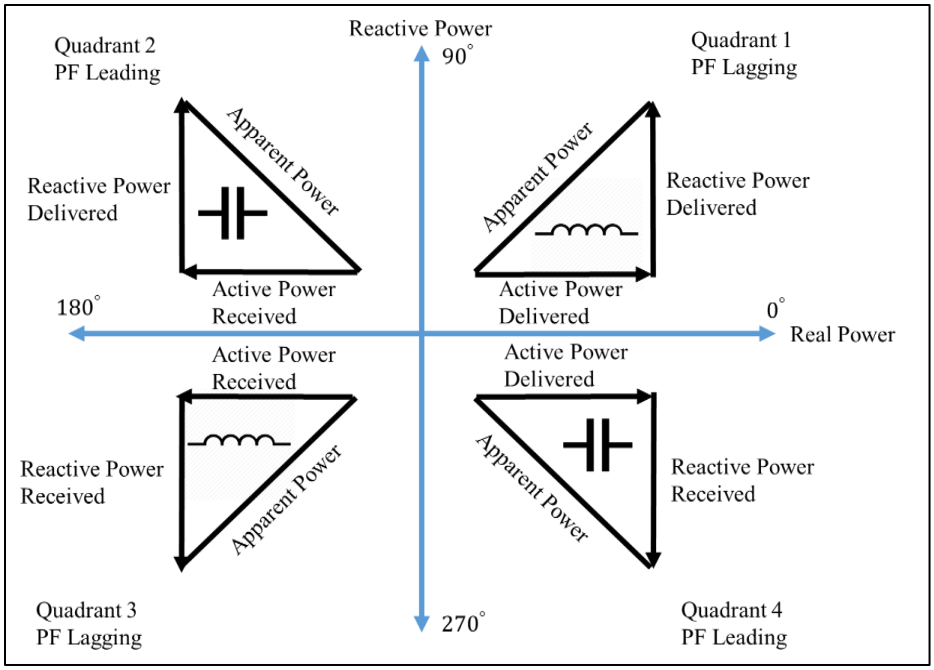

Figure 4.11. Four operating quadrants in FPF control strategy [28]. © 2017 IEEE

Considering Figure 4.12, when the voltage is less than V1, the maximum reactive power is injected. When the voltage is between V2 and V1, reactive power is injected based on the slope S1 shown in Figure 4.12. When voltage falls between V3 and V4, reactive power is absorbed based on the slope S2 illustrated in Figure 4.12. Finally, if the voltage level is greater than V4, the maximum reactive power is absorbed.

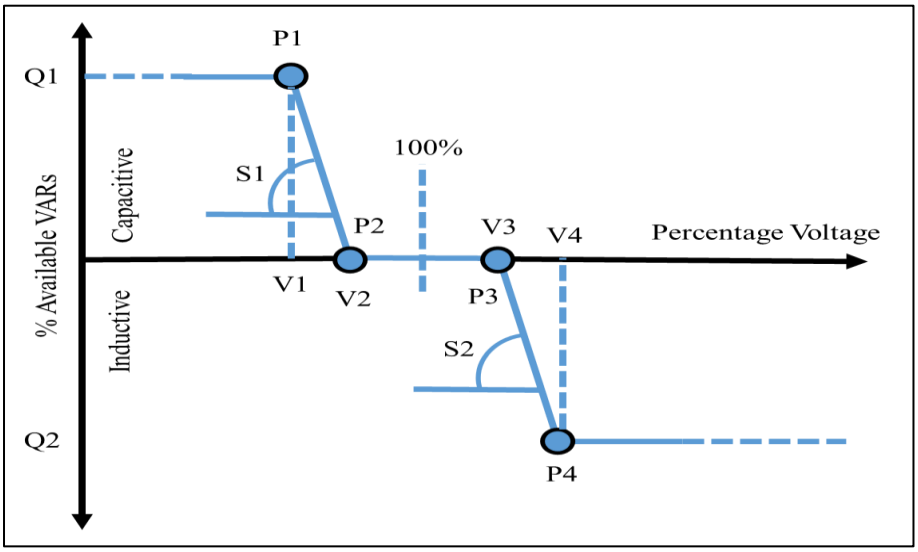

Figure 4.12. VV control strategy characteristics [28]. © 2017 IEEE

In some cases it may be desired to employ hysteresis in the VV control. With hysteresis, different locations can be defined for the points P1-P4 of Figure 4.12. Thus, the path followed by the control when voltage is rising is different from the path followed by the control when voltage is falling. VV control with hysteresis is illustrated in Figure 4.13 [28].

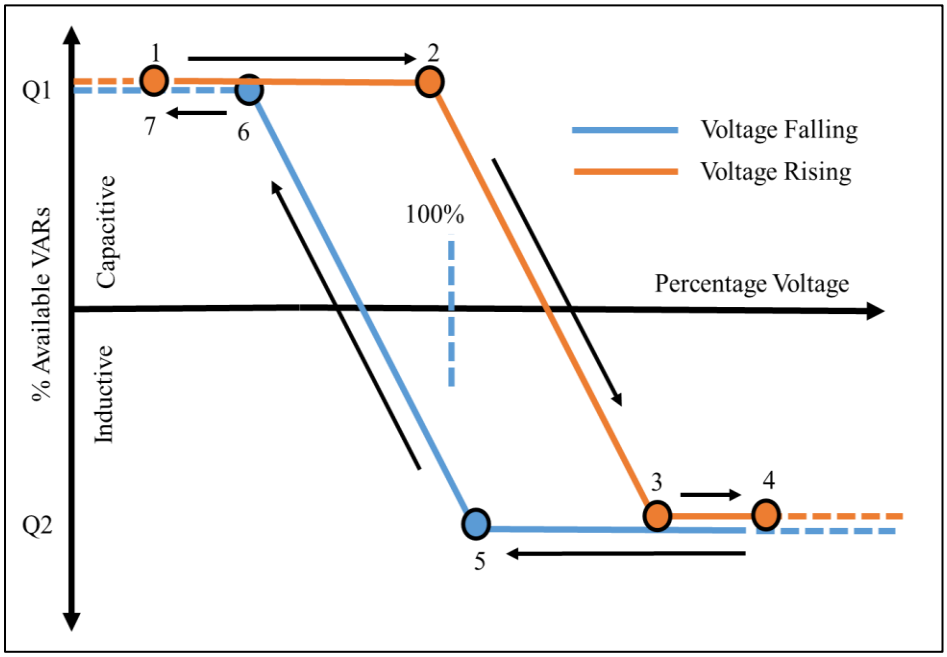

Figure 4.13. VV control strategy with a hysteresis incorporated [28]. © 2017 IEEE

Volt-Watt (VW) Control

The VW control strategy is used to mitigate high voltages induced by high penetration of PV resources at the distribution level. With the VW control, an inverter can gradually reduce its own maximum real power generation as the voltage at the inverter terminals exceeds a configurable limit as shown in Figure 4.14 [96]. Volt-var and Volt-Watt functions can be utilized simultaneously by allocating the kVA of inverters between those functions. However, it is more logical to give precedence to real power generation when both functions are active. This is because the primary application of installing a PV system is to harvest solar energy and deliver real power to loads.

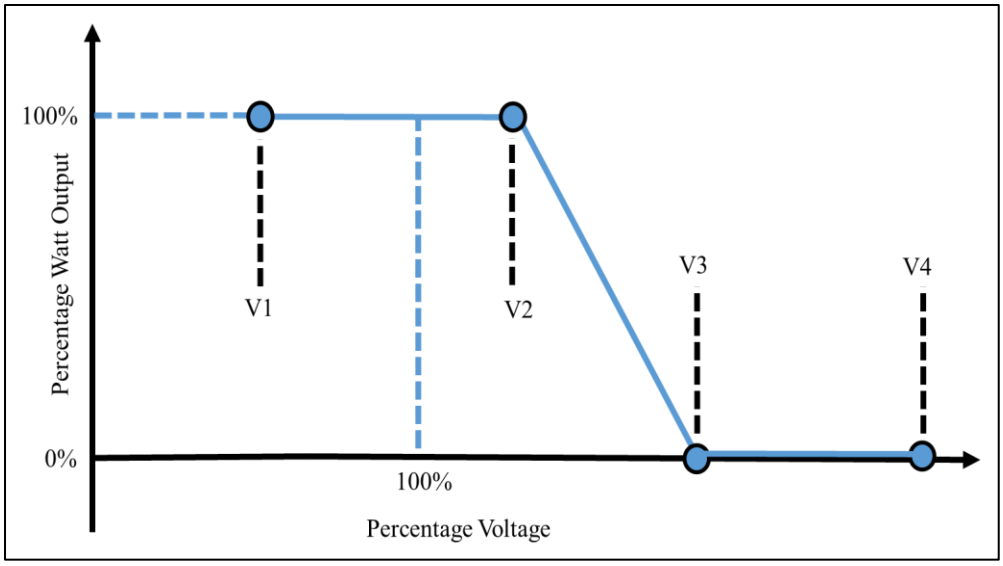

Figure 4.14. VV control strategy characteristics [96]

4.3.2 Volt-var control versus fixed power factor control

A portion of [28] is re-formatted and reused in this section. The first author of [28] is the author of this dissertation and the reuse is in compliance with IEEE policy at the time of writing this dissertation. The policy can be found in the appendix. Note that IEEE holds the copyright of [28], whose citation is expressed in the bibliography.

Case study

The IEEE 13-bus feeder is modified by adding PV generation and is used as the case study to compare voltage regulation of FPF and VV controls. Two 3-phase PV generators are added at busses 671 and 634, with capacities of 1300 and 500 kVA, respectively. The test feeder and PV generator models are illustrated in Figure 4.15. In evaluating the voltage regulation performance of the FPF and VV controls, one second step size simulations are performed covering one hour of operation. The simulations occur at noon when PV generation is at maximum. The solar irradiance profile illustrated in Figure 4.16 is used to simulate solar irradiance fluctuations. In some cases, irradiance drops from 100% to 20% in a matter of seconds. Note that the irradiance profile used is based on real solar irradiance measurements.

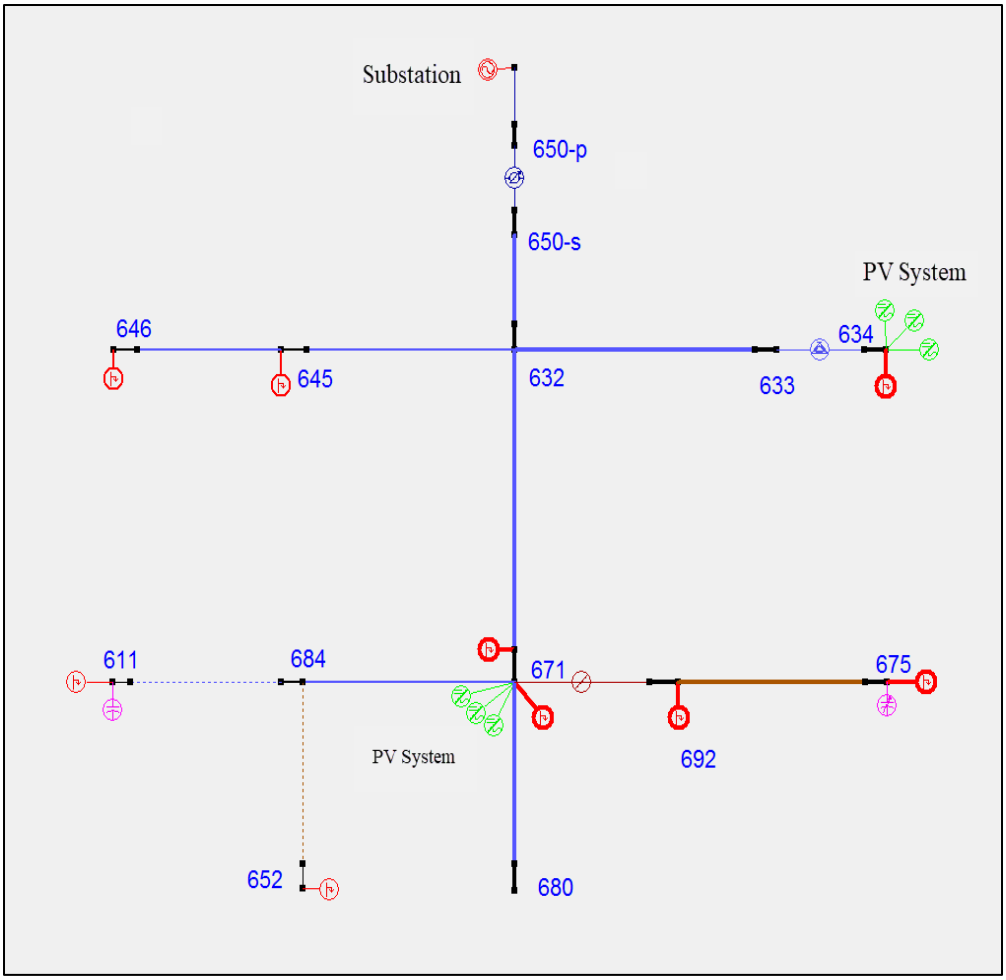

Figure 4.15. IEEE 13-bus feeder with two added PV systems [28]. © 2017 IEEE

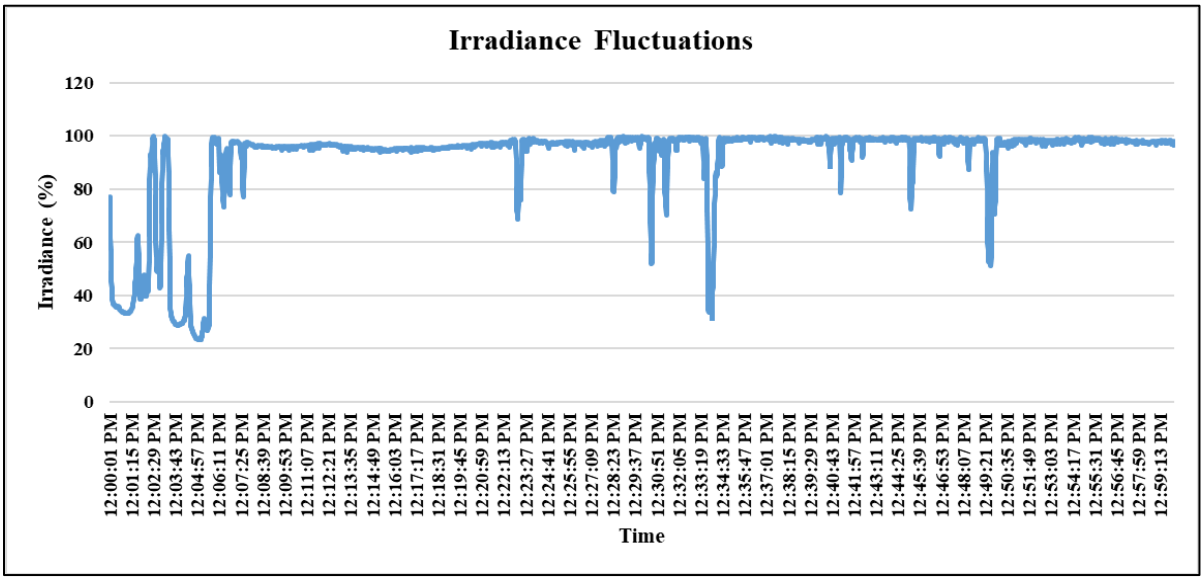

Figure 4.16. Irradiance fluctuations between 12:00 to 13:00 PM [28]. © 2017 IEEE

Voltage regulation performance evaluation

To quantify voltage regulation performance of the FPF and VV controllers over time, a cost function referred to as the Voltage Regulation Index (VRI) is employed. The VRI is defined as

$$VRI = \sum_{t=1}^{t=T} |V(t)_{PU} - 1| \qquad (4.2)$$

where T is 3600 and $V(t)_{PU}$ is the per unit voltage. The VRI is the sum of the absolute values of voltage deviations from the per unit voltage over the simulation time, which is 3600 seconds. A smaller VRI indicates a better voltage regulation performance. The base voltage level is 120 V. A similar cost function is defined for reactive power regardless of its injection/absorption presented by equation 4.3.

$$QI = \sum_{t=1}^{t=T} |Q(t)| \qquad (4.3)$$

where Q(t) is the reactive power injected/absorbed by the inverters at each second.

Simulation results

Different power factors and VV slopes are considered in the simulations, and the VRI is computed for each simulation. Dead bands were not used in the VV control, allowing the VV control to rapidly react to voltage deviations, which resulted in better voltage regulation performance. The simulation results are summarized in Tables 4.4 and 4.5, which for the parametric studies present the control strategies, parameter values, and the VRI values along with the sum of the 3-phase reactive power used in the control, regardless of injection or absorption, for busses 671 and 634. The lowest value of the VRI index achieved at each bus is highlighted in Table 4.4. The time varying voltages at bus 671, which occurred for employing FPF control strategy with leading power factors of 1, 0.95 and 0.9, are illustrated in Figure 4.17. Similarly, the voltages at bus 671 when various slopes are used with the VV control are presented in Figure 4.18.

Table 4.4. Voltage regulation indices computed for VV and FPF controllers [28].

	VR index					
Bus	**Phase A**	**Phase B**	**Phase C**	**Total**	**Control Strategy**	**Characteristics**
761	7.38	123.77	79.05	210.20	Fixed Power Factor	1.0 (Leading)
761	22.68	155.77	27.71	206.16	Fixed Power Factor	0.95 (Leading)
761	22.49	156.24	19.06	197.79	Fixed Power Factor	0.9 (Leading)
761	4.48	114.08	73.31	191.88	Volt-VAR	P1=0.7, P2=1.3
761	3.69	109.92	70.80	184.42	Volt-VAR	P1=0.8, P2=1.2
761	3.88	99.38	64.36	167.62	Volt-VAR	P1=0.9, P2=1.1
	VR index					
Bus	**Phase A**	**Phase B**	**Phase C**	**Total**	**Control Strategy**	**Characteristics**
634	42.92	89.23	40.20	172.35	Fixed Power Factor	1.0 (Leading)
634	72.88	127.55	91.51	291.93	Fixed Power Factor	0.95 (Leading)
634	74.46	129.11	100.11	303.68	Fixed Power Factor	0.9 (Leading)
634	42.89	82.00	40.71	165.60	Volt-VAR	P1=0.7, P2=1.3
634	42.89	78.92	41.03	162.84	Volt-VAR	P1=0.8, P2=1.2
634	42.80	71.15	41.94	155.88	Volt-VAR	P1=0.9, P2=1.1

Table 4.5. Sum of 3600 Absolute Reactive Power Values during QSS Simulations [28].

	Q index (kvar)					
Bus	**Phase A**	**Phase B**	**Phase C**	**3-Phase**	**Control Strategy**	**Characteristics**
761	0	0	0	0	Fixed Power Factor	1.0 (Leading)
761	318730	377821	444495	1141046	Fixed Power Factor	0.95 (Leading)
761	338549	402776	506270	1247595	Fixed Power Factor	0.9 (Leading)
761	4957	52973	44969	102898	Volt-VAR	P1=0.7, P2=1.3
761	6388	75713	64725	146826	Volt-VAR	P1=0.8, P2=1.2
761	10256	133435	115863	259553	Volt-VAR	P1=0.9, P2=1.1
	Q index (kvar)					
Bus	**Phase A**	**Phase B**	**Phase C**	**3-Phase**	**Control Strategy**	**Characteristics**
634	0	0	0	0	Fixed Power Factor	1.0 (Leading)
634	129511	149984	172084	451579	Fixed Power Factor	0.95 (Leading)
634	137424	160518	198902	496845	Fixed Power Factor	0.9 (Leading)
634	5844	14324	8226	28395	Volt-VAR	P1=0.7, P2=1.3
634	8729	20439	12442	41609	Volt-VAR	P1=0.8, P2=1.2
634	17407	35901	25775	79083	Volt-VAR	P1=0.9, P2=1.1

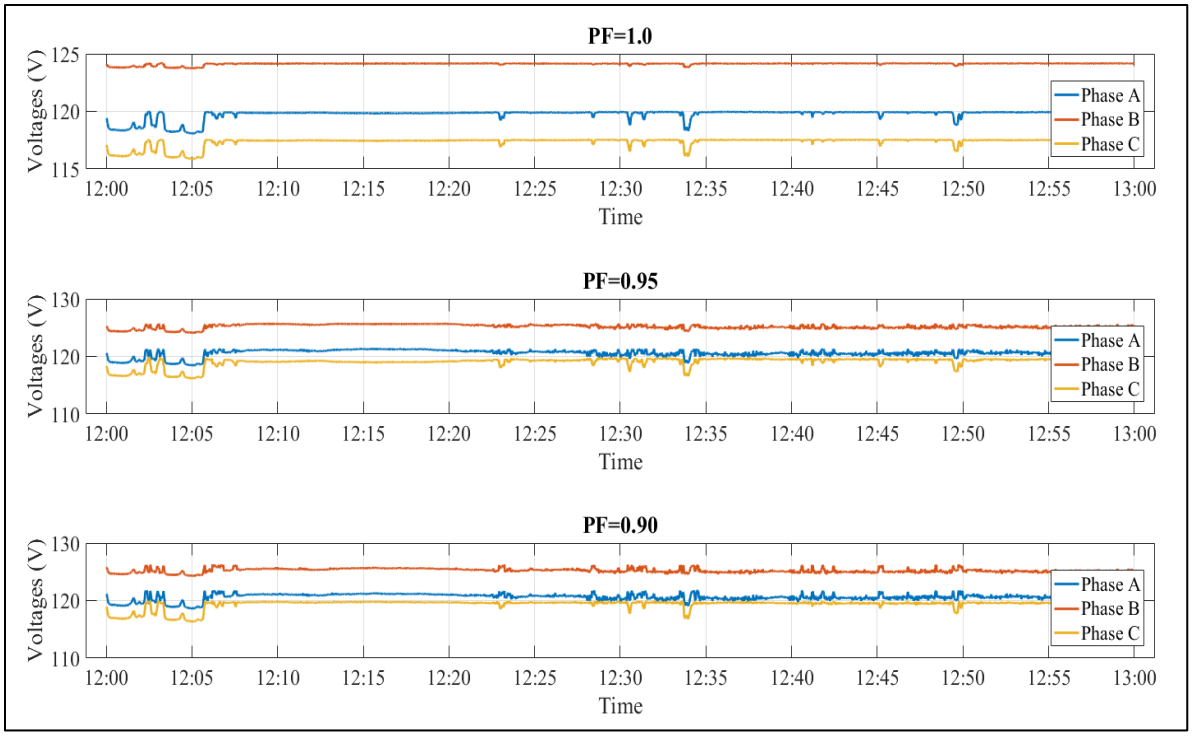

Figure 4.17. 3-phase voltages at bus 671 with FPF control [28]. © 2017 IEEE

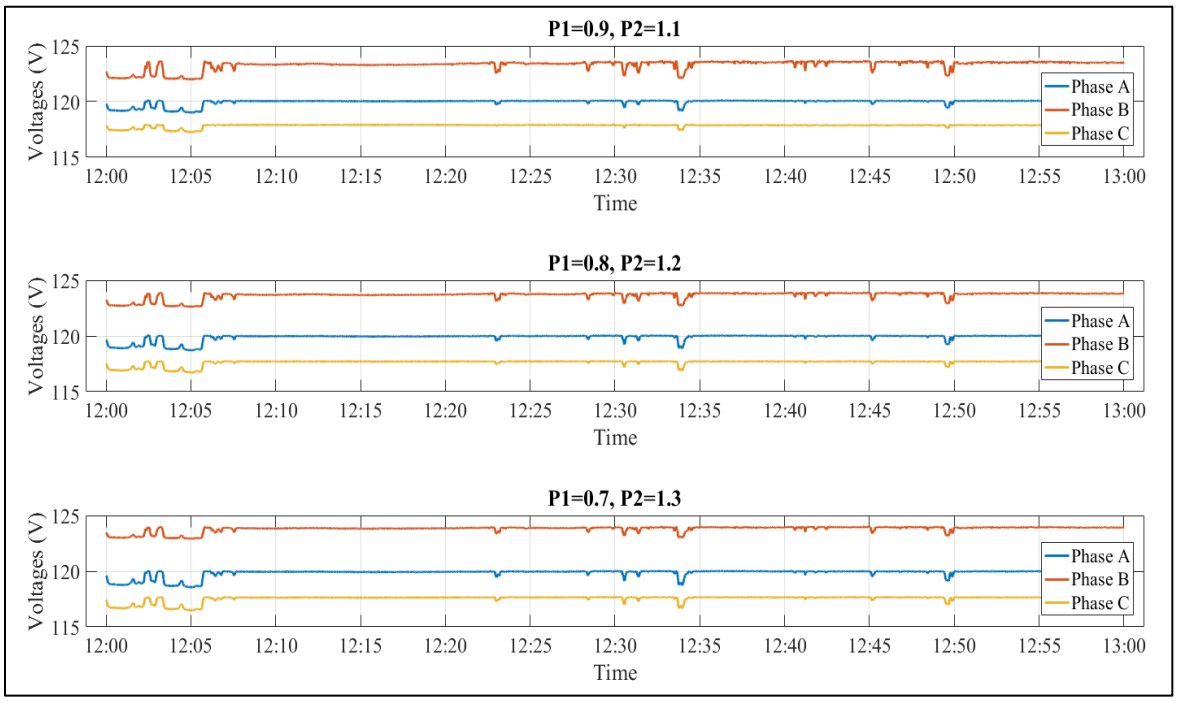

Figure 4.18. 3-phase voltages at bus 671 with VV control [28]. © 2017 IEEE

Reactive power injections or absorptions at bus 671 are illustrated in Figures 4.19 and 4.20 when FPF and VV control strategies are employed respectively.

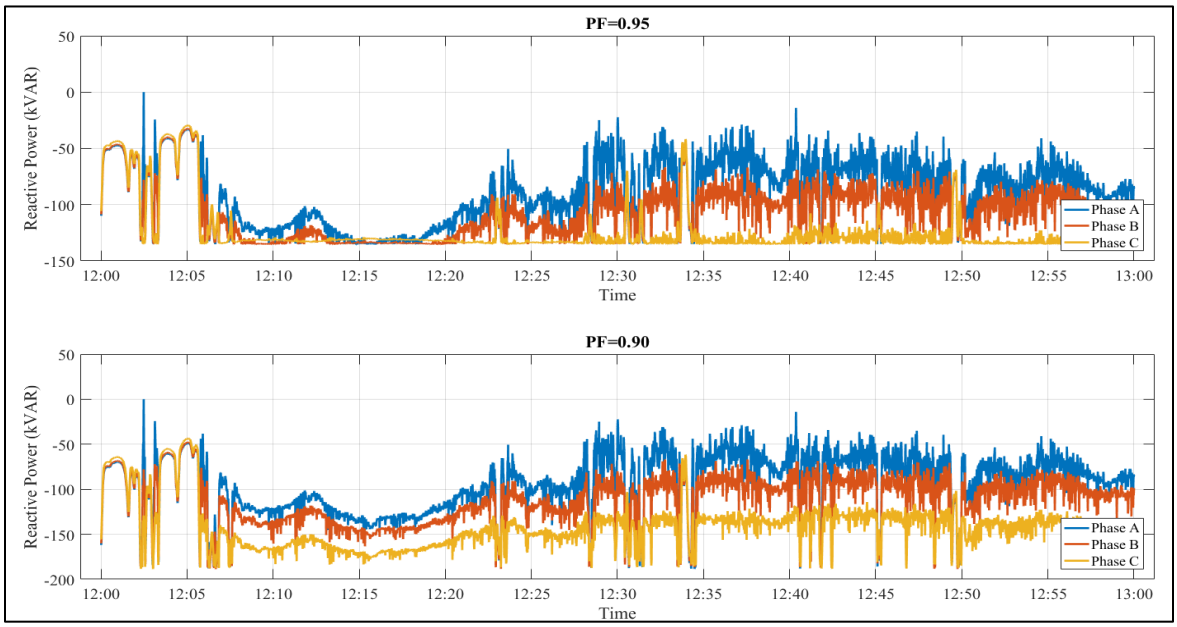

Figure 4.19. Reactive power injections/absorptions of FPF controller at bus 671 during one-hour QSS simulation. Negative values indicate reactive power injection and positive values indicate reactive power absorption [28]. © 2017 IEEE

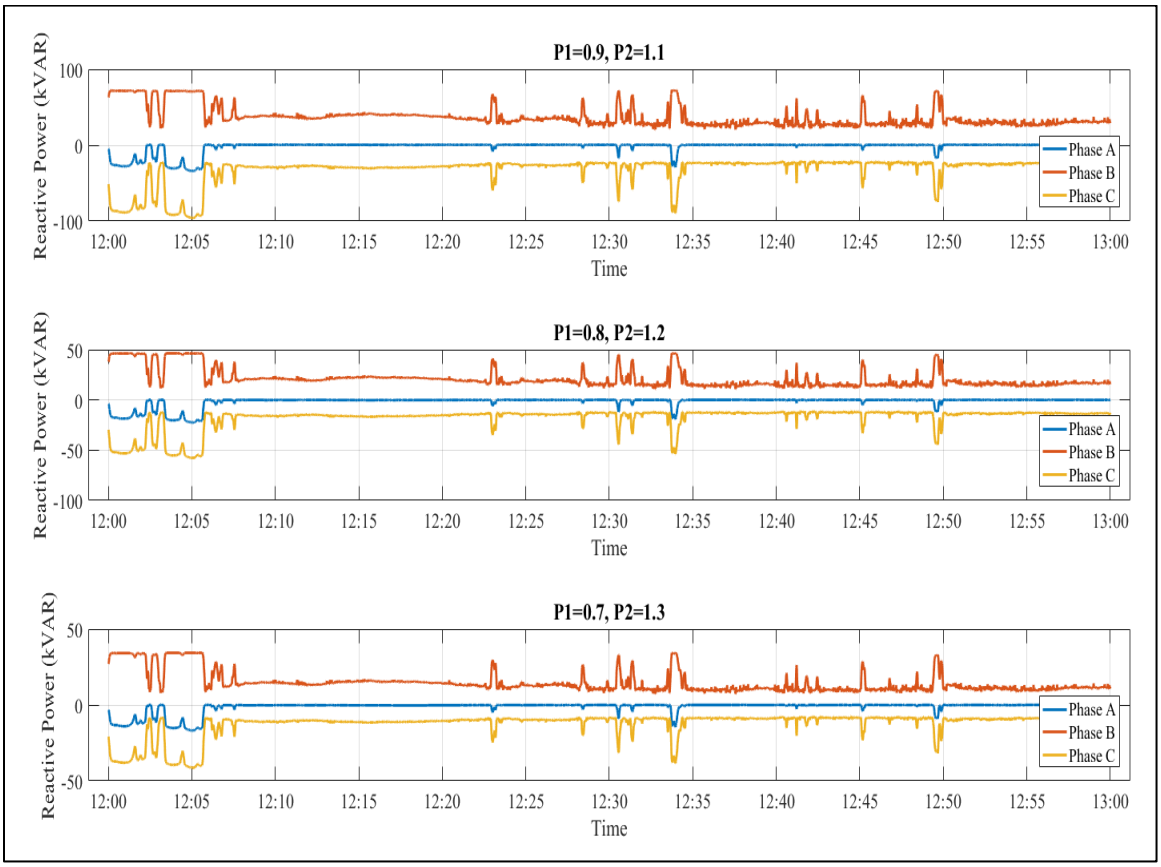

Figure 4.20. Reactive power injections/absorptions of VV controller at bus 671 during one-hour QSS simulation. Negative values indicate reactive power injection and positive values indicate reactive power absorption [28]. © 2017 IEEE

Based on the results presented in Table 4.4, the VV control provides better voltage regulation than the FPF control. Increasing the S1 and S2 slopes of the VV curve of Figure 4.12 results in reducing the VRI. With the FPF controllers, decreasing the power factor from 1.0 to 0.9 results in improving the voltage regulation for bus 671. However, it had a reverse effect on the VRI of bus 634. This is due to the FPF control, which regardless of voltage deviation either injects or absorbs reactive power, and this can result in unwanted voltages deviations.

For the QSS simulations, the VV controllers inject/absorb significantly less reactive power than the FPF control. Based on Table 4.5, the inverter at bus 671 injected/absorbed a total of 259553 kVAR with VV control. However, the same inverter injected/absorbed a total of 1247595 kVAR with a 0.9 leading FPF control, which is approximately six times more reactive power than the VV control. The same trend was observed for bus 634 in terms of total reactive power injection/absorption.

Takeaway

Simulation results showed that the VV control provides more effective voltage regulation than FPF control. Furthermore, it was observed that as much as six times less reactive power injection/absorption occurred when VV control is used.

4.3.3 Volt-Watt control versus unity power factor

Case study

The IEEE 123-bus feeder is modified by adding PV generation and is used as the case study to compare voltage regulation of Unity Power Factor (UPF) and VW controls. Two 3-phase PV generators, both 300 kVA, are added to buses 7 and 83, both of which have voltages over 120V. The test feeder and PV generator models are illustrated in Figure 4.21. Note that all VVC devices are frozen intentionally so as not to interfere in voltage regulation. In evaluating the voltage

regulation performance of the UPF and VV controls, one-second step size QSS simulations are performed, covering one hour of operation. The simulations occur at noon when PV generation is at maximum. The solar irradiance profile illustrated in Figure 4.16 is again used to simulate the irradiance fluctuations.

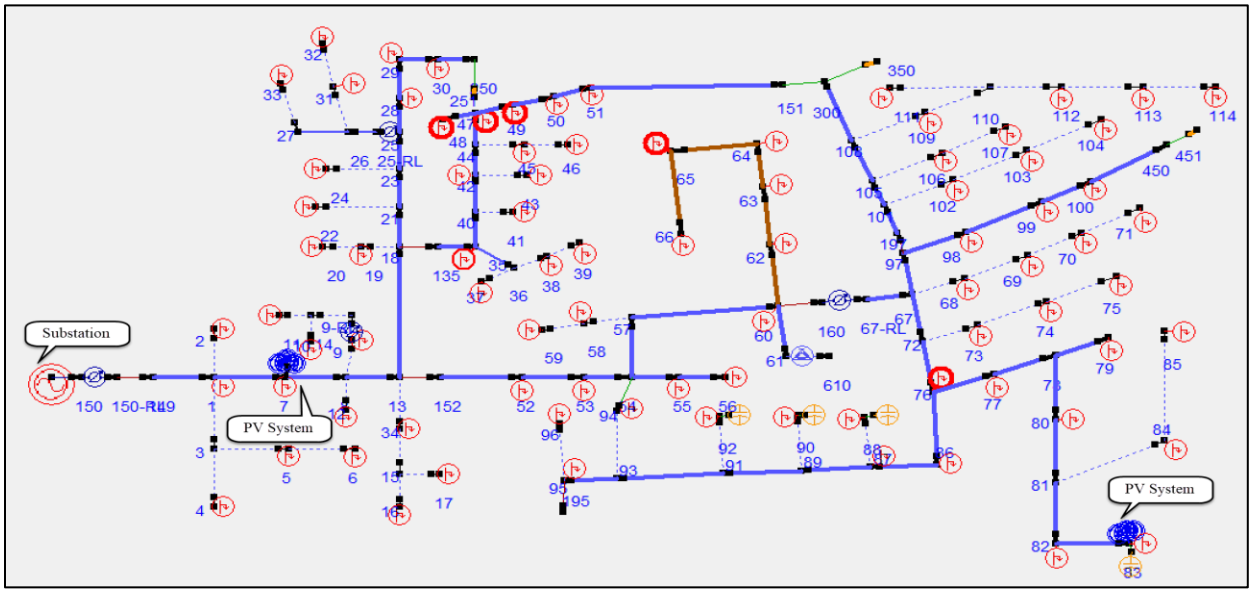

Figure 4.21. The IEEE 123-bus test feeder is modified by adding two PV systems at buses 7 and 83

Simulation results

Table 4.6 presents the VRI of both control strategies at bus 7, which is close to the substation, and bus 83, which is far away from the substation.

Table 4.6. Voltage regulation indices computed for VW and UPF controls

	VRI					
Bus	**Phase A**	**Phase B**	**Phase C**	**Total**	**Control Strategy**	**Characteristics**
7	72.22	133.76	95.67	301.66	Fixed Power Factor	Power Factor=1
7	66.58	127.68	91.41	285.67	Volt-Watt	VW: V1=1, V3=1.05
	VR					
Bus	**Phase A**	**Phase B**	**Phase C**	**Total**	**Control Strategy**	**Characteristics**
83	77	58	67	202	Fixed Power Factor	Power Factor=1
83	53	44	47	145	Volt-Watt	VW: V1=1, V3=1.05

In both locations VW control has a lower VRI, which means a better voltage regulation performance. However, the difference of VRI values is higher at bus 83 by about 25%. As discussed in chapter 3, the sensitivity of voltage to real and reactive power changes increases by the increment of the resistance and reactance between the PCC and the substation. Therefore, curtailing real power by VW at bus 83, which is further from the substation and has greater resistance, decreases the voltage more than bus 7 which is close to the substation.

Figures 4.22 and 4.23 also show the voltage level of bus 83 when UPF and VW controls are applied, respectively. The impact of VW control to reduce voltage, and make them close to the set point of 120V, can be observed from comparing Figures 4.22 and 4.23.

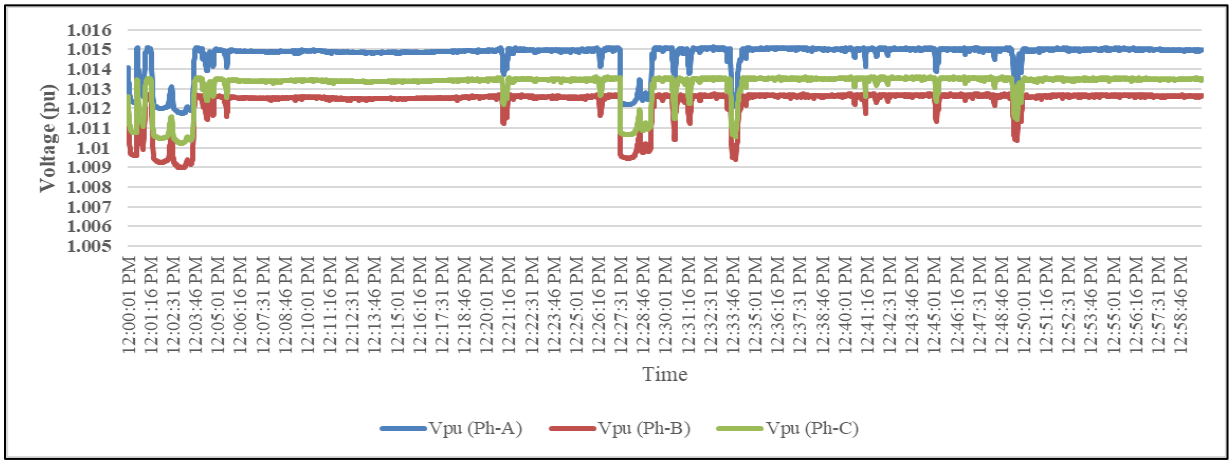

Figure 4.22. Phase voltages of bus 83 under unity power factor

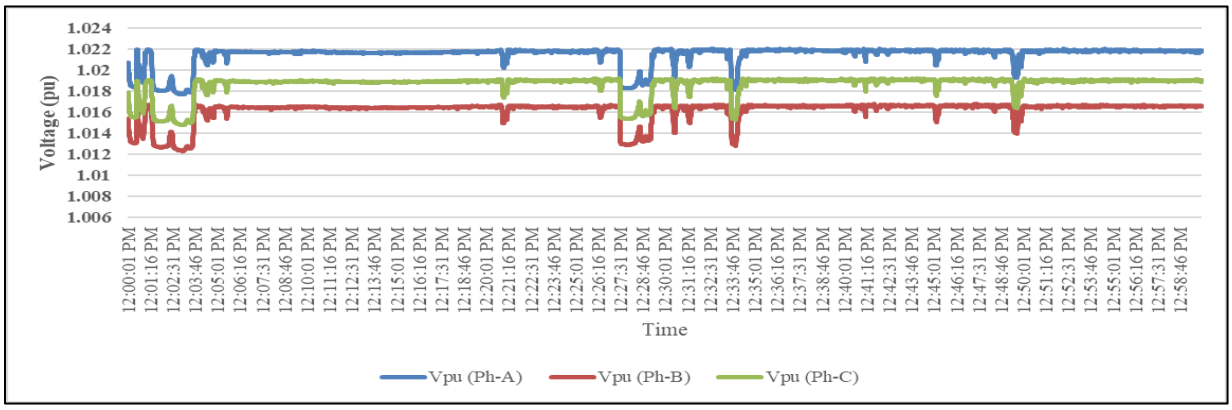

Figure 4.23. Phase voltages of bus 83 under volt-Watt control

Takeaway

Simulation results showed that the VW control can be used in distributed VVC schemes for voltage regulation. This case study also illustrated the effectiveness of Volt-Watt control in handling high voltages, especially at the end-of-feeder locations.

4.4 Conclusion remarks

The goal of this chapter was to provide effective control methods to facilitate high penetration of PV resources. Traditional volt-var control is based on the assumption that the main voltage problem to handle is the under-voltage at the end of distribution feeders. However, that is not the case anymore. With high penetration of distributed PV resources, high voltages can also occur at any location.

This chapter first compared the effectiveness of distributed VVC schemes to accomplish effective voltage regulation to apply conservation voltage reduction. In a case study, a poor performing CVR feeder with traditional VVC devices, was altered into an efficient CVR performer by employing a more distributed VVC configuration, providing 983 MWh of annual energy savings, corresponding to 3.62% reduction in energy usage.

The second part of this chapter compared a fixed power factor control strategy with Volt-var and Volt-Watt control strategies, where voltage regulation is evaluated over an hour of fast and frequent irradiance fluctuations. The QSS simulation results demonstrated that VV and VW controls cloud decrease the voltage regulation index used by 25% in their corresponding case studies.

It seems that distributed VVC schemes, including distributed smart inverters, will be an indisputable portion of any mitigation to the challenges and issues caused by high PV penetration levels, and their winning card is addressing voltage problems at their exact locations.

Chapter 5: Impact of Cloud Shadow on Power Quality

5.1 Introduction and chapter objective

Due to high growth of PV resources in the recent years, additional focus has been placed on their impacts on power quality. Reference [97] has investigated the harmonic interactions between a power system and distributed generation inverters. The authors in [98] have studied power quality behavior of different photovoltaic inverter topologies. Moreover, [99] has assessed a single-phase voltage-controlled grid-connected photovoltaic system with power quality conditioner functionality. Reference [100] has investigated harmonic impact of a 20 kW photovoltaic systems connected to LV distribution networks. However, few studies have explored the impacts of cloud shadow motion on power quality. The objective of this chapter is to investigate the impact irradiance fluctuations, induced by a cloud shadow, on the Total Harmonic Distortion (THD) of voltage and current waveforms in different locations of a power system. In addition, the effect of the impedance between the Point of Common Coupling (PCC) and the utility grid on the voltage THD is assessed through various line lengths.

A portion of [10] is re-formatted and reused in this section. The first author of [10] is the author of this dissertation and the reuse is in compliance with IEEE policy at the time of writing this dissertation. The policy can be found in the appendix. Note that IEEE holds the copyright of [10], whose citation is provided in the bibliography.

5.2 Power quality and power quality indices

Power quality is a term usually used to describe voltage and current quality, reliability and continuity of service, and quality of power supply [101]. The quality of voltage and current can be expressed as how close voltage and current waveforms are to a perfect sinusoidal waveform with a nominal magnitude and frequency. To quantify voltage and current quality, different indices are

proposed in the power quality literature. In the following, some of those power quality indices are briefly discussed.

Individual Harmonic Distortion (IHD), Total Harmonic Distortion (THD), and Total Demand Distortion (TDD) are used to study the voltage and current quality of power systems. IHD, THD and TDD definitions are presented in equations 5.1-5.3, respectively.

$$IHD_i\ (\%) = \frac{h_i}{h_1} * 100 \qquad (5.1)$$

$$THD = \frac{\sqrt[2]{\sum_{i=2}^{max} M_i^2}}{M_1} \qquad (5.2)$$

$$TDD = \frac{\sqrt[2]{\sum_{i=2}^{max} I_i^2}}{I_L} \qquad (5.3)$$

where h_i is the i^{th} harmonic, M_i is the RMS value of the i^{th} harmonic, I_i is the RMS value of the i^{th} harmonic of current and I_L is the peak or maximum load current at the PCC [102]. Computation of TDD requires historical data. Therefore, only IHD and THD of current and voltage waveforms are investigated in this chapter. Furthermore, their variations during a period of cloud shadow movement over are examined and discussed.

5.3 Impact of cloud shadow on power quality

In this section, first the case study is introduced. Then the effects of a cloud shadow on THD of the voltages and currents of the case study are discussed in detail.

5.3.1 Case study

The cases study is a 250-kW grid-connected PV system. Fig. 5.1 shows the model simulated in MATLAB/Simulink environment. The case study is developed based on a Simulink model [103]. The PV array, employed in test system, consists of 86 parallel strings, and each string is

made of seven SunPower SPR-415E solar modules. Figure 5.2 presents the I-V and P-V characteristic curves of one of the modules at two temperatures of 25 and 45 °C. Maximum

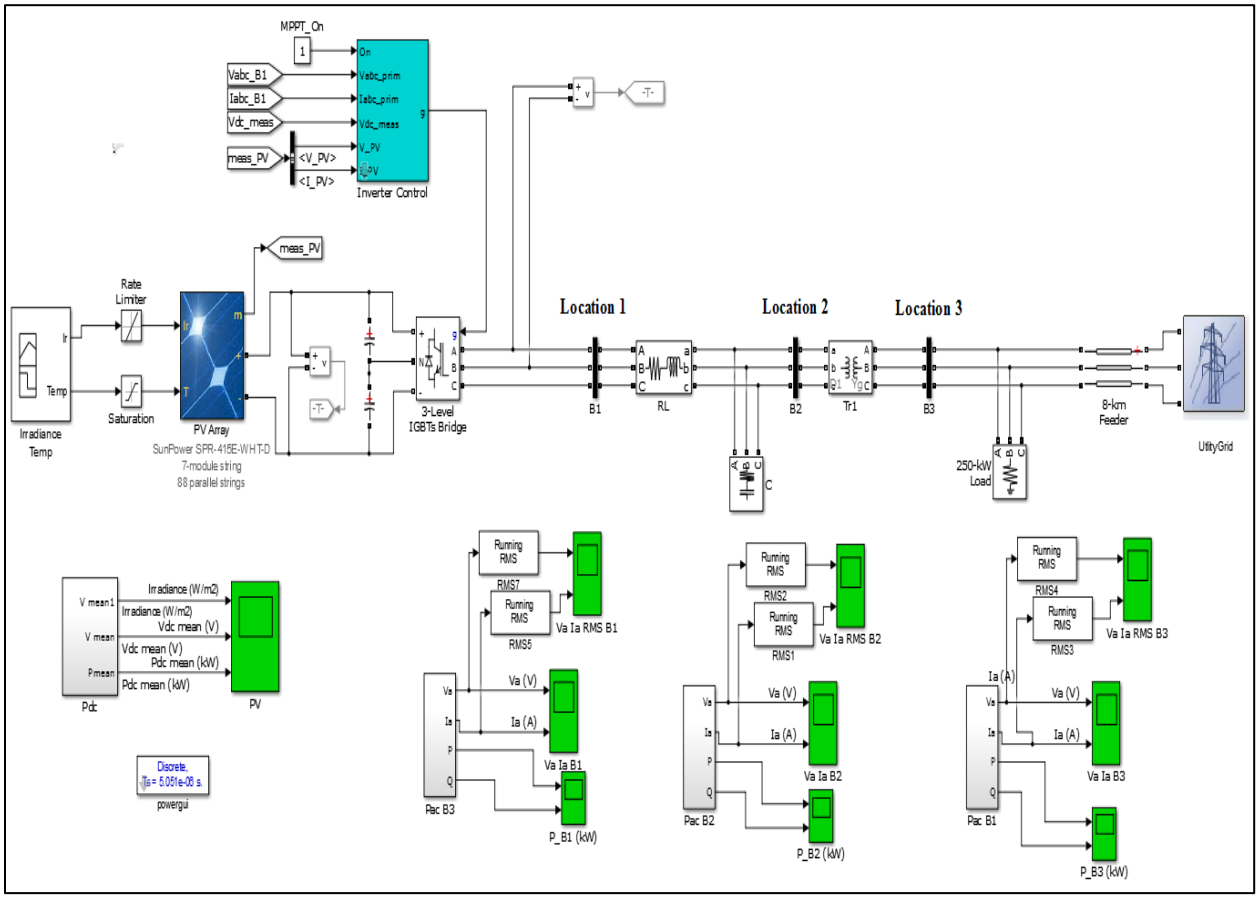

Figure 5.1. Simulated power system in MATLAB/Simulink environment, including a PV system, a local load, and a utility grid [10]. © 2016 IEEE

power of each solar module is about 415W. Hence, the total 602 modules can deliver about 250 kW. A 3-phase inverter is also employed for conversion of DC power to AC power, which is modeled by a 3-level Pulse Width Modulation (PWM)-controlled IGBT Bridge. An RL choke and a small capacitor filter are used to filter out the harmonics generated by the IGBT Bridge. The inverter is connected to the utility grid via a 250-kVA, 250V/25kV transformer.

Maximum Power Point Tracking (MPPT) is achieved based on "Perturb and Observe" technique, which automatically modifies the DC voltage reference signal of the inverter's regulator in order to reach maximum power delivery from the PV array. A PWM generator controls the

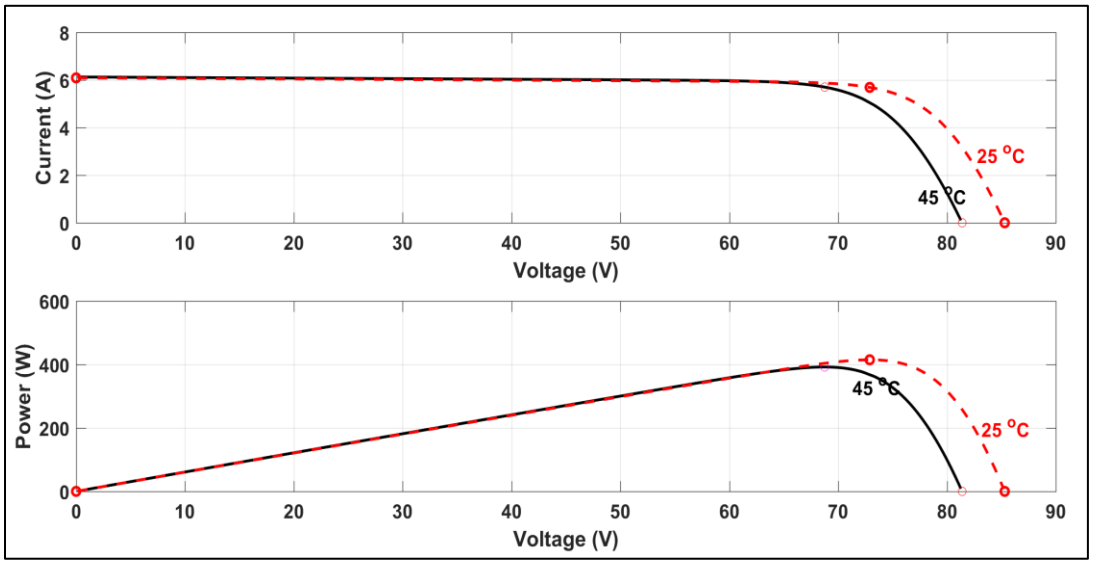

Figure 5.2. I-V and P-V characteristic curves of the solar arrays at 25 and 45 ℃ [10]. © 2016 IEEE

firing signals of the 3-level IGBT Bridge. The utility grid of Figure 5.1 module simulates a distribution network with a voltage level of 25 kV as well as a 120 kV transmission system. The distance between the transformer and the grid is 8 km. The effect of passing a cloud shadow over the PV system on the received irradiance is modeled as shown in Figure 5.3. The received irradiance first decreases from 1000 W/m^2 to 200 W/m^2. Then after the cloud shadow passes over the PV system completely, it returns to 1000 W/m^2 again.

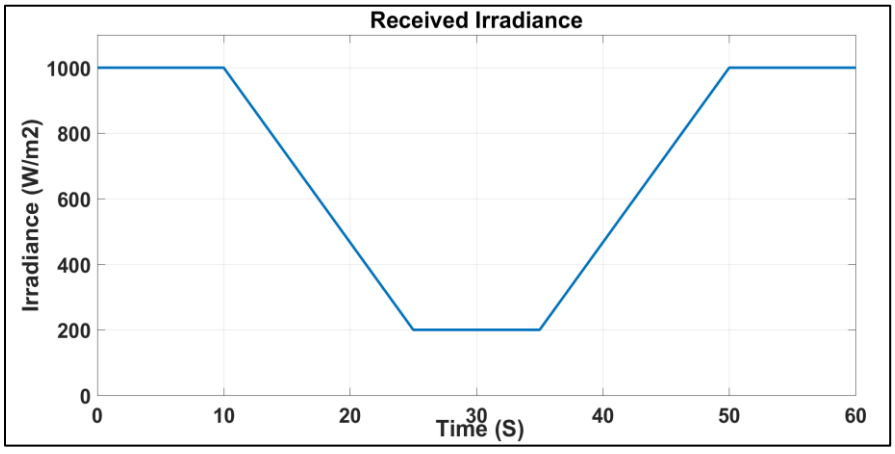

Figure 5.3. Irradiance change due to cloud shadow [10]. © 2016 IEEE

5.3.2 Simulation results

The impact of irradiance variations, due to the cloud shadow, on the power quality of the case study is discussed in this section. Three locations are selected to monitor THD of voltage and current waveforms as well as real and reactive powers during the period the cloud passes over the PV system.

Location 1 monitors the terminals of the 3-level IGBT Bridge. Location 2 is the low-voltage side of the transformer, where harmonics are supposed to be filtered by the choke and the capacitor filter. Location 3 is the high-voltage side of the transformer. The received irradiance by the PV system decreases from 1000 W/m^2 to 200 W/m^2 and then, after 10 seconds, it starts to return to 1000 W/m^2. Figure 5.4 shows the real power generated by the PV system during the simulation time. As illustrated in Figure 5.4, the output power decreases form 250 kW to about 50 kW when the cloud shadow covers the solar arrays completely. Different time points are selected to compute the THD of current and voltage waveforms. A window of 12 cycles is selected for THD calculation according to the IEEE 519-2014 standard [104].

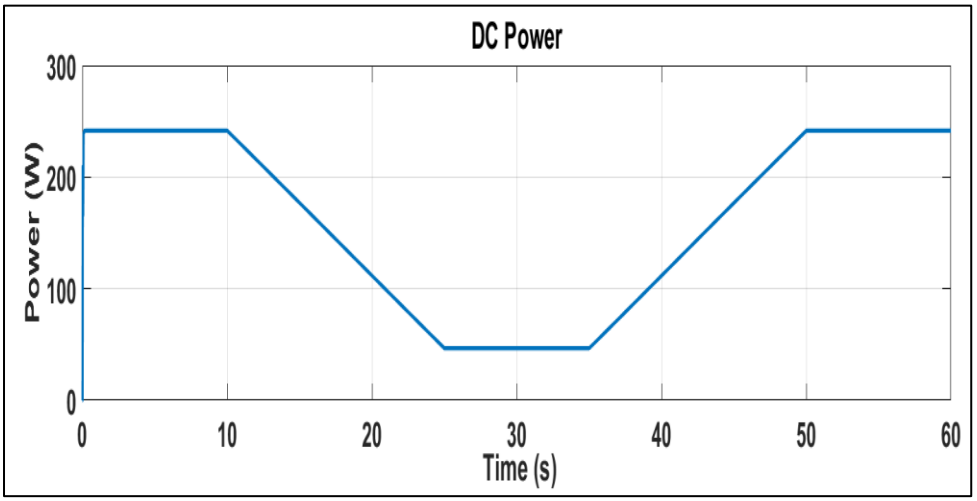

Figure 5.4. Effect of cloud shadow on the output power of the solar arrays [10]. © 2016 IEEE

Figure 5.5 shows three cycles of the current waveform at t=5s, no cloud coverage, t=15s, partial cloud coverage, and t=30s, full cloud coverage, at location 1. The effect of cloud shadow on the current quality can be seen clearly at t=30.

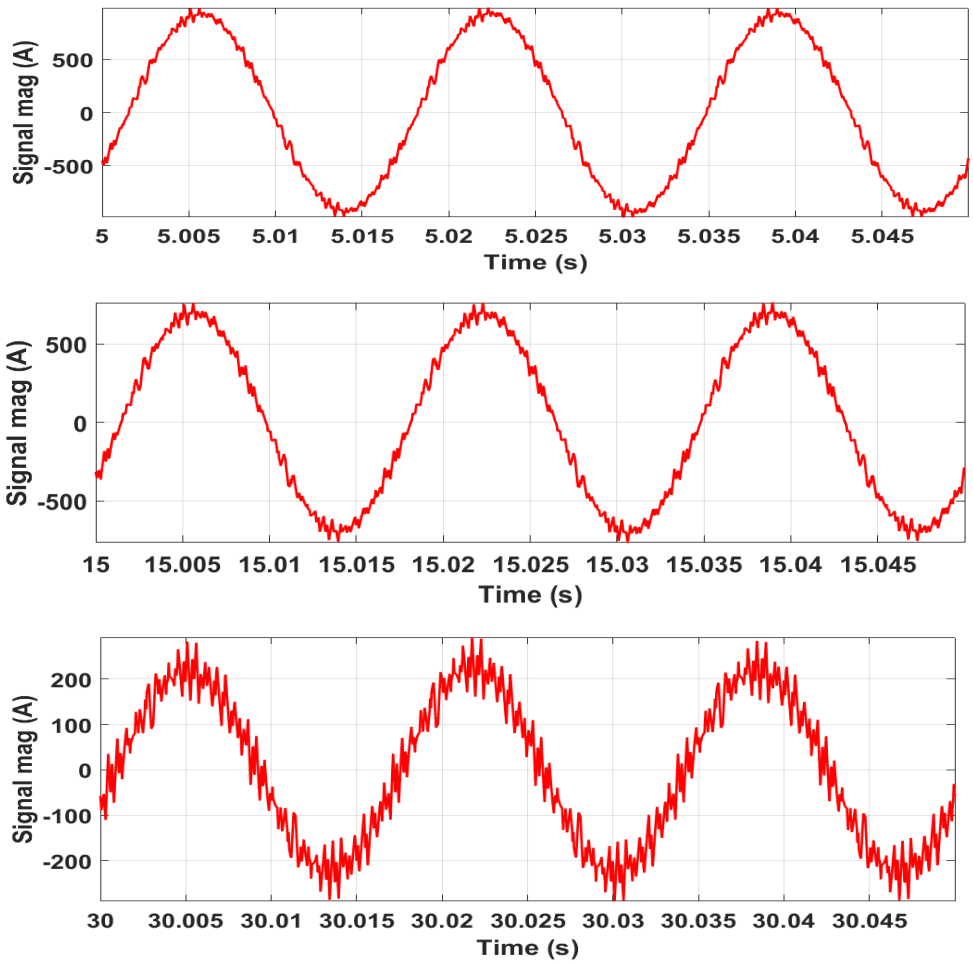

Figure 5.5. Three cycles of current waveform of location 1 at t=5, 15 and 30 s [10]. © 2016 IEEE

Figure 5.6 shows the magnitudes of current waveform harmonics in terms of fundamental percentage, at t=5s, t=15s, and t=30s of location 1. The effect of cloud shadow and the decrease in the received irradiance on the magnitude of fundamental and even harmonics and, consequently the THD could be observed in Figure 5.6. Figure 5.7 presents the variations of the real and reactive powers at location 1 during the simulation.

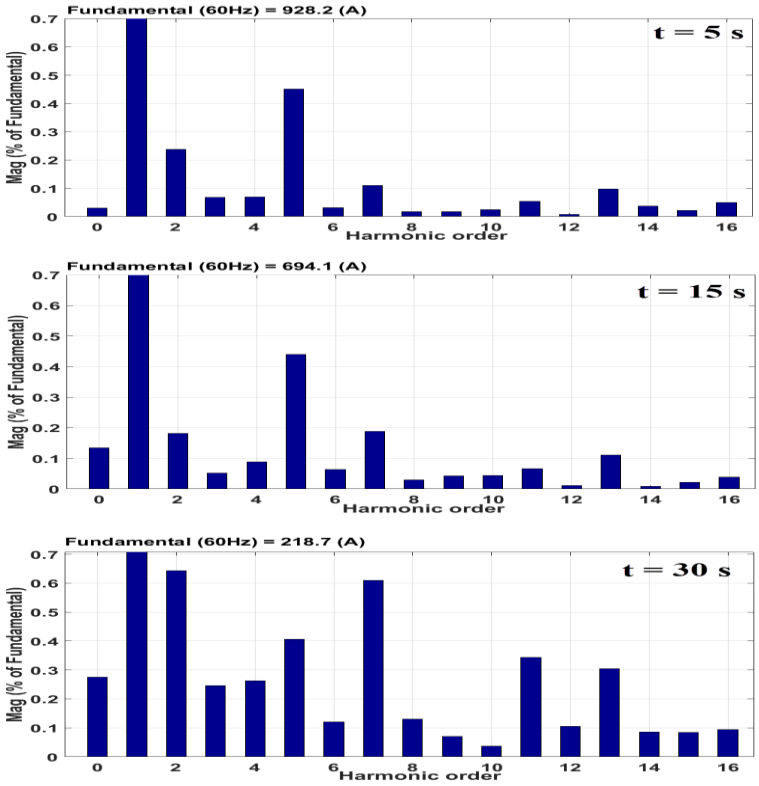

Figure 5.6. Current IHDs of location 1 at t=5, 15, and 30 s [10]. © 2016 IEEE

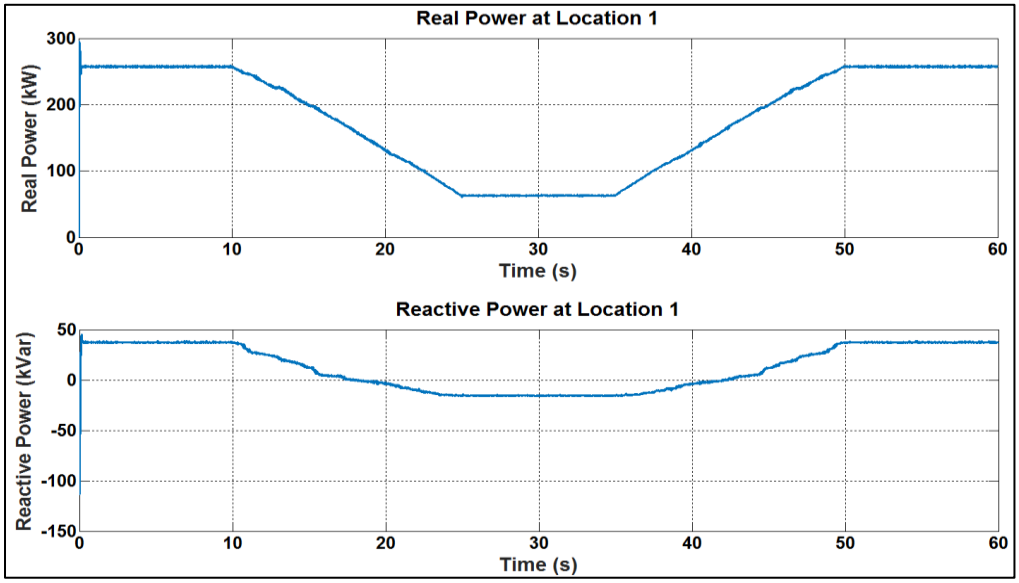

Figure 5.7. Real and reactive power variations at location 1 [10]. © 2016 IEEE

Figure 5.8 shows the three cycles of current waveform at t=5s, t=15s and t=30s at location 2, where is the low-voltage side, or secondary side, of the transformer. The results demonstrate that

the current quality decreases at full cloud coverage at t=30. In comparison to location 1, the power quality has improved due to the presence of the choke and the capacitor filter.

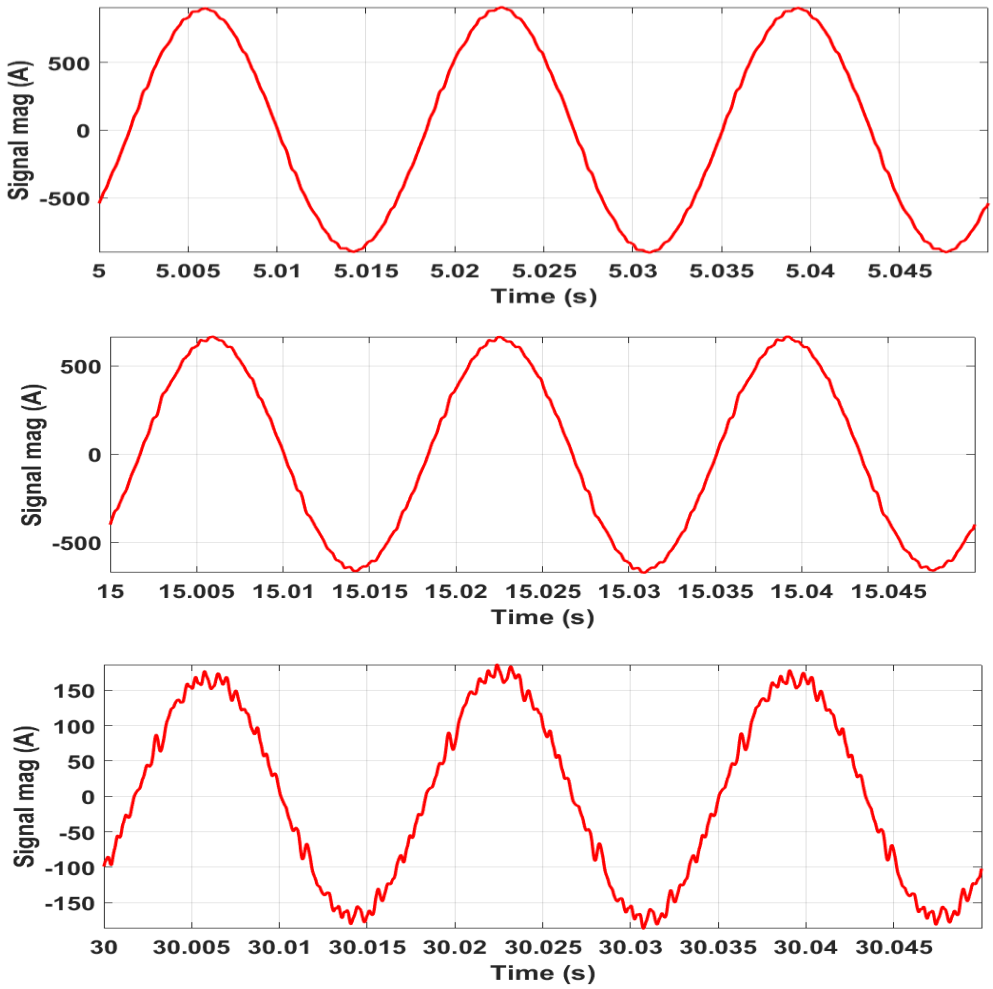

Figure 5.8. Three cycles of current waveform of location 2 at t=5, 15 and 30 s [10]. © 2016 IEEE

Figure 5.9 presents the IHDs of the current waveform of location 2 at t=5s, t=15s, and t=30s. The THD increases by more coverage of the solar arrays by the cloud shadow, and its maximum occurs with full cloud coverage. Decrease in the magnitude of the fundamental delivers the same point. Figure 5.10 presents the real and reactive powers at location 2 during the simulation.

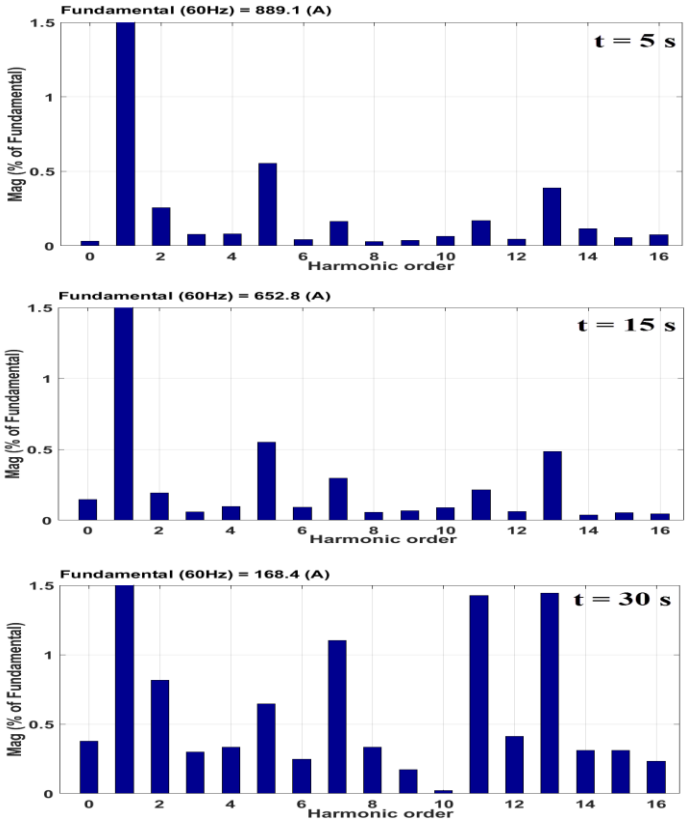

Figure 5.9. Current IHDs of location 1 at t=5, 15, and 30 s [10]. © 2016 IEEE

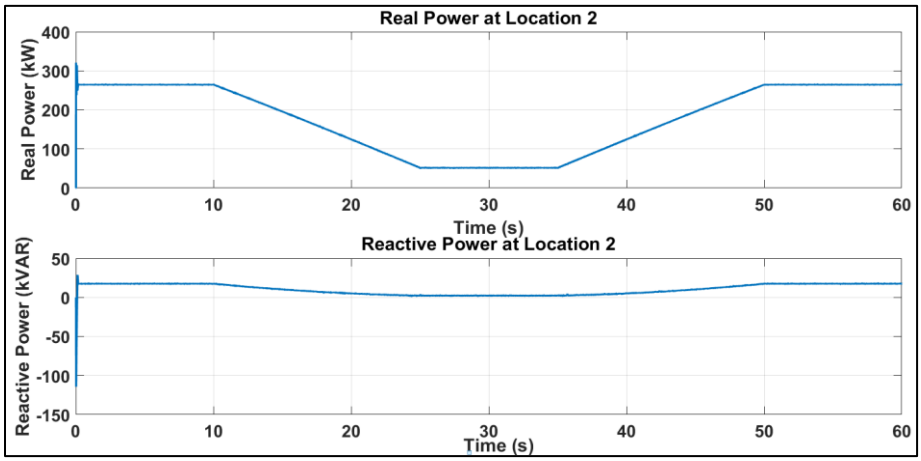

Figure 5.10. Real and reactive power variations at location 2 [10]. © 2016 IEEE

Figure 5.11 shows the three cycles of the current waveform at location 3 at t=5s, t=15s and t=30s. Location 3 is where the PV system is connected to the utility grid. Similar to previously studied locations, the current quality decreases as the cloud shadow covers the solar arrays.

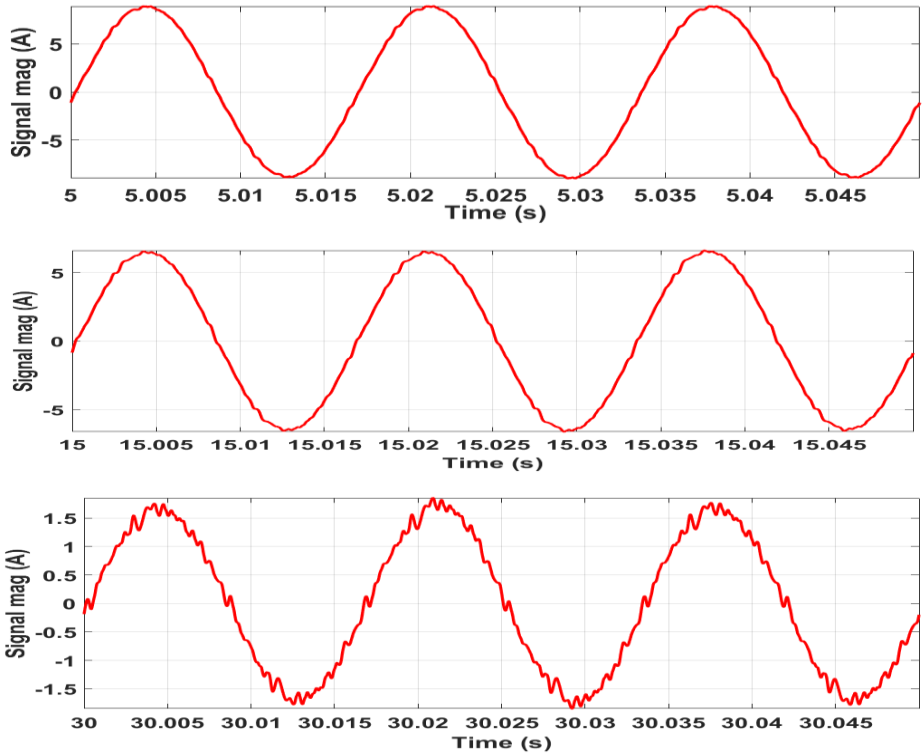

Figure 5.11. Three cycles of current waveform of location 3 at t=5, 15 and 30 s [10]. © 2016 IEEE

Figure 5.12 demonstrates the magnitudes of current waveform harmonics in terms of fundamental percentage, at t=5s, t=15s, and t=30 of location 3. Similar to locations 1 and 2, THD is at maximum when the cloud shadow covers the solar arrays completely. Figure 5.13 shows the real and reactive power variations of location 3.

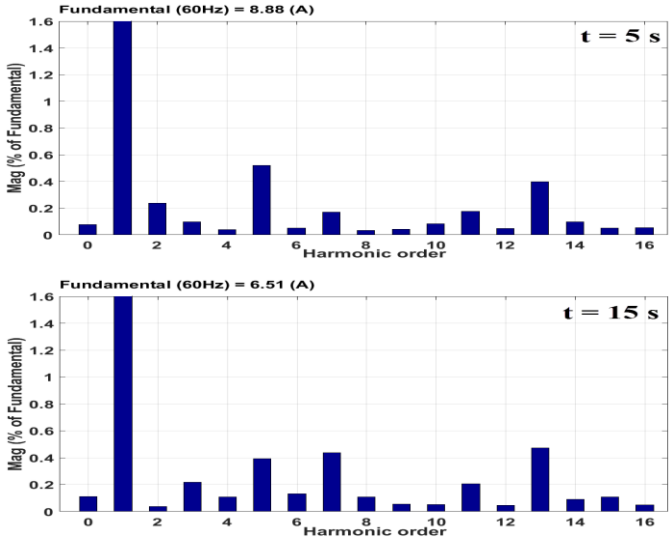

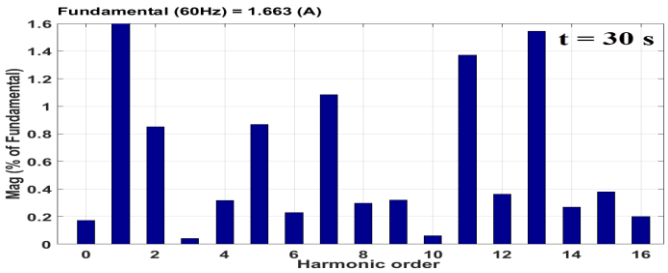

Figure 5.12. IHDs of location 3 at t=5, 15, and 30 s [10]. © 2016 IEEE

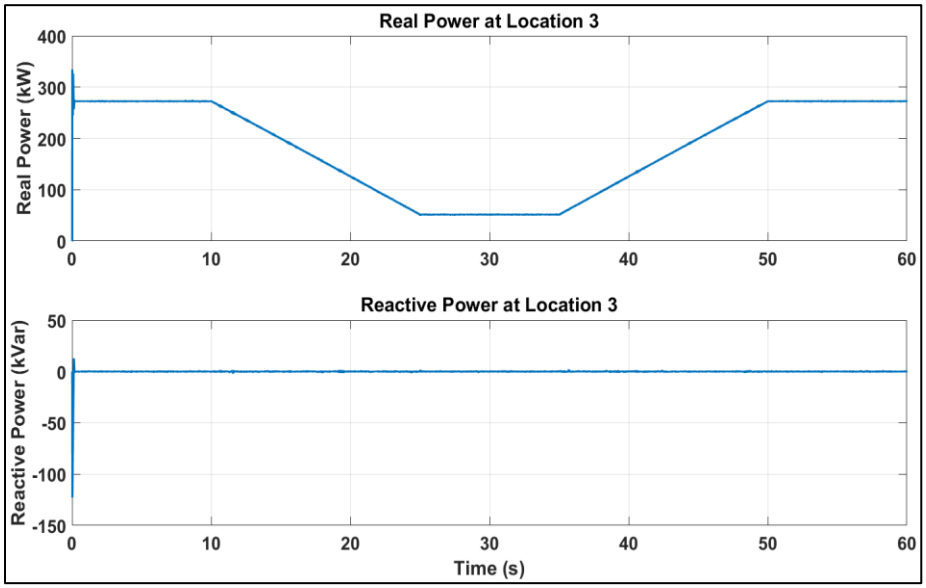

Figure 5.13. Real and reactive power variations at location 3 [10]. © 2016 IEEE

Table 5.1 shows the THD of current and voltage waveforms at the selected locations. Impact of the choke and the filter can be observed in reducing the THD of current and voltage waveforms. Moreover, Table 5.1 illustrates that the THD of the current waveforms increases with the decrease of irradiance, and consequently output power. The Current THD reaches the maximum value when the cloud shadow covers the solar arrays completely, t=30 s. In the same manner, the THD of the current decreases when the irradiance is returning to 1000 W/m^2. The changes in the THD of voltage waveforms are negligible. It is worth mentioning that simulation results can be affected significantly by the control strategy of the PV system inverter.

Table 5.1. summary of simulation results, providing THD of current and voltage waveforms [10]

Time (Second)	5	20	30	45	55
Current THD at Location 1 (%)	4.02	8.28	17.21	5.45	4.03
Current THD at Location 2 (%)	1.26	2.62	6.07	1.87	1.26
Current THD at Location 3 (%)	1.25	2.65	6.14	1.82	1.27
Voltage THD at location 1 (%)	43.00				
Voltage THD at location 2 (%)	2.00				
Voltage THD at location 3 (%)	0.05				

5.4 Impact of impedance between grid and point of common coupling

In this section, the impact of impedance between the utility grid and the PCC is assessed. Three different line lengths of 2, 8, and 14 km are considered. For each line length, THD of voltage waveform at the PCC (location 3) is computed. Simulation results, presented in Table 5.2, demonstrate that the voltage THD at the PCC decreases when the line length decreases. In other words, it illustrates that the impedance between the strong source of the system and the PCC affects the THD of voltage waveform, and its increase results in a higher voltage THD at the PCC.

Table 5.2. Voltage THD at location 1 with line lengths of 2, 8 and 14 km [10]

Line Length (km)	2	8	14
Voltage THD at PCC (%)	0.02	0.05	0.09

5.5 Conclusion remarks

This chapter investigated the impacts of cloud shadow on the dynamics of a 250 kW PV system and assessed the THD and IHD of the voltage, as well as current waveforms in different locations. It was observed that the THD of current waveforms increased and maximized as the cloud shadow covered all the solar arrays. The THD of the current waveform at the point of the PCC increased from 1.25% at no cloud coverage to 6.14% at full cloud coverage.

In addition, the voltage THD at the PCC was assessed in three scenarios in which the line lengths between the PCC and the grid were 2, 8 and 14 km. It was observed that the THD of voltage waveform increased by adding the line length, which eventually means increasing the impedance between the PCC and the gird.

Chapter 6: Conclusions, Contributions and Future Work

6.1 Conclusions

With high growth rate of solar Photovoltaic (PV) resources and ambitious renewable initiatives, seeking 100% pentation level, the intermittent nature of solar energy is causing serious challenges to system planners and operators. Simplified models, analysis approaches, and outdated standards cannot anymore deliver the needed accuracy to assess high penetration of solar energy, which happens to be the fastest-growing renewable energy with an intermittent nature. This dissertation presents a comprehensive analysis approach, which allows more accurate investigation of solar PV resources. Although real-world data sets were used to develop the CMS parameters, the simulation results have not been validated with real PV systems. In this dissertation, problem of high penetration of PV resources is tackled in three aspects of accurate analysis, accurate modeling, and effective control strategy.

The following describes the major contributions of this dissertation:

1. A comprehensive analysis is performed to compare the differences in results of Quasi Steady State (QSS) and Steady State (SS) analysis approaches, and to probe the causes. SS approach is the common practice in industry. A common perception between power engineers is that QSS and SS analysis approaches provide the same results if initial and final inputs of a system are the same, even in the existence of Volt-var controllers. This dissertation with its case studies in Chapter 2 demonstrates that the mentioned assumption is not correct for systems with Volt-var Control (VVC) devices. The final states of a system, one simulated with QSS and one simulated with SS analysis approach, can be very

different due to the nonlinearity of controllers and the paths that the system takes to reach its final state.

2. An extensive comparison is performed between using the flicker curves, presented in IEEE 141-1993 and IEEE 519-1992 standards, and the flickermeter method employed in IEEE 1453-2015 standard in terms of identifying maximum penetration levels. While the flickermeter method is the most updated practice to evaluate voltage flicker, many utilities still use the flicker curves due to its simplicity as well as computational complexity of the flickermeter method. Case studies presented in Chapter 2 show that using flicker curves limits penetration levels significantly and unnecessarily**.** This finding can be used in interconnection studies, allowing higher penetration of solar energy without being worried about violating voltage flicker limits.

3. The main cause of irradiance fluctuations is cloud shadow. However, simulating cloud shapes and shadows seems to be a super complicated task requiring very sophisticated tools and techniques. In fact, simulating cloud shapes is a complex process, but what is important for a power engineer is not simulating cloud shapes, but the impacts of clouds on power systems. This dissertation introduced a novel and practical Cloud Motion Simulator (CMS) that incorporates QSS power-flow analysis and computes flicker severity based on the IEEE 1453-2015 standard. The CMS can be used by engineers without being puzzled by the complex methodologies involved in cloud shape simulations or obstructed by obtaining precise meteorological data for clouds. This dissertation also proposes an innovative method on how six parameters of the CMS can be estimated from statistical analysis of publicly available meteorological data for irradiance and wind speed.

4. Currently, secondary circuits are either ignored or modeled with lumped models. Although using lumped models provides more accurate results compared to completely ignoring secondary circuits, they suffer from many assumptions and simplifications which may not be the case in reality or when used in different distribution networks. The analysis and case studies presented in Chapter 3 demonstrate that without detailed secondary circuit models, accurate penetration levels and precise locations of voltage issues cannot be determined.

5. This dissertation introduces distributed VVC schemes as a solution to future challenges of VVC systems. With the popularity of energy-saving programs such as Conservation Voltage Reduction (CVR), which requires decreasing the voltage level at substations, and high penetration of distributed PV resources, effective voltage regulation cannot be achieved anymore with traditional VVC devices. Furthermore, in Chapter 4 functionality of smart inverters in voltage regulation with controlling real and reactive powers in terms of Volt-var and Volt-Watt control strategies are investigated. The analysis presented shows that smart inverter functions can change the challenge of high penetration of PV resources into an opportunity of effective voltage regulation.

6. Finally, this dissertation for the first time combines the above mentioned contributions to provide a comprehensive, state-of-the-art analysis approach to assess integration of PV resources more accurately without the simplifications and unrealistic assumptions of current analysis approaches. Case studies presented in this dissertation demonstrate that the proposed approach increases the analysis accuracy as well as the penetration levels of PV resources significantly.

6.2 Future work

Although renewable energy resources and their impacts on the power grid have introduced many emerging research fields, the following list provides some potential topics for further investigation:

- Employing battery storage systems in scenarios in which real power needs to be curtailed such as employing Volt-watt controllers. Moreover, how battery storage systems can mitigate the negative impacts of cloud shadows on power quality can be an interesting topic to investigate.

- Using dynamic simulators and investigating the impact of transients on controllers actions. In QSS analysis, transients are not considered, due to the assumption that they will decay before the next time-step. A comparison between dynamic and QSS simulations in term of controller actions and the final state of a system will be valuable.

- Stability analysis of the systems with multiple volt-var controllers and smart inverters. Existence of many VVC devices and their interactions may result in stability issues.

- Developing design strategy for systems with many smart inverters and/or other VVC devices to obtain the best performance. Different objectives can be sought from VVC schemes. Therefore, defining the optimal set points and dead-bands of VVC devices as well as smart inverters settings based on specific VVC objectives, which can change through the day, seems to be a challenging optimization problem.

Bibliography

[1] Muntwyler, Urs. “Towards 100% renewable energy supplies….” 2015 Tenth International Conference on Ecological Vehicles and Renewable Energies (EVER), 2015.

[2] Twidell, John, and Tony Weir. Renewable energy resources. Routledge, 2015.

[3] Asadinejad, Ailin, et al. "Using biomass in power generation for supplying electrical and thermal energy in Iran and evaluation of environmental pollution spread." Journal of Energy and Power Engineering 10.1 (2016): 55-63.

[4] Rahimi, Kaveh, and Masoud Davoudi. "Electric vehicles for improving resilience of distribution systems." Sustainable Cities and Society 36 (2018): 246-256.

[5] Rahimi, Kaveh, and Badrul Chowdhury. "A hybrid approach to improve the resiliency of the power distribution system." North American Power Symposium (NAPS), 2014. IEEE, 2014.

[6] Menyah, Kojo, and Yemane Wolde-Rufael. "CO2 emissions, nuclear energy, renewable energy and economic growth in the US." Energy Policy 38.6 (2010): 2911-2915.

[7] Pollin, Robert, James Heintz, and Heidi Garrett-Peltier. The Economic Benefits of Investing in Clean Energy: How the economic stimulus program and new legislation can boost US economic growth and employment. No. economic_benefits. Political Economy Research Institute, University of Massachusetts at Amherst, 2009.

[8] REN21. 2016. Renewables 2016 Global Status Report (Paris: REN21 Secretariat). ISBN 978-3-9818107-0-7

[9] REN21. 2017. Renewables 2017 Global Status Report (Paris: REN21 Secretariat). ISBN 978-3-9818107-6-9

[10] Rahimi, Kaveh, Saeed Mohajeryami, and Alireza Majzoobi. "Effects of photovoltaic systems on power quality." North American Power Symposium (NAPS), 2016. IEEE, 2016.

[11] Yan, Ruifeng, and Tapan Kumar Saha. "Investigation of voltage stability for residential customers due to high photovoltaic penetrations." IEEE transactions on power systems 27.2 (2012): 651-662.

[12] Parchure, Abhineet, et al. "Investigating PV generation induced voltage volatility for customers sharing a distribution service transformer." IEEE Transactions on Industry Applications 53.1 (2017): 71-79.

[13] Demirok, Erhan, et al. "Local reactive power control methods for overvoltage prevention of distributed solar inverters in low-voltage grids." IEEE Journal of Photovoltaics 1.2 (2011): 174-182.

[14] Hill, Cody A., et al. "Battery energy storage for enabling integration of distributed solar power generation." IEEE Transactions on smart grid 3.2 (2012): 850-857.

[15] Alam, M. J. E., K. M. Muttaqi, and D. Sutanto. "A novel approach for ramp-rate control of solar PV using energy storage to mitigate output fluctuations caused by cloud passing." IEEE Transactions on Energy Conversion 29.2 (2014): 507-518.

[16] Moghaddam, Iman Naziri, Badrul Chowdhury, and Saeed Mohajeryami. "Predictive Operation and Optimal Sizing of Battery Energy Storage with High Wind Energy Penetration." IEEE Transactions on Industrial Electronics (2017).

[17] Mazhari, Iman, et al. "Distributed PV-battery architectures with reconfigurable power conversion units." Applied Power Electronics Conference and Exposition (APEC), 2014 Twenty-Ninth Annual IEEE. IEEE, 2014.

[18] Li, Peng, et al. "Storage aided system property enhancing and hybrid robust smoothing for large-scale PV systems." IEEE Transactions on Smart Grid 8.6 (2017): 2871-2879.

[19] Alam, Md Jan E., Kashem M. Muttaqi, and Danny Sutanto. "A multi-mode control strategy for VAr support by solar PV inverters in distribution networks." IEEE transactions on power systems 30.3 (2015): 1316-1326.

[20] Tonkoski, Reinaldo, Luiz AC Lopes, and Tarek HM El-Fouly. "Coordinated active power curtailment of grid connected PV inverters for overvoltage prevention." IEEE Transactions on Sustainable Energy 2.2 (2011): 139-147.

[21] von Appen, Jan, et al. "Local voltage control strategies for PV storage systems in distribution grids." IEEE Transactions on Smart Grid 5.2 (2014): 1002-1009.

[22] Pompodakis, Evangelos E., et al. "Photovoltaic systems in low-voltage networks and overvoltage correction with reactive power control." IET Renewable Power Generation 10.3 (2016): 410-417.

[23] Kabir, M. N., et al. "Coordinated control of grid-connected photovoltaic reactive power and battery energy storage systems to improve the voltage profile of a residential distribution feeder." IEEE Transactions on industrial Informatics 10.2 (2014): 967-977.

[24] Gabash, Aouss, and P. U. Li. "Reverse active-reactive optimal power flow in ADNs: Technical and economical aspects." Energy Conference (ENERGYCON), 2014 IEEE International. IEEE, 2014.

[25] Davoudi, Masoud. Increasing Hosting Capacity of Distribution Systems For Renewable Distributed Generation By Means of Network Reconfiguration. Diss. The University of North Carolina at Charlotte, 2017.

[26] Davoudi, Masoud, Valentina Cecchi, and Julio Romero Agüero. "Increasing penetration of Distributed Generation with meshed operation of distribution systems." North American Power Symposium (NAPS), 2014. IEEE, 2014.

[27] Agrawal, Ashish, et al. "Performance of PV generation feedback controllers: Power factor versus Volt-VAR control strategies." North American Power Symposium (NAPS), 2015. IEEE, 2015.

[28] K. Rahimi, A. Tbaileh, R. Broadwater, J. Woyak and M. Dilek, "Voltage regulation performance of smart inverters: Power factor versus volt-VAR control," 2017 North American Power Symposium (NAPS), Morgantown, WV, 2017, pp. 1-6. doi: 10.1109/NAPS.2017.8107407

[29] Jahangiri, Pedram, and Dionysios C. Aliprantis. "Distributed Volt/VAr control by PV inverters." IEEE Transactions on power systems 28.3 (2013): 3429-3439.

[30] Fazeli, Meghdad, et al. "Exploiting PV inverters to support local voltage—A small-signal model." IEEE Transactions on Energy Conversion 29.2 (2014): 453-462.

[31] Lopes, JA Pecas, et al. "Integrating distributed generation into electric power systems: A review of drivers, challenges and opportunities." Electric power systems research 77.9 (2007): 1189-1203.

[32] Tbaileh, Ahmad, et al. "Graph Trace Analysis: An object-oriented power flow, verifications and comparisons." Electric Power Systems Research 147 (2017): 145-153.

[33] Elyas, Seyyed Hamid, Asghar Akbari Foroud, and Hamed Chitsaz. "A novel method for maintenance scheduling of generating units considering the demand side." International Journal of Electrical Power & Energy Systems 51 (2013): 201-212.

[34] Molzahn, Daniel K. "Computing the feasible spaces of optimal power flow problems." IEEE Transactions on Power Systems 32.6 (2017): 4752-4763.

[35] Majzoobi, Alireza, and Amin Khodaei. "Application of microgrids in supporting distribution grid flexibility." IEEE Transactions on Power Systems 32.5 (2017): 3660-3669.

[36] Vittal, Eknath, Mark O'Malley, and Andrew Keane. "A steady-state voltage stability analysis of power systems with high penetrations of wind." IEEE Transactions on Power Systems 25.1 (2010): 433-442.

[37] Hamidi, R. Jalilzadeh, and H. Livani. "Myopic real-time decentralized charging management of plug-in hybrid electric vehicles." Electric Power Systems Research 143 (2017): 522-532.

[38] Doostan, Milad, et al. "Concurrent placement of distributed generation resources and capacitor banks in distribution systems." North American Power Symposium (NAPS), 2016. IEEE, 2016.

[39] Gunther, Erich W., and H. Mebta. "A survey of distribution system power quality-preliminary results." IEEE transactions on Power Delivery 10.1 (1995): 322-329.

[40] IEEE Recommended Practice for Electric Power Distribution for Industrial Plants," in IEEE Std 141-1993 , vol., no., pp.1-768, April 29 1994

[41] IEEE Recommended Practices and Requirements for Harmonic Control in Electrical Power Systems," in IEEE Std 519-1992 , vol., no., pp.1-112, April 9 1993

[42] IEEE Recommended Practice for the Analysis of Fluctuating Installations on Power Systems," in IEEE Std 1453-2015 (Revision of IEEE Std 1453-2011) , vol., no., pp.1-74, Oct. 30 2015

[43] Morf, Heinrich. "The stochastic two-state cloud cover model STSCCM." Solar Energy 85.5 (2011): 985-999.

[44] Marotz, Glen A., and James A. Henry. "Satellite-derived cumulus cloud statistics for western Kansas." Journal of Applied Meteorology 17.11 (1978): 1725-1736.

[45] Lohmann, Gerald M., et al. "Simulating clear-sky index increment correlations under mixed sky conditions using a fractal cloud model." Solar Energy 150 (2017): 255-264.

[46] Cai, Chengrui, and Dionysios C. Aliprantis. "Cumulus cloud shadow model for analysis of power systems with photovoltaics." IEEE Transactions on Power Systems 28.4 (2013): 4496-4506.

[47] Barbieri, Florian, Sumedha Rajakaruna, and Arindam Ghosh. "Very short-term photovoltaic power forecasting with cloud modeling: A review." Renewable and Sustainable Energy Reviews 75 (2017): 242-263.

[48] P. Gupta, K. Rahimi, R. Broadwater and M. Dilek, "Importance of detailed modeling of loads/PV systems connected to secondary of distribution transformers," 2017 North American Power Symposium (NAPS), Morgantown, WV, 2017, pp. 1-6.

[49] Peppanen, Jouni, et al. "Secondary Low-Voltage Circuit Models—How Good is Good Enough?." IEEE Transactions on Industry Applications 54.1 (2018): 150-159.

[50] Shirek, Greg J., et al. "Modeling Secondary Services in Engineering and Mapping." IEEE Transactions on Industry Applications 1.48 (2012): 254-262.

[51] Short, Tom A. "Advanced metering for phase identification, transformer identification, and secondary modeling." IEEE Transactions on Smart Grid 4.2 (2013): 651-658.

[52] Taylor, J. A., T. A. Short, and B. Bushey. "Efficiency impacts of distribution secondaries." Transmission and Distribution Conference and Exposition (T&D), 2012 IEEE PES. IEEE, 2012.

[53] Hoff, Thomas E., and Richard Perez. "Modeling PV fleet output variability." Solar Energy 86.8 (2012): 2177-2189.

[54] Lave, Matthew, and Jan Kleissl. "Cloud speed impact on solar variability scaling–Application to the wavelet variability model." Solar Energy 91 (2013): 11-21.

[55] Lave, Matthew, Jan Kleissl, and Joshua S. Stein. "A wavelet-based variability model (WVM) for solar PV power plants." IEEE Transactions on Sustainable Energy 4.2 (2013): 501-509.

[56] Dyreson, Ana. Predicting spatial smoothing for solar PV power using the wavelet variability model. Diss. Northern Arizona University, 2014.

[57] Stein, Joshua, Clifford Hansen, and Matthew J. Reno. The Variability Index: A New and Novel Metric for Quantifying Irradiance and PV Output Variability. No. SAND2012-2088C. Sandia National Laboratories, 2012.

[58] Dyreson, Ana, et al. "Comparison of solar irradiance smoothing using a 45-sensor network and the wavelet variability model." 43rd ASES National Solar Conference 2014, SOLAR 2014, Including the 39th National Passive Solar Conference and the 2nd Meeting of Young and Emerging Professionals in Renewable Energy. American Solar Energy Society, 2014.

[59] IEEE Standard for Interconnecting Distributed Resources with Electric Power Systems," in IEEE Std 1547-2003 , vol., no., pp.1-28, July 28 2003

[60] Jain, Himanshu, et al. "Studying the Impact of Solar PV on Power System Dynamics Using Integrated Transmission and Distribution Network Models." Journal of Energy Engineering 144.1 (2017): 04017072.

[61] Jain, Himanshu, et al. "Integrated transmission & distribution system modeling and analysis: Need & advantages." Power and Energy Society General Meeting (PESGM), 2016. IEEE, 2016.

[62] Deng, Weisi, et al. "Risk-Based Probabilistic Voltage Stability Assessment in Uncertain Power System." Energies 10.2 (2017): 180.

[63] California Energy Commission, European Renewable Distributed Generation Infrastructure Study: Lessons Learned from Electricity Markets in Germany and Spain - Consultant Report, CEC400-2011- 011, December, 2011.

[64] Malashenko, Elizaveta, Stephen Appert, and Wendy al-Mukdad. "Advanced inverter technologies report." California Public Utilities Commission (2013): 1-13.

[65] IEEE Standard for Interconnecting Distributed Resources with Electric Power Systems - Amendment 1," in IEEE Std 1547a-2014 (Amendment to IEEE Std 1547-2003) , vol., no., pp.1-16, May 21 2014

[66] Mather, Barry A. "Quasi-static time-series test feeder for PV integration analysis on distribution systems." Power and Energy Society General Meeting, 2012 IEEE. IEEE, 2012.

[67] Rahimi, Kaveh, et al. "Quasi-Steady-State computation of voltage flicker with cloud motion simulator." Power and Energy Conference at Illinois (PECI), 2017 IEEE. IEEE, 2017.

[68] Billinton, Roy, Hua Chen, and R. Ghajar. "Time-series models for reliability evaluation of power systems including wind energy." Microelectronics Reliability 36.9 (1996): 1253-1261.

[69] Rahimi, Kaveh, et al. "Computation of Voltage Flicker with Cloud Motion Simulator." IEEE Transactions on Industry Applications (2017).

[70] Ebad, Mehdi, and William Mack Grady. "An approach for assessing high-penetration PV impact on distribution feeders." Electric Power Systems Research 133 (2016): 347-354.

[71] Garrett, D. L., and S. M. Jeter. "A photovoltaic voltage regulation impact investigation technique. I. Model development." IEEE Transactions on Energy Conversion 4.1 (1989): 47-53.

[72] Davis, Anthony B., and Alexander Marshak. "Solar radiation transport in the cloudy atmosphere: a 3D perspective on observations and climate impacts." Reports on Progress in Physics 73.2 (2010): 026801.

[73] Nelson, Joel A. "Effects of cloud-induced photovoltaic power transients on power system protection." (2010).

[74] Wu, Qiang, D. H. Popović, and David J. Hill. "Avoiding sustained oscillations in power systems with tap changing transformers." International journal of electrical power & energy systems 22.8 (2000): 597-605.

[75] Popović, D., I. A. Hiskens, and D. J. Hill. "Investigations of load-tap changer interaction." International Journal of Electrical Power & Energy Systems 18.2 (1996): 81-97.

[76] Cullen, Scott. "Trees and wind: wind scales and speeds." Journal of Arboriculture 28.5 (2002): 237-242.

[77] IEEE Guide for Conducting Distribution Impact Studies for Distributed Resource Interconnection," in IEEE Std 1547.7-2013 , vol., no., pp.1-137, Feb. 28 2014. doi: 10.1109/IEEESTD.2014.6748837

[78] IEC 61000-4-15, Edition 2-08-2010—Electromagnetic compatibility (EMC)—Part 4-15: Testing and measurement techniques—Flickermeter—Functional and design specifications.

[79] ANSI C84.1-2006, American National Standard for Electric Power Systems and Equipment-Voltage Ratings (60 Hertz); http://www.nema.org /media/pr/20070116a.cfm; accessed 5/17/2011.

[80] Giraldez Miner, Julieta I., et al. Simulation of Hawaiian Electric Companies Feeder Operations with Advanced Inverters and Analysis of Annual Photovoltaic Energy Curtailment. No. NREL/TP-5D00-68681. National Renewable Energy Laboratory (NREL), Golden, CO (United States), 2017.

[81] Ding, Fei, et al. Photovoltaic Impact Assessment of Smart Inverter Volt-VAR Control on Distribution System Conservation Voltage Reduction and Power Quality. No. NREL/TP-5D00-67296. National Renewable Energy Lab.(NREL), Golden, CO (United States), 2016.

[82] Nagarajan, Adarsh, et al. "Network reduction algorithm for developing distribution feeders for real-time simulators." IEEE Power and Energy Society General Meeting. 2017.

[83] Nelson, Austin, et al. Hawaiian Electric Advanced Inverter Grid Support Function Laboratory Validation and Analysis. No. NREL/TP-5D00-67485. National Renewable Energy Lab.(NREL), Golden, CO (United States), 2016.

[84] American National Standard for Transformers-- Underground-Type Three-Phase Distribution Transformers 2500 kVA and Smaller; High Voltage: 34,500 GrdY/29 920 Volts and Below; Low Voltage: 480 Volts and Below--Requirements," in ANSI C57.12.24-2000 , vol., no., pp.1-18, Jan. 21 2000

[85] Conti, S., S. Raiti, and G. Vagliasindi. "Voltage sensitivity analysis in radial MV distribution networks using constant current models." Industrial Electronics (ISIE), 2010 IEEE International Symposium on. IEEE, 2010.

[86] Youssef, Karim Hassan. "A new method for online sensitivity-based distributed voltage control and short circuit analysis of unbalanced distribution feeders." IEEE Transactions on Smart Grid 6.3 (2015): 1253-1260.

[87] Agalgaonkar, Yashodhan P., Bikash C. Pal, and Rabih A. Jabr. "Distribution voltage control considering the impact of PV generation on tap changers and autonomous regulators." IEEE Transactions on Power Systems 29.1 (2014): 182-192.

[88] Aghatehrani, Rasool, and Rajesh Kavasseri. "Reactive power management of a DFIG wind system in microgrids based on voltage sensitivity analysis." IEEE Transactions on Sustainable Energy 2.4 (2011): 451-458.

[89] Ong, Sean, et al. Land-use requirements for solar power plants in the United States. No. NREL/TP-6A20-56290. National Renewable Energy Laboratory (NREL), Golden, CO., 2013.

[90] Rahimi, Kaveh, et al. "Selecting and Redesigning Distribution Feeders for CVR Benefits." Global Journal of Research In Engineering (2016).

[91] Willis, H. Lee. Power distribution planning reference book. CRC press, 2004.

[92] Gellings, Clark W. The smart grid: enabling energy efficiency and demand response. The Fairmont Press, Inc., 2009.

[93] Schneider, Kevin P., et al. Evaluation of conservation voltage reduction (CVR) on a national level. No. PNNL-19596. Pacific Northwest National Laboratory (PNNL), Richland, WA (US), 2010.

[94] Broadwater, Robert P., et al. "Minimum loss optimization in distribution systems: discrete ascent optimal programming." Electric power systems research 36.2 (1996): 113-121.

[95] Kersting, William H. "Radial distribution test feeders." IEEE Transactions on Power Systems 6.3 (1991): 975-985.

[96] Seal, B. "Common functions for smart inverters, version 3." EPRI Report 3002002233 21 (2014).

[97] Wang, Fei, Jorge L. Duarte, and Marcel AM Hendrix. "Analysis of harmonic interactions between DG inverters and polluted grids." Energy Conference and Exhibition (EnergyCon), 2010 IEEE International. IEEE, 2010.

[98] Heskes, P. J. M., and Johan Heinrich Richter Enslin. Power quality behaviour of different photovoltaic inverter topologies. Energy research Centre of the Netherlands ECN, 2003.

[99] Mastromauro, Rosa A., et al. "A single-phase voltage-controlled grid-connected photovoltaic system with power quality conditioner functionality." IEEE Transactions on Industrial Electronics 56.11 (2009): 4436-4444.

[100] Papaioannou, Ioulia T., et al. "Harmonic impact of small photovoltaic systems connected to the LV distribution network." Electricity Market, 2008. EEM 2008. 5th International Conference on European. IEEE, 2008.

[101] Chattopadhyay, Surajit, Madhuchhanda Mitra, and Samarjit Sengupta. "Sag, Swell, Interruption, Undervoltage and Overvoltage." Electric Power Quality. Springer Netherlands, 2011. 39-42.

[102] Dugan, Roger C., Mark F. McGranaghan, and H. Wayne Beaty. "Electrical power systems quality." New York, NY: McGraw-Hill,| c1996 (1996).

[103] Mathworks official website, “250-kW Grid-Connected PV Array, 2016. ”[Online]. Available: https://www.mathworks.com/help/physmod/sps/examples/250-kw-grid-connected-pv-array.html

[104] IEEE Recommended Practice and Requirements for Harmonic Control in Electric Power Systems," in IEEE Std 519-2014 (Revision of IEEE Std 519-1992) , vol., no., pp.1-29, June 11 2014s

Appendix

Reuse of IEEE articles

Some chapters of this dissertation are written based on several IEEE published papers, each of which the author of this dissertation was the first author. At the time of writing this dissertation, the reuses are in compliance with the IEEE reuse policy for Theses and Dissertations, where a formal reuse license is not required. The policy can be accessed at:

https://www.ieee.org/publications_standards/publications/rights/permissions_faq.pdf

Reuse of GJ article

A section of Chapter 4 is written based on [90]. The following is GJ policy published on the first page of [90] which allows the reuse of the article in this dissertation.

"This is a research/review paper, distributed under the terms of the Creative Commons Attribution-Noncommercial 3.0 Unported License http://creativecommons.org/licenses/by-nc/3.0/), permitting all non commercial use, distribution, and reproduction in any medium, provided the original work is properly cited."

More info on Creative Commons Attribution-Noncommercial 3.0 can be found at:

https://creativecommons.org/licenses/by-nc/3.0/us/